creative commons
COMMONS DEED

저작자표시-비영리-변경금지 2.0 대한민국

이용자는 아래의 조건을 따르는 경우에 한하여 자유롭게

- 이 저작물을 복제, 배포, 전송, 전시, 공연 및 방송할 수 있습니다.

다음과 같은 조건을 따라야 합니다:

저작자표시. 귀하는 원저작자를 표시하여야 합니다.

비영리. 귀하는 이 저작물을 영리 목적으로 이용할 수 없습니다.

변경금지. 귀하는 이 저작물을 개작, 변형 또는 가공할 수 없습니다.

- 귀하는, 이 저작물의 재이용이나 배포의 경우, 이 저작물에 적용된 이용허락조건을 명확하게 나타내어야 합니다.
- 저작권자로부터 별도의 허가를 받으면 이러한 조건들은 적용되지 않습니다.

저작권법에 따른 이용자의 권리는 위의 내용에 의하여 영향을 받지 않습니다.

이것은 이용허락규약(Legal Code)을 이해하기 쉽게 요약한 것입니다.

Disclaimer

dCollection

이학박사학위논문

RNF20의 지방대사 조절과 신장암에서의 기능 연구

Roles of RNF20, an E3 Ubiquitin Ligase,

in Hepatic Lipid Metabolism and Kidney Cancer

2017년 2월

서울대학교 대학원

생명과학부

이 재 호

RNF20의 지방대사 조절과 신장암에서의 기능 연구

Roles of RNF20, an E3 Ubiquitin Ligase, in Hepatic Lipid Metabolism and Kidney Cancer

지도교수 김 재 범

이 논문을 이학박사 학위논문으로 제출함

2017년 2월

서울대학교 대학원

생명과학부

이 재 호

이재호의 박사학위논문을 인준함

2017년 2월

위 원 장 이 건 수 (인)

부위원장 김 재 범 (인)

위 원 설 재 홍 (인)

위 원 곽 철 (인)

위 원 송 재 환 (인)

Roles of RNF20, an E3 Ubiquitin Ligase,

in Hepatic Lipid Metabolism and Kidney Cancer

A dissertation submitted in partial fulfillment of

the requirement for degree of

DOCTOR OF PHILOSOPHY

To the Faculty of the

School of Biological Sciences

At

SEOUL NATIONAL UNIVERSITY

By

Jae Ho Lee

February, 2017

Data Approved

_____

_____

_____

_____

_____

_____

ABSTRACT

Roles of RNF20, an E3 Ubiquitin Ligase, in Hepatic Lipid Metabolism and Kidney Cancer

Jae Ho Lee

Lipid metabolism is crucial for cell growth and survival by regulating energy homeostasis, signaling cascade, and membrane integrity. Accordingly, abnormal regulation of lipid metabolism is closely associated with metabolic disorders and tumorigenesis. In liver, *de novo* lipogenesis is hormonally and nutritionally controlled by sterol regulatory element-binding protein 1c (SREBP1c). SREBP1c is a key transcription factor for fatty acid synthesis during the postprandial state. Hepatic SREBP1c is rapidly suppressed by fasting signals to prevent futile lipogenic pathways. However, the molecular mechanisms that control SREBP1c turnover in response to fasting status are not thoroughly understood. Moreover, accumulating evidences have demonstrated that activated SREBP1c is involved in lipid storage in cancer cells. Although SREBP1c is associated with tumor development, progression and migration, eventually leading to poor prognosis, it remains unclear how SREBP1c would contribute to ectopic lipid storage and tumorigenesis in cancer cells.

In the chapter one, I demonstrated that SREBP1c is ubiquitinated by ring finger protein 20 (RNF20), an E3 ubiquitin ligase. The RNF20-induced SREBP1c

ubiquitination suppresses hepatic lipid metabolism upon protein kinase A (PKA), a major signaling molecule for nutritional deprivation. In hepatocytes, glucagon and activated PKA stimulate RNF20 expression and subsequently downregulate lipogenic activity. In obese *db*/*db* mice, hepatic RNF20 overexpression alleviates fatty liver by reducing lipogenic activity via SREBP1c suppression. This study suggests that RNF20 would act as a negative regulator of hepatic lipid metabolism through SREBP1c degradation upon PKA activation. Thus, these findings enhance our understandings of how SREBP1c is able to turn off hepatic lipid metabolism during fasting.

In the chapter two, I revealed that downregulation of RNF20 promotes tumorigenesis in clear cell renal cell carcinoma (ccRCC), which is characterized by ectopic lipid accumulation, following consequent activation of SREBP1c. In ccRCC tumor tissues, RNF20 is downregulated, accompanied with lipogenic activation and poor prognosis. In cultured ccRCC cells and xenograft studies, RNF20 overexpression represses lipogenesis and cell proliferation by inhibiting SREBP1c. In this study, pituitary tumor-transforming gene 1 (PTTG1) has been identified as a novel target gene of SREBP1c, and PTTG1 plays a crucial role in cell cycle progression in ccRCC through SREBP1c. In ccRCC cells, suppression of SREBP1 by either genetic knockdown or pharmacological inhibitor betulin attenuates cell proliferation, accompanied with decreased expression of PTTG1 and cell cycle genes.

Taken together, this study provides a clue to understand how SREBP1c is regulated by RNF20 to modulate lipid homeostasis and underscores the close relationship between lipid metabolism and tumorigenesis in ccRCC, where the

RNF20-SREBP1c axis would be important for lipogenesis and cell cycle progression. Therefore, these data suggest that RNF20 might be a useful target for ameliorating metabolic disorders and certain cancers associated with increased lipid metabolism, particularly with SREBP1c.

Key words: RNF20, SREBP1c, PTTG1, PKA, Ubiquitination, Lipogenesis, Tumorigenesis, ccRCC

Student number: 2011-30914

TABLE OF CONTENTS

LIST OF FIGURES

LIST OF TABLES

BACKGROUNDS

I. Lipid metabolism in liver

About 40% of the body's caloric intake is derived from lipids. Lipids consist of diverse water-insoluble molecules including triacylglycerides, phosphoglycerides, sterols, and sphingolipids. Various lipid metabolites act as energy sources, signaling molecules, and structural components of cellular membranes. For example, fatty acids are one of key components of triacylglycerides, which are primarily used for energy storage. Phosphoglycerides, together with sterols and sphingolipids, represent the major structural components of cellular membranes. Furthermore, lipids contribute to act as insulating material in the subcutaneous tissues. Lipid metabolites are also involved in signaling pathways by acting as second messengers. Thus, it is likely that alteration in lipid metabolism would influence various cellular processes including cell growth, proliferation, differentiation, and survival (Bretscher and Raff, 1975; Divecha and Irvine, 1995; Liscovitch and Cantley, 1994).

Liver is one of the key organs in the regulation of lipid metabolism. In liver, fatty acids are originated from three major sources; (i) absorption from dietary lipid (chylomicrons), (ii) hydrolysis of triglycerides from adipose tissues (lipolysis), and (iii) liver-specific lipases de-esterify triglycerides to release free fatty acids (Lands, 1965; Nguyen et al., 2008). As a central organ for cholesterol metabolism (Schroepfer, 1981), liver synthesizes various lipoproteins involved in transporting cholesterol and other lipid metabolites throughout the body (Schaefer et al., 1978). Thus, lipid metabolism is regulated by energy demands (Figure 1).

Figure 1. Homeostatic regulation of hepatic lipid metabolism. Signals from sites of lipid storage communicate the energy state of the body to the central nervous system, which also receives environmental inputs. The central nervous system integrates these signals and responds to control behavior, energy uptake, storage, and utilization (modified from Ashrafi *et al*, 2007)

Figure 1

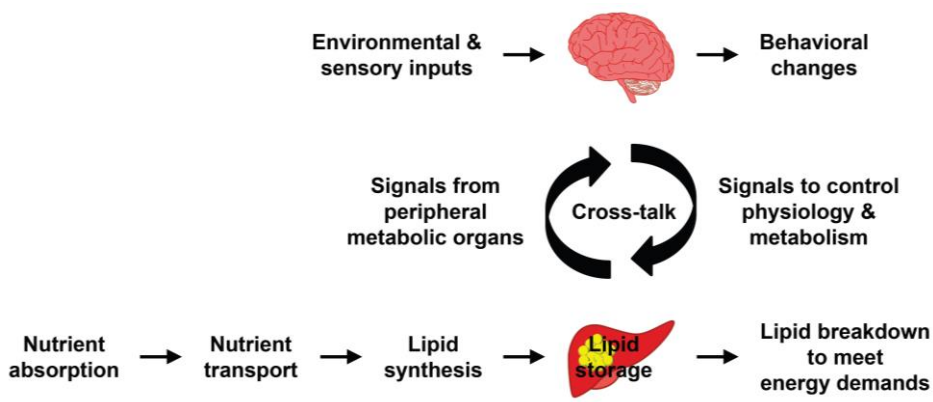
Environmental & sensory inputs
Behavioral changes
Signals from peripheral metabolic organs
Cross-talk
Signals to control physiology & metabolism
Nutrient absorption
Nutrient transport
Lipid synthesis
Lipid storage
Lipid breakdown to meet energy demands

1. *De novo* lipogenesis

Excess energy supply beyond energy needs is converted into storage with various forms of lipid metabolites. Fatty acid synthesis and their further processes into phospholipids and triglycerides are referred as *de novo* lipogenesis. Any metabolite that yields acetyl-CoA is a potential supplier for lipogenesis. *De novo* lipogenesis is a complicated anabolic pathway that is composed of sequential processes. The first step of lipogenic reactions is the transportation of acetyl-CoA across the inner mitochondrial membrane into the cytoplasm and conversion of citrate to acetyl-CoA by ATP-citrate lyase (ACLY). The resulting acetyl-CoA is carboxylated to become malonyl-CoA by acetyl-CoA carboxylase (ACC), which is the key rate-limiting step for synthesis of fatty acid. Malonyl-CoA is further processed to generate long-chain fatty acids by fatty acid synthase (FASN). Following step is the desaturation of long-chain fatty acids catalyzed by stearoyl-CoA desaturase (SCD). For instance, palmitic acid (C16:0) and stearic acid (C18:0) can be unsaturated to their respective monounsaturated forms palmitoleic acid (C16:1) and oleic acid (C18:1), which is catalyzed in endoplasmic reticulum (ER) membrane and provides fatty acids for phospholipid biosynthesis. And further acylation steps are mediated by several enzymes such as glycerol-3-phosphate acyltransferase (GPAT) and diacylglycerol acyltransferase (DGAT) to synthesize triglycerides (Karmen et al., 1963; Pearce, 1983). Further elongation and oxidation can occur in either mitochondrion or ER.

2. Lipolysis and fatty acid oxidation

Liver is also involved in lipid retrieval. The major source of lipids entering

to liver is free fatty acids released from adipose tissue and transported in systemic blood plasma complexed with albumin. Lipolysis is mainly catalyzed in cytosol and further processed in mitochondria. Triglycerides are hydrolyzed by several lipases including adipose tissue lipase (ATGL), hormone sensitive lipase (HSL), and monoacylglycerol lipase (MGL) (Jensen, 1997; Zechner et al., 2005). Hydrolyzed free fatty acids are transported into mitochondria through carnitine-palmitoyl transferase (CPT). In the matrix of mitochondria, fatty acid β-oxidation is the catabolic process in which fatty acid molecules are broken down to generate acetyl-CoA, which enters the tricarboxylic acid (TCA) cycle. TCA cycle generates numerous biochemical energy sources including adenosine triphosphate (ATP), precursors of certain amino acids, and the reducing agent NADH that is used in numerous cellular reactions (Krebs, 1948).

3. Lipid transport

Lipid delivery is a key metabolic process for transportation of lipid metabolites via various lipoproteins in bloodstream. Most metabolic tissues facilitate lipid uptake to utilize lipids as energy sources. In intestine, transposable forms of lipids are converted into lipoprotein particles, which are water-soluble in bloodstream. There are five types of lipoproteins such as chylomicrons, very low-density lipoprotein (VLDL), intermediate-density lipoprotein (IDL), low-density lipoprotein (LDL), and high-density lipoprotein (HDL). Chylomicrons are the largest lipoprotein produced in the intestine. Chylomicrons regulate transport of exogenous lipid metabolites into liver, heart, muscle, and adipose tissues, which is required for lipoprotein lipase (LPL). Both HDL and LDL contain high cholesterol

contents and play a key role in the regulation of cholesterol homeostasis. In contrast, both VLDL and IDL contain high triglyceride contents (Jackson et al., 1976; Karmen et al., 1963). Each lipoprotein has a different subset of surface proteins which bind to corresponding surface receptors in target cells for delivering their contents.

II. Hormonal and nutritional regulation of *de novo* lipogenesis

De novo lipogenesis encompasses the processes of fatty acid synthesis and subsequent triglyceride synthesis, which are active in liver and adipose tissue. Lipogenic flux is tightly controlled by hormonal and nutritional changes (Girard et al., 1994; Kersten, 2001). During postprandial state, glucose increases lipogenesis by stimulating the release of insulin and inhibiting the release of glucagon from the pancreas. Insulin is the most important hormonal factor influencing lipogenesis. Insulin promotes lipogenesis by activating insulin downstream signaling cascades. In contrast, fasting reduces lipogenesis, which is accompanied with an increased rate of lipolysis. Thus, lipolysis eventually leads to net loss of triglycerides. Fasting is associated with significant changes in plasma hormone. For example, fasting decreases plasma insulin, while fasting increases plasma growth hormone and glucagon. Collectively, hormonal and nutritional changes are crucial factors to maintain energy homeostasis by regulating lipid metabolism in liver and adipose tissue.

1. Transcriptional regulation of *de novo* lipogenesis

During fasting-feeding cycle, most enzymes that are involved in *de novo*

lipogenesis are regulated at the transcriptional level. As an anabolic hormone, insulin transcriptionally activates most lipogenic pathway with transcription factors such as sterol regulatory element-binding protein 1c (SREBP1c) and liver X receptors (LXRs) (Farmer, 2006; Wang et al., 2015). In hepatocytes, overexpression of SREBP1c directly activates lipogenic genes such as *FASN*, *ACC*, and *SCD1* even in the absence of insulin, whereas dominant-negative form of SREBP1c counteracts insulin-dependent induction of those genes. It has been well established that SREBP1c plays a critical role to activate lipogenic programming (Foretz et al., 1999; Kim and Spiegelman, 1996). In liver, overexpression of SREBP1c leads to increased hepatic lipid accumulation and insulin resistance (Shimano et al., 1997). In accordance with these, insulin-resistant obese animals with hepatic steatosis express elevated SREBP1c in liver (Ferre and Foufelle, 2010). On the other hand, LXRs are member of nuclear receptor superfamily and are activated by oxysterols. Among two LXR isoforms, LXRα is abundantly expressed in lipogenic tissues such as liver and adipose tissue and it stimulates lipogenic gene expression by upregulating SREBP1c as a target gene (Janowski et al., 1996). *LXRα* deficient mice decreased expression of SREBP1c, FAS, ACC, and SCD1 (Kalaany et al., 2005). In addition, it has been shown that the effect of glucose on the expression of lipogenic genes is modulated by carbohydrate-responsive element-binding protein (ChREBP) (Postic et al., 2007). In hepatocytes, activation of ChREBP in response to glucose results in the import of ChREBP into the nucleus where it binds to carbohydrate responsive elements (ChoREs). Although ChREBP activates a similar subset of genes of SREBP1c, ChREBP does not affect expression of SREBP1c. *ChREBP* deficient mice reduce basal and high-

carbohydrate diet-stimulated hepatic expression of FASN, ACC, and L-PK (Ishii et al., 2004). Thus, these factors coordinately stimulate lipogenic gene expression in response to nutrients and hormones during feeding and fasting cycle (Table 1).

2. Regulation of lipogenesis by hormonal and nutritional changes

During postprandial state, insulin stimulates conversion of excess energy into triglycerides for long-term energy storage (Saltiel and Kahn, 2001). Insulin binds to the insulin receptor (IR) and activates phosphoinositide-3 kinase (PI3K) pathways through activating tyrosine kinase activity of IR. The activation of IR, insulin receptor substrates (IRSs), and PI3K leads to stimulate phosphoinositide-3-dependent protein kinase 1 (PDK1), which in turn phosphorylates the serine/threonine kinase Akt/PKB (Taniguchi et al., 2006). Activated Akt/PKB phosphorylates several factors including mechanistic target of rapamycin (mTOR) and SREBP1c, which directly or indirectly mediate the effects of insulin on certain gene expression such as lipogenic pathways (Porstmann et al., 2008). On the contrary, during fasting state, glucose-producing system is activated in liver to supply glucose into the brain. The systemic adaptation to low glucose state is mediated by catabolic hormones such as glucagon, glucocorticoids, and catecholamine, whereas it is counter-regulated by insulin (Jiang and Zhang, 2003). Glucagon, secreted from pancreatic α-cells under fasting conditions, binds to the membrane receptor coupled to GTP-binding proteins so that it induces intracellular cyclic adenosine monophosphate (cAMP) level, which in turn activates protein kinase A (PKA) pathways (Shabb, 2001). In hepatocytes, PKA phosphorylates SREBP1c and consequently suppresses lipogenic activity (Lu and Shyy, 2006).

Table 1

Table 1. Lipogenic transcription factors and the types of modifications that activate or repress its target genes

Transcription factor	Binding site	Target genes	Activation	Repression
SREBP1c	SRE 5'-TCACNCCAC-3'	*SREBP1c*, *ACC*, *FASN*, *SCD1*, *ACLY*, *GPAT*, *PK*, and *GK*	• P-S117, S63, and T426 by MAPK • Ac-K289 and K309 by p300	• P-S31 and S314 by PKA • P-S372 by AMPK • deAc-K289 and K309 by SIRT1
LXR	LXRE 5'-AGGTCAN$_4$AGGTCA-3'	*SREBP1c*, *LXR*, *ACC*, *FASN*, and *ChREBP*	• *O*-GlcNAcylation or *O*-GlcNAc	• P-S195, S196, S200, and S291 by PKA
ChREBP	ChoRE 5'-CAYGNGN$_5$CNCRTG-3'	*ACC*, *FASN*, *SCD1*, *ACLY*, and *L-PK*	• deP-S196 and T666 by PP2A • Ac-K672 by p300 • *O*-GlcNAcylation or *O*-GlcNAc	• P-S196 and T666 by PKA • P-140 and 196 by PKA • P-586 by AMPK
USF1	E-Box 5'-CANNTG-3'	*SREBP1c*, *ACC*, *FASN*, *SCD1*, *ACLY*, and *GPAT*	• P-S262 by DNA-PK • Ac-K237 by PCAF	• deAc-K237 by HDAC9

Glucocorticoids, which are steroid hormones synthesized in the adrenal cortex, are released as part of acute stress response and mediate many metabolic actions. Similar to glucagon, glucocorticoids have an inhibitory effect of lipogenesis in adipose tissue (Leung and Munck, 1975). In addition, catecholamine is released from adrenal medulla as an adaptive response to emotional and physical stresses such as starvation and exercise. Catecholamine promotes catabolic metabolisms including lipolysis and fatty acid oxidation, whereas it represses anabolic lipid synthesis upon stress (Sharman, 1973). Nonetheless, the factors that are involved in SREBP1c suppression under fasting conditions are poorly understood.

3. Hepatic lipid accumulation and NAFLD

Non-alcoholic fatty liver disease (NAFLD) is associated with excessive lipid accumulation in hepatocytes and is the most common liver disease affecting 10-30% of the general population. NAFLD encompasses a serial spectrum of conditions characterized by hepatic steatosis in individuals without significant alcohol consumption nor viral, congenital, and autoimmune liver disease markers (Cohen et al., 2011). NAFLD is resulted from an imbalance between lipid availability from *de novo* lipogenesis and lipid disposal via fatty acid oxidation or transport (Hebbard and George, 2011). In NAFLD, accumulated extra lipid often causes inflammation and eventually induces scar in liver. Thus, hepatic steatosis can progress to NASH (non-alcoholic steatohepatitis). Subsequently, NAFLD and NASH lead to development of cirrhosis and hepatocellular carcinoma (HCC). Furthermore, NAFLD is related to insulin resistance and metabolic syndromes.

III. Sterol regulatory element-binding proteins (SREBPs)

SREBPs play key roles in lipid homeostasis from yeast to humans (Osborne, 2000). SREBP1c was cloned by the Spiegelman group as an adipocyte determination and differentiation-dependent factor 1 (*ADD1*) (Tontonoz et al., 1993) and was independently cloned by the Brown and Goldstein group as a member of SREBP transcription factor family, which are involved in cholesterol metabolism by binding to the sterol regulatory element in the promoter of LDL receptor (*LDLR*) gene (Wang et al., 1993). Since the members of SREBP family exhibit similar amino acid sequences and structures, they appear to share several molecular regulatory mechanisms to modulate their target genes (Horton et al., 2002).

1. SREBP isoforms

SREBPs belong to the basic helix-loop-helix-leucine zipper (bHLH-LZ) family of transcription factors. In mammals, three SREBP isoforms, including SREBP1a, SREBP1c (also known as ADD1), and SREBP2, are encoded by two genes (Horton et al., 2002). Both SREBP1a and SREBP1c are generated from a single *SREBF1* gene through the use of alternative transcription start sites encoding different first exons that are spliced into a common second exon, designated 1a and 1c, whereas SREBP2 is transcribed from a separate *SREBF2* gene (Shimomura et al., 1997). SREBP1c mainly regulates fatty acid metabolism whereas SREBP2 primarily controls cholesterol metabolism (Eberle et al., 2004b).

Each SREBP precursor is composed of three functional domains; (i) a NH_2-terminal domain that contains acidic transactivation domain and DNA binding domain, (ii) two hydrophobic transmembrane spanning domains interrupted by a

short loop that projects into the lumen of the ER, and (iii) a COOH-terminal domain that recruits regulatory protein complexes (Figure 2). Upon activation, ER anchored SREBP precursor proteins undergo complex proteolytic processes, leading to release the NH_2-terminal active form of SREBPs (Yang et al., 2002). Subsequently, the NH_2-terminal active form of SREBPs is translocated into the nucleus, where it stimulates target gene expression by binding to sterol response elements (SREs) or E-Box (CANNTG) in the promoter/enhancer regions of their own target genes (Amemiya-Kudo et al., 2000). While SREBP1a is highly expressed in most cultured cell lines, SREBP1c is predominantly expressed in metabolic tissues such as liver and adipose tissue (Shimomura et al., 1997). Overexpression of SREBP1c selectively promotes the expression of lipogenic genes, whereas deletion of SREBP1c leads to decrease expression of lipogenic enzymes (Liang et al., 2002). On the other hand, SREBP2 is responsible for cholesterol synthetic genes. Transgenic mice overexpressing SREBP2 shows preferential induction of genes involved in cholesterol biosynthesis (Horton et al., 1998b).

2. Nutritional control of SREBP1c

SREBP1c is selectively regulated by several metabolic cues such as insulin and fasting/refeeding regimes in the liver, adipose tissue, and skeletal muscle (Bizeau et al., 2003; Horton et al., 1998a; Kim et al., 1998). During nutrient-rich conditions, insulin, which is released from pancreatic β-cells, stimulates the expression and activity of SREBP1c, leading to increase in *de novo* lipogenesis. Insulin activates SREBP1c through at least two levels; (i) it increases

Figure 2. Domain structure of SREBP1c. SREBP1c controls lipid metabolism by regulating the expression of enzymes required for fatty acid synthesis. SREBP1c is synthetized as precursor forms bound to the endoplasmic reticulum membranes. Upon activation, the precursor undergoes a sequential two step cleavage process to release the NH_2-terminal active domain in the nucleus.

Figure 2

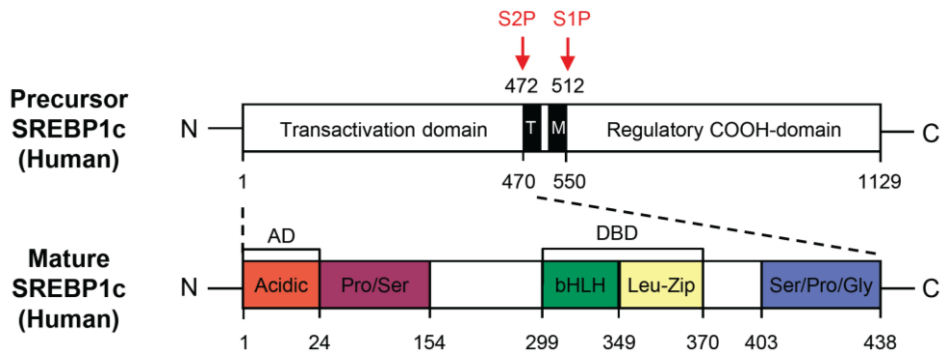
S2P
S1P
472
512
Precursor
SREBP1c
(Human)
N
Transactivation domain
T
M
Regulatory COOH-domain
C
1
470
550
1129
AD
DBD
Mature
SREBP1c
(Human)
N
Acidic
Pro/Ser
bHLH
Leu-Zip
Ser/Pro/Gly
C
1
24
154
299
349
370
403
438

SREBP1c transcription, (ii) it stimulates post-translational modifications including proteolytic cleavage of SREBP1c from an inactive ER membrane-bound precursor to release the NH_2-terminal active form, which is capable of translocating to the nucleus to promote target gene expression. Several studies have demonstrated that inhibition of PI3K by chemical inhibitors or expression of dominant-negative Akt inhibits ER-to-Golgi transport and proteolytic activation of SREBP1c (Du et al., 2006). Since fasting/refeeding responses of lipogenic gene expression are severely blunted in *SREBP1c* deficient mice (Liang et al., 2002), SREBP1c has been considered as a key factor to mediate fatty acid metabolism upon nutritional changes.

Under nutritionally deprived states, the expression of SREBP1c and lipogenic genes is suppressed by glucagon, which is secreted from pancreatic α-cells. Activation of PKA and/or AMP-activated protein kinase (AMPK), results in decrease in SREBP1c expression, eventually leading to downregulate lipogenesis (Foretz et al., 1998; Zhou et al., 2001). Although SREBP1c-mediated lipogenic program is rapidly repressed by nutritional deprivations, it is largely unknown how SREBP1c and lipogenic programming might be shut down upon fasting.

3. Post-translational regulation of SREBP1c

The precursor of SREBP1c is retained in the ER membrane by SREBP cleavage-activating protein (SCAP) and insulin-induced gene (INSIG) proteins (Yang et al., 2002). Under the certain conditions such as depletion of phosphatidylcholine or polyunsaturated fatty acids, SCAP escorts the precursor of SREBP1c from the ER to the Golgi apparatus (Walker et al., 2011). The precursor

of SREBP1c is sequentially cleaved by certain proteases, translocating the mature form of SREBP1c into the nucleus (Sakai et al., 1998; Wang et al., 1994). It has been suggested that Akt and mechanistic target of rapamycin complex 1 (mTORC1) might be involved in SREBP1c processing upon insulin (Bakan and Laplante, 2012). Akt-mediated SREBP1c phosphorylation increases the affinity of SCAP-SREBP1c complex found on COPⅡ-coated vesicles, which accelerates the transport of SREBP1c to the Golgi, where SREBP1c can undergo proteolysis (Yellaturu et al., 2009). Also, mTORC1 and its downstream target kinases such as ribosomal protein S6 kinase β1 (S6K1) modulate SREBP1c processing upon insulin (Owen et al., 2012). In the nucleus, the activity and stability of mature SREBP1c appears to be regulated by several post-translational modifications such as phosphorylation, sumoylation, acetylation, and ubiquitination (Figure 3). For instance, SREBP1c is phosphorylated by glycogen synthase kinase 3 (GSK3), which is inactivated by Akt (Kim et al., 2004). In addition, SREBP1c is phosphorylated and repressed by PKA, resulting in decrease of the transcription of SREBP1c target genes (Lu and Shyy, 2006). SREBP1c is also modulated by the small ubiquitin-related modifier (SUMO)-1 (Hirano et al., 2003; Lee et al., 2014a). Besides, SREBP1c undergoes acetylation and deacetylation processes. SREBP1c is acetylated by p300/CREB-binding protein (CBP) under high glucose and insulin conditions (Naar et al., 1999), whereas SREBP1c is deacetylated by sirtuin 1 (SIRT1). SIRT1-dependent deacetylation of SREBP1c inhibits its binding to its target gene promoters. Accordingly, deacetylation of SREBP1c promotes its ubiquitination and degradation (Ponugoti et al., 2010; Walker et al., 2010).

Figure 3. Post-translational modifications of SREBP1c. Regulation of SREBP1c occurs at the level of SREBP1c expression, proteolytic processing, transcriptional activity, and post-translational modifications. Multiple signals regulate ER-to-Golgi transport and the proteolytic activation of SREBP1c by controlling INSIG. SREBP1c is rapidly modulated by post-translational modifications, including phosphorylation, sumoylation, acetylation, and ubiquitination.

Figure 3

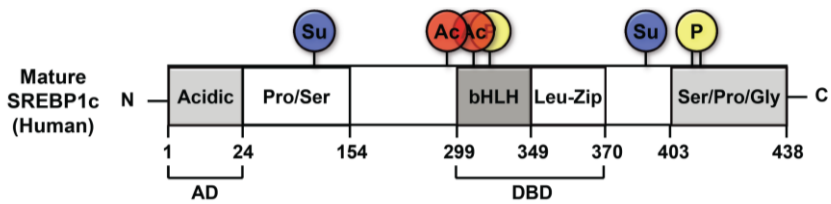

PTM	Mediator	Signal cue	Site of SREBP	Function	Ref
Acetylation	CBP/p300	Co-activator	hSREBP1a (K-324 / 333) hSREBP1c (K-289 / 309)	Stabilized by prevent Ub	Nature (1999) MCB (2003)
De-acetylation	SIRT1	Fasting	hSREBP1a (K-324 / 333) hSREBP1c (K-289 / 309)	De-stabilized by promote Ub	G&D (2010) JBC (2010)
Phosphorylation	GSK-3β	DNA-binding	hSREBP1a (T-426, S-430) hSREBP2 (S-433)	Fbw7 recruitment → Ub ↑	JBC (2004) Cell Meta (2005)
	Growth hormone	-	hSREBP1a (S-117) hSREBP2 (S-432 / 455)	Inhibit Sumo → Trx ↑	JBC (2008) Atheros (2010)
	AMPK	S17834	hSREBP1c (S-372) hSREBP2 (?)	Decrease processing → Trx ↓	Cell Meta (2011)
	PKA	Fasting	hSREBP1a (S-338) hSERBP1c (S-314)	Insulin effect ↓ DNA-binding ↓	BBRC (2005) AJP (2006)
			hSERBP1c (S-314)	Promote Sumo → Ub ↑ RNF20 ↑ → Ub ↑	MCB (2014) Hepa (2014)
	SIK	-	mSREBP1c (S-265/266) mSREBP1c (S-329)	Trx ↓	JBC (2009)
Sumoylation	-	-	hSREBP1a (K-123 / 418) hSREBP2 (K-464)	Trx ↓	JBC (2003)
	PKA	Fasting	hSREBP1c (K-153) rSREBP1c (K-98)	De-stabilized by promote Ub	MCB (2014)

Together, it has been proposed that various post-translational modifications of SREBP1c appear to affect lipid metabolism upon nutritional and hormonal changes.

IV. Lipid metabolism in cancer

Cancer cells differ from normal cells in many aspects that allow them to abnormal cell growth and become invasive. Cancer cells undergo a complex metabolic reprogramming characterized by changes in anaerobic glycolysis and lipid synthetic processes (DeBerardinis et al., 2008; Schulze and Harris, 2012). The relevance of metabolic rearrangement of cancer cells has been included in the updated version of the review "Hallmarks of Cancer" where dysregulation of energy metabolism is included as one of emerging hallmarks (Hanahan and Weinberg, 2000, 2011). Tumorigenesis is dependent on the metabolic reprogramming as both direct and indirect consequences of oncogenic signaling (DeBerardinis et al., 2008). Cancer cells need to generate large amounts of precursors for macromolecule biosynthesis to allow the accumulation of cellular building blocks during cell growth and proliferation. Most cancer cells utilize aerobic glycolysis to support the production of intermediates for the synthesis of lipids, proteins and nucleic acids (Vander Heiden et al., 2009). In addition, cancer cells have increased glutamine uptake and glutaminolysis, which replenish intermediates of the TCA cycle that are redirected into biosynthetic reactions; a process known as anaplerosis (Hensley et al., 2013). The alterations in intracellular and extracellular metabolites that can accompany cancer-associated metabolic reprogramming have profound effects on gene expression, cellular differentiation, and the tumor microenvironment (Hsu and Sabatini, 2008).

1. Aberrant lipogenesis in cancer

During tumorigenesis, lipids contribute to several aspects including tumor growth, energy and redox homeostasis, and metastasis. Certain cancer cells often show an increased *de novo* lipogenesis (Menendez and Lupu, 2007). Fatty acids are the major building blocks for the synthesis of phospholipids and triglycerides, which are mainly used for membrane biogenesis and energy storage, respectively (Bretscher and Raff, 1975; Divecha and Irvine, 1995). In cancer cells, most lipid metabolites are derived from *de novo* lipogenesis rather than from extracellular lipid uptake (Medes et al., 1953). Thus, increased lipogenesis provides the majority of lipids required for rapid proliferation of cancer cells. It has been reported that the shift from lipid uptake to *de novo* lipogenesis in cancer cells leads to increased membrane lipid saturation, resulting in higher levels of saturated and monounsaturated phospholipids, potentially protecting cancer cells from oxidative damage by reducing lipid peroxidation (Santos and Schulze, 2012). In addition, lipids are important signaling molecules in tumorigenesis (Spiegel et al., 1996). Some lipid metabolites are parts of paracrine hormones and growth factors, including prostaglandins, lyophosphatidic acid (LPA) or steroid hormones. Many studies have demonstrated that inhibition of several lipogenic enzymes such as FASN, ACC, and SCD1 can repress cancer cell growth (Currie et al., 2013). Although aberrant lipogenesis likely contributes to tumorigenesis in cancers, it has been poorly elucidated which factors are linked to lipid metabolism for tumorigenesis.

2. Hyperactivation of SREBP1c in metabolic disease and cancers

It has been suggested that SREBP1c would be closely associated with type 2 diabetes, insulin resistance, and pathogenesis of metabolic diseases (Shao and Espenshade, 2012). Accordingly, sequence variations at *SREBF1* locus are linked to type 2 diabetes and increased expression of SREBP1c with genetic polymorphisms is associated with metabolic syndromes including cardiovascular diseases (Eberle et al., 2004a). Furthermore, hepatic SREBP1c is elevated in several animal models with insulin resistance and NAFLD (Marchesini et al., 2001; Muoio and Newgard, 2006). In addition, it has been reported that SREBP1c and its target genes are enhanced in certain cancers (Griffiths et al., 2013; Guo et al., 2014) and that SREBP1c promotes proliferation, migration, and invasion in glioblastoma and prostate cancers (Guo et al., 2009; Huang et al., 2012). On the other hand, it has been shown that inhibition of SREBP1c attenuates tumor growth in glioblastoma xenografts and that SREBP1c is defined a gene signature associated with poor survival in glioblastoma (Guo et al., 2009). Together, these findings imply that SREBP1c may play an important function in tumorigenesis, accompanied with lipid metabolism.

V. Purpose of this study

SREBP1c is tightly controlled by nutritional and hormonal changes to maintain whole-body energy homeostasis. To date, most studies have focused on the lipogenic roles of SREBP1c by coupling insulin action in metabolic organs. During postprandial states, insulin promotes SREBP1c activity to upregulate lipogenic programing. Conversely, hepatic SREBP1c is rapidly suppressed by

fasting signals to prevent futile lipogenic pathways. However, the molecular mechanisms that control SREBP1c turnover in response to nutritional deprivation are not thoroughly elucidated (Figure 4). Both animal models and human subjects with metabolic complications such as obesity, NAFLD, and certain cancers constitutively exhibit elevated SREBP1c. Thus, the elucidation of molecular mechanisms by which SREBP1c and lipogenic activity might be downregulated upon physiological cues appears to be important. Excess lipid accumulation is one of the hallmarks in clear cell renal cell carcinoma (ccRCC), the most common subtype of kidney cancers. To date, it has not been thoroughly understood the relationship between lipid metabolism and tumorigenesis in ccRCC.

In this study, I have elucidated two novel findings for SREBP1c; (i) the suppression of SREBP1c during fasting and (ii) upregulation of SREBP1c in ccRCC. In the chapter one, to reveal which factors are involved in the inactivation of SREBP1c, I attempted to identify SREBP1c-interacting proteins by mass spectrometry analysis. I have identified that ring finger protein 20 (RNF20) is a novel E3 ubiquitin ligase for SREBP1c. Also, I have shown that RNF20-induced SREBP1c degradation downregulates hepatic lipid metabolism upon PKA activation. In the chapter two, I demonstrated that downregulation of RNF20 stimulates tumorigenesis through SREBP1c activation in ccRCC. Moreover, in cultured ccRCC cells and xenograft models, RNF20 overexpression repressed lipogenesis and cell proliferation by inhibiting SREBP1c. To further explore which factors might be involved in SREBP1c-induced cell cycle progression in ccRCC, I tried to identify novel SREBP1c target genes, particularly, involving in cell cycle regulation. I discovered that pituitary tumor-transforming gene 1 (PTTG1) is a

Figure 4. The unsolved question on the molecular mechanisms of SREBP1c suppression upon fasting. SREBP1c is a key transcription factor for *de novo* lipogenesis during the postprandial state. During nutritional deprivation, SREBP1c is rapidly suppressed by fasting signals to turn off lipogenic program. However, the molecular mechanisms that control SREBP1c activity in response to fasting status are not thoroughly understood.

Figure 4

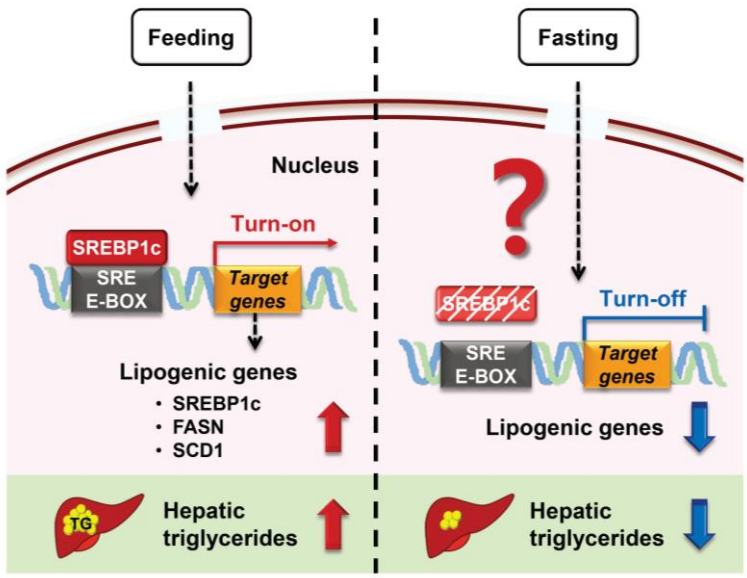
Feeding
Fasting
Nucleus
Turn-on
SREBP1c
SRE
E-BOX
Target
genes
Lipogenic genes
• SREBP1c
• FASN
• SCD1
TG
Hepatic
triglycerides
SREBP1c
Turn-off
SRE
E-BOX
Target
genes
Lipogenic genes
Hepatic
triglycerides

novel target gene of SREBP1c and plays a crucial role in cell cycle control in ccRCC. Therefore, I would like to propose the idea that RNF20 would act as a tumor suppressor gene through inhibiting SREBP1c which modulates not only lipid metabolism but also cell cycle progression in ccRCC.

CHAPTER ONE:

Ring finger protein 20 regulates hepatic lipid metabolism through protein kinase A-dependent sterol regulatory element-binding protein 1c degradation

Abstract

SREBP1c is a key transcription factor for *de novo* lipogenesis during the postprandial state. During nutritional deprivations, hepatic SREBP1c is rapidly suppressed by fasting signals to prevent lipogenic pathways. However, the molecular mechanisms that control SREBP1c turnover in response to fasting status are not thoroughly understood. To elucidate which factors are involved in the inactivation of SREBP1c, I attempted to identify SREBP1c-interacting proteins by mass spectrometry analysis. As a result, RNF20 was identified as a novel E3 ubiquitin ligase for SREBP1c. In this work, I reveal that RNF20 physically interacts with SREBP1c, leading to degradation of SREBP1c via ubiquitination. In accordance with these findings, RNF20 represses the transcriptional activity of SREBP1c and turns off the expression of lipogenic genes that are targets of SREBP1c. In contrast, knockdown of RNF20 stimulates the expression of SREBP1c and induces lipogenic activity in primary hepatocytes. Furthermore, activation of PKA with glucagon or forskolin enhances the expression of RNF20 and potentiates the ubiquitination of SREBP1c via RNF20. In wild-type and *db*/*db* mice, adenoviral overexpression of RNF20 markedly suppresses FASN promoter activity and reduces the level of hepatic triglycerides, accompanied by a decrease in the hepatic lipogenic program. Taken together, these data suggest that RNF20 acts as a negative regulator of hepatic fatty acid metabolism through degradation of SREBP1c upon PKA activation. Knowledge regarding this process enhances understanding of how SREBP1c is able to turn off hepatic lipid metabolism during nutritional deprivation.

Introduction

Sterol regulatory element-binding proteins (SREBPs) play key roles in lipid homeostasis from yeast to humans (Osborne, 2000; Tontonoz et al., 1993). In mammals, three different SREBP isoforms, including SREBP1a, SREBP1c (also known as ADD1), and SREBP2, are encoded by two genes: *SREBF1* and *SREBF2*. SREBP1 regulates fatty acid metabolism, whereas SREBP2 controls cholesterol metabolism (Horton et al., 2002). When the cellular sterol level is low, SREBP cleavage-activating protein (SCAP) escorts the SREBP precursors from the endoplasmic reticulum (ER) to the Golgi, where SREBPs are cleaved by Site-1 and Site-2 proteases (Yang et al., 2002). Subsequently, the mature forms of SREBPs are translocated into the nucleus and stimulate the expression of target genes (Briggs et al., 1993; Wang et al., 1993). SREBP1a and SREBP1c are generated through transcription from alternative promoters and splicing from a single *SREBF1* gene.

In metabolic tissues such as adipose tissue and liver, SREBP1c is the predominant isoform of SREBP1 (Shimomura et al., 1997; Tontonoz et al., 1993). SREBP1c governs *de novo* lipogenesis by stimulating its target genes, including fatty acid synthase (*FASN*), acetyl-CoA carboxylase1 (*ACC1*), stearoyl-CoA desaturase1 (*SCD1*), and long-chain fatty acid elongase (*ELOVL6*) (Eberle et al., 2004b; Kim and Spiegelman, 1996; Kumadaki et al., 2008). Furthermore, SREBP1c is sensitively regulated by nutritional and hormonal changes to achieve energy balance. For example, SREBP1c is suppressed by fasting, whereas SREBP1c is activated by feeding in adipose tissue and liver (Horton et al., 1998a; Kim et al., 1998). In parallel, the expression of most lipogenic genes, including *FASN*, *ACC1*, and *SCD1*, is also modulated in a fashion analogous to that of

nutritionally regulated SREBP1c (Foufelle et al., 1994; Girard et al., 1994; Kim et al., 1998). Accordingly, it has been reported that various hormones, such as insulin, glucagon, and adrenaline, participate in the regulation of SREBP1c and its target lipogenic genes (Foretz et al., 1999; Zhang et al., 2003). Insulin, a key postprandial hormone, stimulates the expression and activity of SREBP1c to accommodate anabolic processes, such as fatty acid synthesis, upon feeding (Flier and Hollenberg, 1999; Kim et al., 1998). In contrast, glucagon, a key catabolic hormone, suppresses the activity of SREBP1c in fasting states, leading to a decrease in lipogenesis (Lu and Shyy, 2006).

In the nucleus, mature SREBPs are very unstable and are rapidly degraded by the proteasome (Hirano et al., 2003; Hirano et al., 2001). Previous reports have shown that SREBP1 is phosphorylated by glycogen synthase kinase-3 beta (GSK-3β), which leads to F-box- and WD repeat domain-containing 7 (FBXW7)-dependent ubiquitination of SREBP1 (Punga et al., 2006; Sundqvist et al., 2005). However, a recent *in vivo* study revealed that inhibition of FBXW7 does not alter the expression of SREBP1c or lipogenic genes in the liver (Kumadaki et al., 2011).

Although SREBP1c-mediated lipogenic program in liver is rapidly repressed by nutritional deprivations, the factors that are involved in the suppression of SREBP1c activity during fasting have not been thoroughly characterized. In this study, I demonstrate that ring finger protein 20 (RNF20) promotes polyubiquitination and degradation of SREBP1c. Overexpression of RNF20 represses SREBP1c activity, leading to a decrease in the expression of lipogenic genes. In obese *db*/*db* mice, RNF20 overexpression alleviates hepatic steatosis by reducing the lipogenic program via SREBP1c downregulation.

Furthermore, activated protein kinase A (PKA), a major signaling cascade that mediates the fasting state, induces degradation of SREBP1c by increasing RNF20 expression. Taken together, these data suggest that RNF20 plays a critical role in the regulation of hepatic lipid metabolism by modulating the protein stability and transcriptional activity of SREBP1c during hormonal changes.

Materials and Methods

Cell culture and reagents

HEK293T, COS-1, and H4IIE cells were maintained in Dulbecco's modified Eagle's medium (DMEM) supplemented with 10% fetal bovine serum (FBS, Gibco/BRL) and cultured at 37℃ in a 5% CO_2 incubator. Cycloheximide (CHX), H-89, insulin, T0901317 were purchased from Sigma-Aldrich (St. Louis, MO, USA). Forskolin and MG132 were purchased from Calbiochem (San Diego, CA, USA).

Plasmids and recombinant adenoviruses

The nuclear form of SREBP1c, encoding amino acids 1–403 of rat SREBP1c, was cloned into the pcDNA3.1-Myc A plasmid (Invitrogen, Carlsbad, CA) and p3×FLAG-CMV-10 vector (Sigma-Aldrich). The full-length RNF20 cDNA was cloned into the pcDNA3.1-Myc A and p3×FLAG-CMV-10 vectors. A small interfering RNA duplex for RNF20 was generated by GenePharma (Shanghai, China), and its target sequence was as follows: forward 5'-GGAGAGAGAACGAGAGAAA (dTdT)-3'. The FASN-luciferase plasmid containing a –220 to +25 bp fragment of the FASN promoter ahead of a luciferase reporter gene was described previously (Kim et al., 1998). An RNF20-expressing adenovirus was generated through homologous recombination between a linearized transfer vector, pAd-Track, and the adenoviral vector pAd-Easy, as previously described (He et al., 1998). Ad-RNF20 contained the full-length murine RNF20 cDNA with a C-terminal Myc-tag. An adenovirus encoding GFP only (Ad-Mock) was used as a control in all experiments. I produced adenoviruses in HEK293A

cells and purified them by CsCl gradient centrifugation, as described previously (Becker et al., 1994). Ad-FASN luc was generated based on FASN (–150/–43) luciferase as described (Dentin et al., 2007; Magana et al., 2000).

Primary hepatocyte culture and infection with adenovirus

Eight-week-old C57BL/6 male mice from Samtako (South Korea) were used for isolation of primary hepatocytes. After the animals were anesthetized, primary hepatocytes were isolated as previously described (Berry and Friend, 1969). Briefly, total liver tissues were perfused with HBSS buffer (50 mM HEPES [pH 7.4], 5.5 mM glucose, 138 mM NaCl, 5.4 mM KCl, 4.17 mM $NaHCO_3$, 0.34 mM Na_2HPO_4 [dibasic], and 0.44 mM KH_2PO_4) into the portal vein. After perfusion, the liver tissues were dissociated into hepatocytes using collagenase buffer (HBSS buffer supplemented with 0.25% type IV collagenase (Sigma-Aldrich) and 5 mM $CaCl_2$). Subsequently, the isolated hepatocytes were washed with serum-free M199 medium (HyClone, South Logan, USA) and suspended in M199 medium supplemented with 10% FBS, 100 units/mL penicillin, and 100 mg/mL streptomycin. Cell viability was assessed by the trypan blue exclusion test. Isolated hepatocytes were seeded at a density of 2.5×10^6 cells/dish in 100-mm tissue culture dishes and maintained at 37℃ in 5% CO_2. After cell attachment (approximately 4 hours), the culture media were replaced with fresh media. For adenoviral infections, hepatocytes were cultured for approximately 16 hours after cell attachment and subsequently incubated for 5 hours at 37℃ in serum-free M199 either with or without adenovirus. Then, the culture media were replaced with fresh media, and the cells were incubated for 24 hours.

Flag affinity purification of the SREBP1c complex

Adenoviruses encoding green fluorescent protein (GFP) or Flag-SREBP1c, which contains the transcriptionally active fragment of rat SREBP1c (amino acids 1–403) fused with a Flag-tag, were used to infect primary hepatocytes. The infected hepatocytes were then gently washed with ice-cold phosphate-buffered saline (PBS) and lysed in hypotonic buffer (20 mM HEPES [pH 7.9], 1 mM EDTA, 1 mM EGTA, 1 mM DTT, 0.5 mM PMSF, 0.2% Nonidet P-40 (NP-40), and protease inhibitor cocktail (Roche, Rotkreuz, Switzerland)). After incubation in hypotonic buffer for 10 minutes, the homogenates were centrifuged at 8,000 rpm for 1 minute at 4℃, and the supernatants (cytosolic fraction) were transferred to a fresh tube. The pellet was homogenized in ice-cold high salt buffer (10 mM HEPES [pH 7.9], 420 mM NaCl, 20% glycerol, 1 mM EDTA, 1 mM EGTA, 1 mM DTT, 0.5 mM PMSF, and protease inhibitor cocktail) on a rotating shaker for 30 minutes at 4℃ and subsequently centrifuged at 12,000 rpm for 15 minutes at 4℃. Consequently, the supernatants (nuclear fraction) were incubated with anti-Flag M2-agarose affinity gel (Sigma-Aldrich) for 2 hours at 4℃ on a rotating shaker. The beads were then rinsed four times for 10 minutes each in washing buffer (20 mM HEPES [pH 7.9], 150 mM NaCl, 0.5 mM EDTA, 0.5 mM PMSF, 1% Triton X-100, and protease inhibitor cocktail), followed by elution with sodium dodecyl sulfate (SDS) buffer (250 mM Tris-HCl [pH 6.6], 10% SDS, 50% glycerol, 500 mM DTT, and 0.5% bromophenol blue). The eluates were then subjected to mass spectrometry.

GST pull-down assay

GST pull-down assays were performed as previously described (Lee et al., 2003). Briefly, GST and GST-SREBP1c recombinant proteins were bound to glutathione beads and incubated with ^{35}S-Met-labeled RNF20 protein. The beads were washed with Tris-buffered saline containing 0.1% Tween-20 (TBST, 25 mM Tris-HCl [pH 8.0], 137 mM NaCl, 2.7 mM KCl, and 0.1% Tween-20) and analyzed by autoradiography after SDS-PAGE.

Western blot analysis

The cells were lysed on ice with modified radioimmunoprecipitation assay (RIPA) buffer (50 mM Tris-HCl [pH 7.4], 150 mM NaCl, 1 mM EDTA, 1 mM PMSF, 1% NP-40, 0.25% Na-deoxycholate, and protease inhibitor cocktail) and subjected to immunoprecipitation or western blotting analyses. For immunoprecipitation, equal amounts of the total cell extracts were incubated with Myc or Flag antibody, and the immunoprecipitated complexes were collected using protein A-sepharose beads (GE Healthcare, UK). Further, the pellets were washed extensively and subjected to western blotting analyses according to previously described protocols (Kim et al., 2009). The following antibodies were used in the western blotting analyses: RNF20 (Abcam, MA; #ab32629; 1:1,000), FASN (Cell Signaling, MA; #3180; 1:1,000), GAPDH (AbFrontier, South Korea; #LF-PA0018; 1:1,000), Pol II (Santa Cruz Biotechnology, CA; #SC-5943; 1:1,000), Lamin B1 (Abcam; #ab16048; 1:1,000), β-actin (Sigma-Aldrich; #A5316; 1:2,000), Flag-tag (Sigma-Aldrich; #F1804; 1:1,000), Myc-tag (Cell Signaling; #2276; 1:1,000) and HA-tag (Covance Research, PA; #16B12; 1:1,000). SREBP1 antibodies were

produced by AbFrontier using the nuclear form of recombinant SREBP1 as an immunogen. Relative amounts of each protein were calculated using ImageJ software.

Cell-based ubiquitination assay

COS-1 cells were transfected with plasmids encoding Myc-SREBP1c, Flag-RNF20 and HA-ubiquitin in the presence or absence of forskolin (20 μM). After transfection for 36 hours, the cells were incubated with MG132 (10 μM) for 12 hours and lysed with cold RIPA buffer. Equal amounts of total cell lysates were incubated with the Myc antibodies for 2 hours at 4℃. Immunocomplexes were collected using protein-A sepharose beads for 1 hour at 4℃. Further, the immunoprecipitates were washed with RIPA buffer and subjected to SDS-PAGE followed by western blotting analyses with anti-HA antibodies.

Transient transfection and luciferase assay

HEK293T cells were transiently transfected with several DNA constructs according to the calcium-phosphate method described previously (Seo et al., 2004a). After incubation for 24 hours, transfected cells were harvested and assayed for luciferase and β-galactosidase activity. Total cell extracts were prepared with lysis buffer (25 mM Tris-phosphate [pH 7.8], 10% glycerol, 2 mM CDTA, 2 mM DTT, and 1% Triton X-100), and the activities of luciferase and β-galactosidase were measured according to the manufacturer's instructions (Promega). The relative luciferase activity was normalized to β-galactosidase activity in each sample. Transfections of SREBP1c, RNF20 and the siRNA duplex for RNF20 into

COS-1 and mouse primary hepatocytes were carried out with Lipofectamine2000^{TM} reagent (Invitrogen) according to the manufacturer's instructions.

Immunocytochemistry

Flag-tagged nuclear SREBP1c and Myc-tagged RNF20 plasmids were co-transfected into HeLa cells cultured in a 6-well plate. After transfection for 24 hours, the cells were rinsed with PBS and fixed in 4% paraformaldehyde for 10 minutes. The fixed cells were incubated with 0.5% Triton X-100-PBS for 5 minutes and 3% bovine serum albumin (BSA)-PBS for 1 hour. The cells were then incubated with anti-Flag (Sigma-Aldrich; #F1804; 1:200) and anti-Myc (Cell Signaling; #2276; 1:200) antibodies at 4℃ overnight followed by incubation with fluorophore-conjugated secondary antibodies (1:200) for 1 hour in the dark at room temperature. All images were recorded and processed under equivalent conditions.

Oil Red O staining

To assess intracellular lipid accumulation, hepatocytes were fixed with 10% formaldehyde (Merck, Germany) in PBS and stained with Oil Red O as described previously (Kim et al., 2010). Mouse primary hepatocytes were transfected with siRNA targeted against RNF20 in M199 medium. After 48 hours, the transfected cells were washed twice with PBS, fixed for 1 hour with 3.7% formaldehyde in PBS and subsequently dehydrated with 100% propylene glycol (AMRESCO, USA) for 5 minutes. After removing the propylene glycol, Oil Red O dye was added to the plate and incubated overnight. Subsequently, Oil Red O was removed, and 85%

propylene glycol was added to the plate, which was allowed to stand for 5 minutes. Finally, excess dye was washed away with distilled water until the background was clear. To detect hepatic lipid contents in liver section, OCT compound-embedded, snap-frozen liver tissues were fixed and stained with Oil Red O. Images were obtained using an EVOS® ORIGINAL microscope (Advanced Microscopy Group) and a Nikon TMS inverted microscope.

RNA isolation and quantitative RT-PCR

Cell As described previously (Jeong et al., 2010), total RNA was isolated with TRIzol reagent (Molecular Research Center, OH, USA), and cDNA was synthesized with M-MuLV reverse transcriptase (Fermentas, MD, USA). qRT-PCR analyses were performed with the MyiQ quantitative real-time PCR detection system (Bio-Rad Laboratories, CA, USA) using SYBR Green I (BioWhittaker Molecular Applications). The relative levels of each mRNA were normalized to the levels of TBP, GAPDH, or cyclophilin mRNA. The qRT-PCR primers used in this study were synthesized by Bioneer, and the primer sequences are listed in Table 2.

Animals

All animal experiments were approved by the Seoul National University Animal Experiment Ethics Committee. Male C57BL/6 mice were obtained from Samtako (South Korea), and *db*/*db* mice were obtained from Central Lab (South Korea). The animals were housed in colony cages in 12 hours light/12 hours dark cycles. Standard chow (Purina Mills) was given *ad libitum*.

Table 2. Primers sequences for qRT-PCR

Species	Gene	Sequence (5' to 3')	Direction
Mouse	RNF20	TGCAGATGACCTCAAAGCAC	Forward
		TCATCACACTTGGGCACATT	Reverse
	FASN	GCCTACACCCAGAGCTACCG	Forward
		GCCATGGTACTTGGCCTTG	Reverse
	SCD1	CCGGAGACCCCTTAGATCGA	Forward
		TAGCCTGTAAAGATTTCTGCAAACC	Reverse
	ELOVL6	TGCCATGTTCATCACCTTGT	Forward
		TACTCAGCCTTCGTGGCTTT	Reverse
	SREBP1a	GGCCGAGATGTGCGAACT	Forward
		TTGTTGATGAGCTGGAGCATGT	Reverse
	SREBP2	GCGTTCTGGAGACCATGGA	Forward
		ACAAAGTTGCTCTGAAAACAAATCA	Reverse
	HMGCR	CTTGTGGAATGCCTTGTGATTG	Forward
		AGCCGAAGCAGCACATGAT	Reverse
	SQS	CCAACTCAATGGGTCTGTTCCT	Forward
		TGGCTTAGCAAAGTCTTCCAACT	Reverse
	LDLR	AGGCTGTGGGCTCCATAGG	Forward
		TGCGGTCCAGGGTCATCT	Reverse
	PPARγ	TCACAAGAGCTGACCCAATGG	Forward
		GGCTCTACTTGATCGACTTTG	Reverse
	LXRα	GGAGGCAACACTTGCATCCT	Forward
		AGGGCTGTAGGCTCTGCTGA	Reverse
	ChREBP	GCATCCTCATCCGACCTTTA	Forward
		GATGCTTGTGGAAGTGCTGA	Reverse
	FBXW7	CCATGTTCAGCAACACCAAC	Forward
		TGGAACTGGGGCTCTATCAC	Reverse
	G6Pase	ACACCGACTACTACAGCAACAG	Forward
		CCTCGAAAGATAGCAAGAGTAG	Reverse
	GAPDH	TTCACCACCATGGAGAAGG	Forward
		CTAAGCAGTTGGTGGTGCAG	Reverse
	TBP	GGGAGAATCATGGACCAGAA	Forward
		CCGTAAGGCATCATTGGACT	Reverse
Mouse	SREBP1c	GGAGCCATGGATTGCACATT	Forward
		CAGGAAGGCTTCCAGAGAGG	Reverse
Rat	RNF20	GCATCACACCATGTCTCAGG	Forward
		CACCCGCTCTAGGACTTCAG	Reverse

In vivo imaging system

Ten-week-old C57BL/6 mice and nine-week-old *db*/*db* mice were injected through the tail vein with adenoviruses encoding GFP (Ad-Mock), RNF20 (Ad-RNF20) and FASN luciferase (Ad-FASN-luc). After 7 days, adenovirus-infected mice were injected intraperitoneally with 100 mg/kg sterile D-luciferin. The mice were then anaesthetized with Zoletil® and imaged using the IVIS™ 100 Imaging System (Xenogen) as described previously (Dentin et al., 2007).

Oral glucose tolerance test

For the oral glucose tolerance test, *db*/*db* mice were fasted for 12 hours and basal blood samples were taken, followed by oral glucose administration (1.5 g/kg of body weight). Blood samples were drawn at 15, 30, 45, 60, and 90 minutes after administration.

Hepatic triglyceride analysis

Hepatic triglycerides were measured in cell lysates using a colorimetric assay and expressed as μg of lipid per mg of cellular protein as described previously (Jo et al., 2013). In brief, liver tissue samples were homogenized in 5% Triton X-100, and total tissue extracts were incubated in a water bath at 80℃ and subsequently cooled down to room temperature twice. After centrifugation at 12,000 rpm for 5 minutes at room temperature, the supernatant was collected and used in triglyceride assays. Measurement of hepatic triglycerides was performed using the Infinity™ triglycerides reagent (Thermo Scientific).

Statistical analysis

All observed data are presented as the mean ± standard deviation (SD). Error bars represent SD, and *P* values were calculated by Student's *t* test. The SD values were considered statistically significant at $*P < 0.05$ and $**P < 0.01$.

Results

SREBP1c is decreased by ubiquitination upon PKA activation.

Ectopic SREBP1c is tightly regulated by hormonal and nutritional changes to reflect the energy status (Foretz et al., 1999; Zhang et al., 2003). When I examined the protein stability of SREBP1c in the presence of cycloheximide, an inhibitor of protein synthesis, the degradation rate of nuclear SREBP1c was reduced in the presence of MG132, an inhibitor of the 26S proteasome (Figures 5A and 5B), indicating that the rapid turnover of SREBP1c protein might be mediated by proteasomal degradation. Although it has been demonstrated that the cAMP/PKA pathway is involved in the suppression of SREBP1c (Lu and Shyy, 2006; Yamamoto et al., 2007; Yellaturu et al., 2005), it is largely unknown how PKA affects SREBP1c protein stability. To address this issue, primary hepatocytes were treated with forskolin, an activator of the PKA cascade. The level of SREBP1 protein was reduced by forskolin (Figures 5C and 5D), while that of SREBP1 protein was restored by MG132 in a dose-dependent manner (Figures 6A and 6B), implying that PKA would be involved in the regulation of SREBP1c protein stability through the ubiquitin-proteasome system. Next, to investigate whether SREBP1c is indeed ubiquitinated by PKA activation, cell-based ubiquitination assays were carried out. As shown in Figure 6C, forskolin efficiently polyubiquitinated the SREBP1c protein, while H-89, the inhibitor of PKA, greatly attenuated forskolin-induced SREBP1c ubiquitination. Therefore, these data suggest that SREBP1c is degraded by ubiquitination upon PKA activation.

Figure 5. PKA activation decreases SREBP1c protein stability. (A) Mouse primary hepatocytes were treated with cycloheximide (20 μM) for the indicated periods with or without MG132 (20 μM) treatment for 3 hours. After the preparation of nuclear extracts, western blotting analyses were performed with the indicated antibodies. DMSO, dimethyl sulfoxide; CHX, cycloheximide; nSREBP1, nuclear SREBP1. **(B)** Quantification of the amounts of nSREBP1 protein in the presence of MG132 in Figure 5A. Relative level of nSREBP1 protein was calculated by ImageJ software and normalized with Pol II using nonlinear regression curve fit™ program (GraphPad Prism). The level of nSREBP1 protein at time zero in each condition was normalized to 100%. **(C)** Mouse primary hepatocytes were treated with forskolin (50 μM) for 6 hours and harvested at the indicated time points after cycloheximide (50 μM) treatment. After isolating nuclear extracts, western blotting analyses were performed with the indicated antibodies. **(D)** Quantification of the amounts of nSREBP1 protein in the presence of forskolin in Figure 5C. Relative level of nSREBP1 protein was calculated by ImageJ software and normalized with Lamin B1 using nonlinear regression curve fit™ program (GraphPad Prism). The level of nSREBP1 protein at time zero in each condition was normalized to 100%.

Figure 5

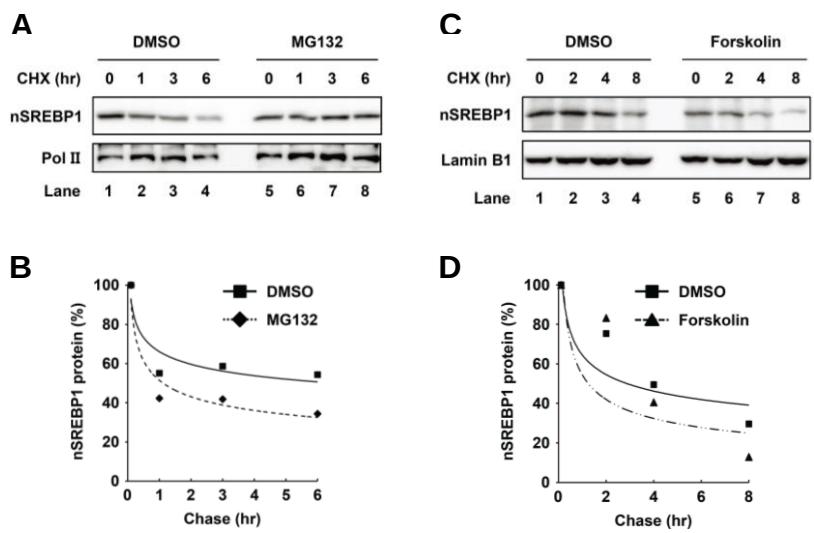
A
DMSO
MG132
CHX (hr) 0 1 3 6 0 1 3 6
nSREBP1
Pol II
Lane 1 2 3 4 5 6 7 8
C
DMSO
Forskolin
CHX (hr) 0 2 4 8 0 2 4 8
nSREBP1
Lamin B1
Lane 1 2 3 4 5 6 7 8
B
nSREBP1 protein (%)
DMSO
MG132
Chase (hr)
D
nSREBP1 protein (%)
DMSO
Forskolin
Chase (hr)

Figure 6. SREBP1c is decreased by ubiquitination upon PKA activation. **(A)** Mouse primary hepatocytes were treated with or without forskolin (50 μM) in the presence of MG132 with indicated dose for 4 hours. Nuclear extracts were isolated and analyzed by western blotting analyses with the indicated antibodies. **(B)** Quantification of the amounts of nSREBP1 protein in Figure 6A. Relative level of nSREBP1 protein was calculated by ImageJ software and normalized with Lamin B1. The level of nSREBP1 protein without MG132 and forskolin was normalized to 100%. **(C)** COS-1 cells were co-transfected with plasmids encoding Myc-SREBP1c and HA-ubiquitin. After transfection, the cells were treated with MG132 (10 μM) for 12 hours and subsequently pretreated with H-89 (20 μM) for 1 hour. Then, the cells were treated with or without forskolin (20 μM) for another 3 hours. Total cell lysates were subjected to co-immunoprecipitation with anti-Myc antibody, followed by western blotting analyses with the indicated antibodies. IP, immunoprecipitation; IB, immunoblotting; IgG, immunoglobulin G. All experiments were repeated independently at least three times, and representative results are shown.

Figure 6

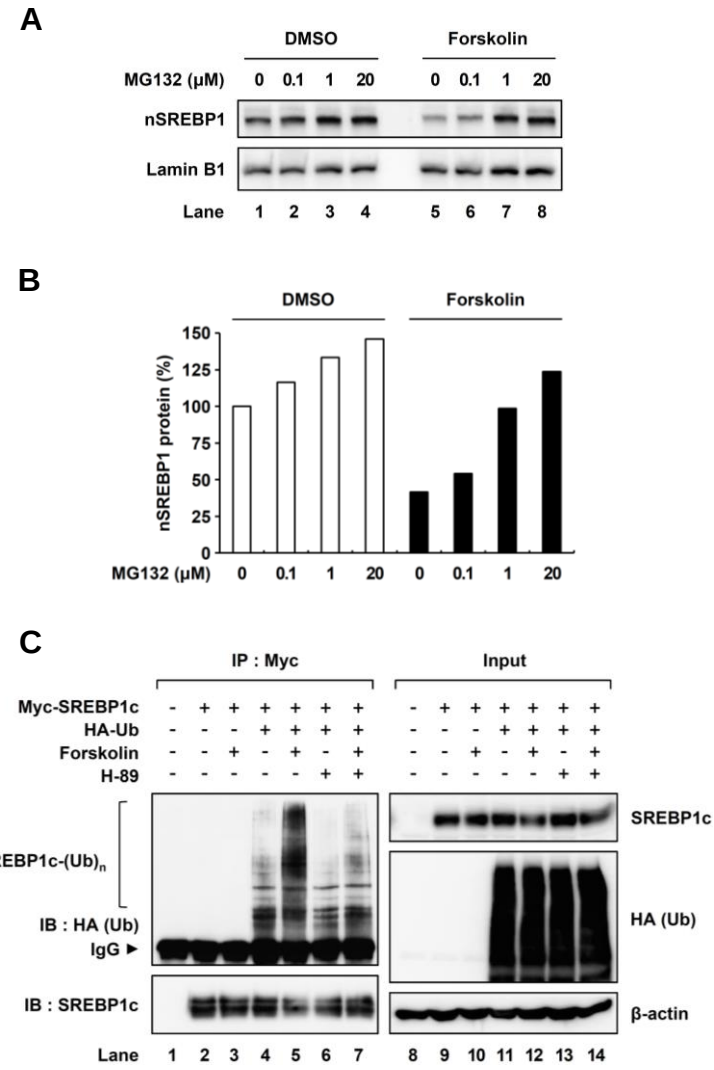
A
DMSO
Forskolin
MG132 (μM) 0 0.1 1 20 0 0.1 1 20
nSREBP1
Lamin B1
Lane 1 2 3 4 5 6 7 8
B
DMSO
Forskolin
nSREBP1 protein (%)
150
125
100
75
50
25
0
MG132 (μM) 0 0.1 1 20 0 0.1 1 20
C
IP : Myc
Input
Myc-SREBP1c
HA-Ub
Forskolin
H-89
SREBP1c-(Ub)n
IB : HA (Ub)
IgG ►
IB : SREBP1c
SREBP1c
HA (Ub)
β-actin
Lane 1 2 3 4 5 6 7 8 9 10 11 12 13 14

RNF20 physically interacts with SREBP1c.

To investigate which factors are involved in the degradation and ubiquitination of nuclear SREBP1c protein, I attempted to identify SREBP1c-interacting proteins; particularly, I was eager to identify an E3 ubiquitin ligase. Mouse primary hepatocytes were infected with adenovirus expressing nuclear SREBP1c, and affinity purifications were conducted. Mass spectrometry analyses indicated that RNF20 (also known as BRE1A) was a potential SREBP1c-interacting protein (Figures 7A and 7B). To validate the physical interaction between RNF20 and SREBP1c, GST pull-down assays were performed. Because SREBP1c forms homodimers, ^{35}S-Met labeled SREBP1c was used as a positive control (Figure 8A, lane 5). RNF20 protein was detected in the fractions eluted from the GST-SREBP1c protein complex (Figure 8A, lane 6). Further, when I biochemically tested the physical interaction between RNF20 and SREBP1c, RNF20 was co-immunoprecipitated with SREBP1c (Figure 8B), indicating that RNF20 could physically interact with SREBP1c. Moreover, I observed that endogenous RNF20 formed immuno-complex with endogenous SREBP1 in liver nuclear extracts (Figure 8C). In parallel immunocytochemistry experiments, exogenous Flag-SREBP1c and Myc-RNF20 proteins co-localized in the nucleus (Figure 8D), implying that RNF20 can interact with SREBP1c in the nucleus.

RNF20 promotes ubiquitination and degradation of SREBP1c.

Given that the E3 ubiquitin ligase RNF20 associates with SREBP1c, the effect of RNF20 on SREBP1c stability was examined. As shown in Figure 9A, the level of SREBP1c protein was decreased by RNF20 in a dose-dependent manner.

Figure 7. Nuclear SREBP1c interacting proteins are identified by using affinity purification. (A) Mouse primary hepatocytes were infected with adenovirus expressing either GFP alone (Mock) or Flag-tagged nuclear SREBP1c (Flag-SREBP1c). Nuclear extracts were subjected to flag affinity purification followed by SDS-PAGE. After affinity purification, SREBP1c interacting candidate proteins were visualized by silver staining. **(B)** The list of nuclear SREBP1c interacting candidates identified by affinity purification with LC-MS/MS analyses.

Figure 7

A

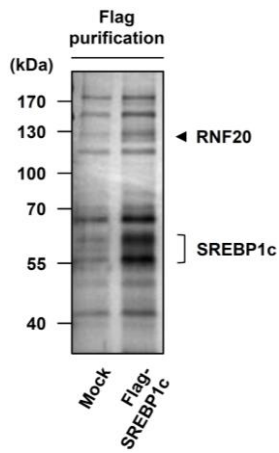

B

The list of nuclear SREBP1c interacting candidates

Accession	Reference	Definition
108885300	H2AV_MOUSE	Histone H2A. variant
51703341	UBIQ_ MOUSE	Ubiquitin
62512148	TBX3_MOUSE	T-box transcription factor TBX3
6678980	GADD45β_MOUSE	Growth arrest and DNA-damage-inducible 45 beta
84027767	BRE1A_MOUSE	RING finger protein 20 (RNF 20)
56749099	GOLI_MOUSE	RING finger protein 130 (RNF 130)
81866361	CCAR1_MOUSE	Cell division cycle and apoptosis regulator protein 1
41688490	CHFR_MOUSE	Checkpoint with forkhead and RING finger domains protein
81886163	NACC1_MOUSE	Nucleus accumbens-associated protein 1

Figure 8. RNF20 physically interacts with SREBP1c. (A) GST pull-down assays were performed as described in "Materials and Methods". Inputs of *in vitro*-translated ^{35}S-Met-labeled SREBP1c (nuclear form) and RNF20 are shown in lanes 1 and 2, respectively. Radioisotope-labeled proteins were mixed with GST or GST-SREBP1c recombinant proteins, and GST pull-down analyses were performed. GST, glutathione S-transferase. **(B)** HEK293T cells were transiently co-transfected with Flag-SREBP1c and/or Myc-RNF20 expression vectors. After preparing total cell lysates, co-immunoprecipitation with anti-Flag antibody and western blotting analyses were performed with the indicated antibodies. IP, immunoprecipitation; IB, immunoblotting; IgG, immunoglobulin G. **(C)** Nuclear extracts were isolated from mouse livers and subsequently co-immunoprecipitated with IgG or the indicated antibody. Immuno-protein complexes were detected by western blotting analyses with the indicated antibodies. nSREBP1, nuclear SREBP1. **(D)** Immuno-cytochemistry analyses of co-expressed Flag-SREBP1c and Myc-RNF20 in HeLa cells. DAPI, 4',6-diamidino-2-phenylindole; Scale bar, 10 μm.

Figure 8

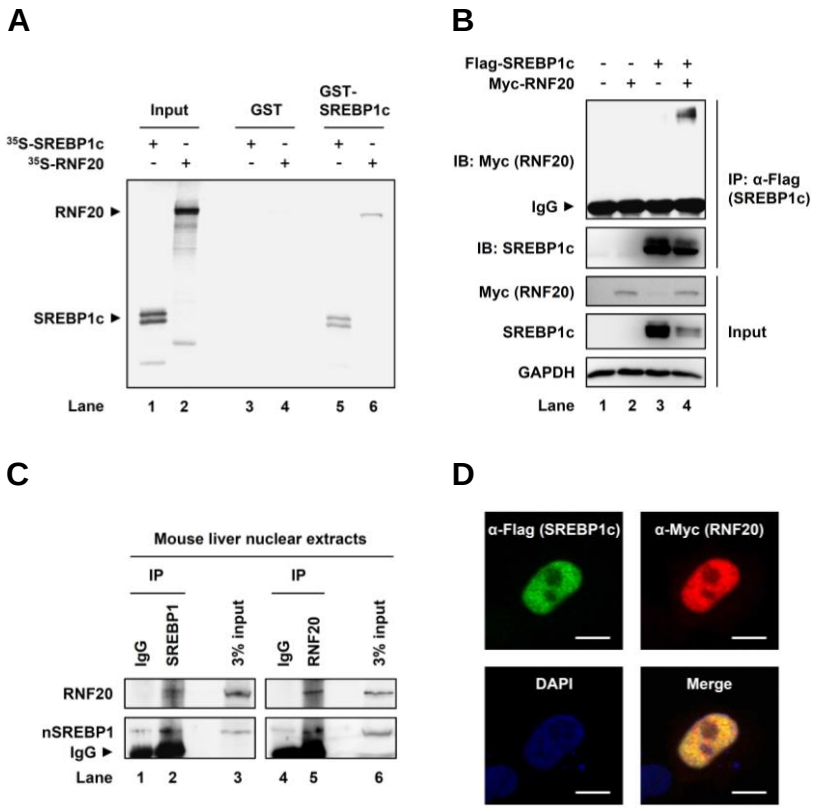
A
Input
GST
GST-SREBP1c
35S-SREBP1c
35S-RNF20
RNF20
SREBP1c
Lane 1 2 3 4 5 6
B
Flag-SREBP1c
Myc-RNF20
IB: Myc (RNF20)
IgG
IB: SREBP1c
IP: α-Flag (SREBP1c)
Myc (RNF20)
SREBP1c
GAPDH
Input
Lane 1 2 3 4
C
Mouse liver nuclear extracts
IP
IP
IgG
SREBP1
3% input
IgG
RNF20
3% input
RNF20
nSREBP1
IgG
Lane 1 2 3 4 5 6
D
α-Flag (SREBP1c)
α-Myc (RNF20)
DAPI
Merge

Moreover, the RNF20-induced reduction of SREBP1c protein was alleviated by MG132 (Figure 9A, lane 6), indicating that RNF20 would stimulate SREBP1c degradation via ubiquitin-proteasomal degradation. Consistent with these data, cycloheximide-chase assays revealed that the half-life of SREBP1c was shortened by ectopic expression of RNF20 (Figure 9B). Next, as RNF20 exhibits E3 ubiquitin ligase activity, I tested whether SREBP1c is ubiquitinated by RNF20. As shown in Figure 10A, RNF20 greatly promoted the level of SREBP1c polyubiquitination. To confirm whether endogenous RNF20 plays a role in SREBP1c ubiquitination, I investigated the effect of RNF20 knockdown via siRNA on the ubiquitination of SREBP1c. I found that suppression of RNF20 relieved the level of SREBP1c polyubiquitination (Figure 10B). These data indicate that RNF20 can act as an E3 ubiquitin ligase for SREBP1c and can accelerate polyubiquitination and degradation of SREBP1c protein.

RNF20 suppresses the transcriptional activity of SREBP1c.

To understand the biological significance of SREBP1c degradation by RNF20, I investigated the transcriptional activity of SREBP1c with or without RNF20 overexpression. Consistent with previous reports (Kim et al., 1998; Seo et al., 2004b), SREBP1c transactivated the promoters of *FASN* and adiponectin (*Acrp30*) genes, whereas coexpression with RNF20 suppressed the transcriptional activity of SREBP1c (Figure 11A). When the level of SREBP1 protein was investigated with or without RNF20 overexpression in primary hepatocytes, RNF20 overexpression clearly decreased in endogenous and ectopic nuclear SREBP1 protein (Figure 11B). Moreover, RNF20 overexpression indeed decreased

Figure 9. RNF20 represses the protein stability of SREBP1c. (A) HEK293T cells transfected with Flag-SREBP1c and/or Myc-RNF20 expression vectors were incubated with or without MG132 (20 μM) for 4 hours, and total cell lysates were subjected to SDS-PAGE followed by western blotting analyses with the indicated antibodies. **(B)** COS-1 cells transfected with Myc-SREBP1c and/or Myc-RNF20 expression vectors were harvested at 0, 2, 4, and 8 hours after cycloheximide treatment (30 μM). After isolating total cell lysates, western blotting analyses were performed with the indicated antibodies. CHX, cycloheximide.

Figure 9

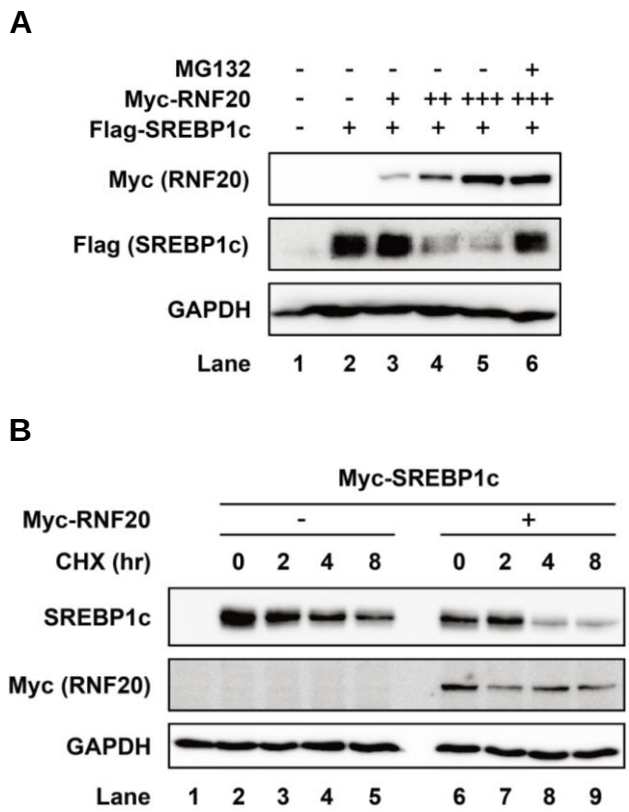
A
MG132 - - - - - +
Myc-RNF20 - - + ++ +++ +++
Flag-SREBP1c - + + + + +
Myc (RNF20)
Flag (SREBP1c)
GAPDH
Lane 1 2 3 4 5 6
B
Myc-SREBP1c
Myc-RNF20 - +
CHX (hr) 0 2 4 8 0 2 4 8
SREBP1c
Myc (RNF20)
GAPDH
Lane 1 2 3 4 5 6 7 8 9

Figure 10. RNF20 mediates ubiquitination and degradation of SREBP1c. **(A)** COS-1 cells were co-transfected with Myc-SREBP1c, HA-tagged ubiquitin and/or Flag-RNF20 expression vectors. After incubation for 36 hours, the cells were treated with MG132 (10 μM) for 12 hours. Total cell lysates were isolated and subjected to cell-based ubiquitination assays. IP, immunoprecipitation; IB, immunoblotting; IgG, immunoglobulin G. **(B)** COS-1 cells were transfected with non-specific control siRNA (siControl) or RNF20-specific siRNA (siRNF20). After incubation for 36 hours, the cells were incubated with MG132 (10 μM) for 12 hours. Total cell lysates were isolated and subjected to cell-based ubiquitination assays. The data shown are representative results of at least three independent experiments.

Figure 10

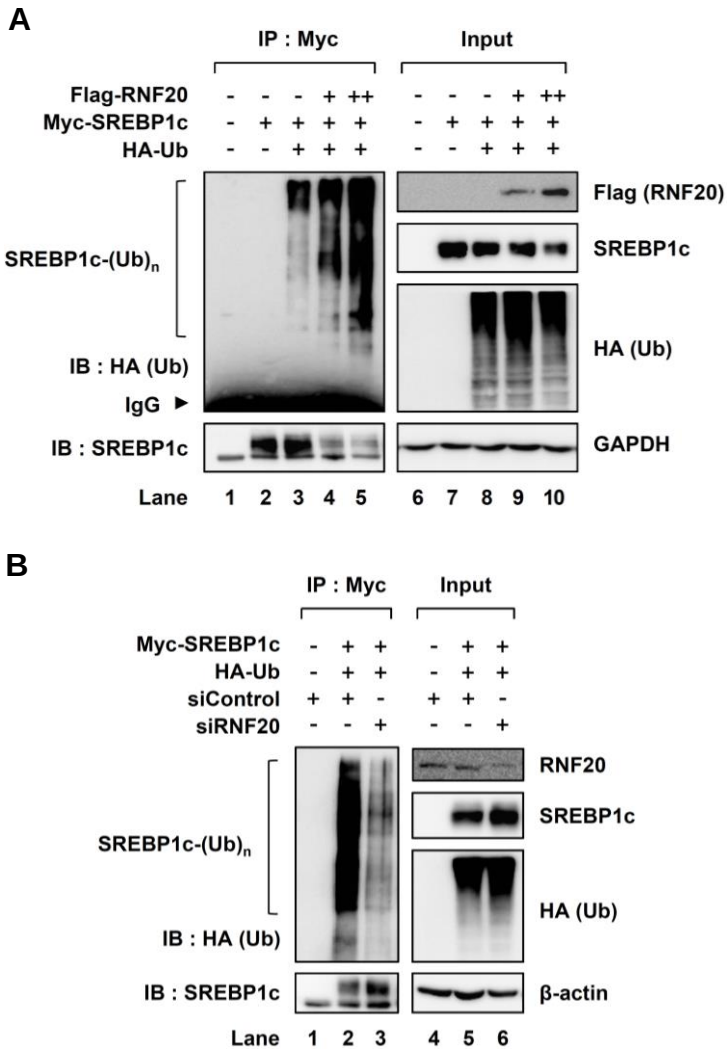
A
IP : Myc
Input
Flag-RNF20 - - - + ++ - - - + ++
Myc-SREBP1c - + + + + - + + + +
HA-Ub - - + + + - - + + +
SREBP1c-(Ub)n
IB : HA (Ub)
IgG
IB : SREBP1c
Flag (RNF20)
SREBP1c
HA (Ub)
GAPDH
Lane 1 2 3 4 5 6 7 8 9 10
B
IP : Myc
Input
Myc-SREBP1c - + + - + +
HA-Ub - + + - + +
siControl + + - + + -
siRNF20 - - + - - +
SREBP1c-(Ub)n
IB : HA (Ub)
IB : SREBP1c
RNF20
SREBP1c
HA (Ub)
β-actin
Lane 1 2 3 4 5 6

elevated endogenous SREBP1 protein in the presence of insulin and/or T0901317, a LXR agonist (Figure 11C). Next, to address the question whether RNF20 could affect the expression of SREBP1c target genes, I analyzed the mRNA levels of its target genes in RNF20 and/or SREBP1c-overexpressing hepatocytes. In primary hepatocytes, RNF20 overexpression alone significantly decreased many lipogenic genes including *SREBP1c*, *FASN*, *SCD1*, *ACC1*, and *ELOVL6* (Figure 12A, lane 2). Consistent with previous reports (Horton et al., 2002; Kim et al., 1998), SREBP1c elevated the mRNA expression of lipogenic genes such as *FASN*, *SCD1*, and *ELOVL6* in primary hepatocytes (Figure 12A, lane 3). However, the effects of RNF20 overexpression on lipogenic suppression were marginal in SREBP1c-overexpressing hepatocytes (Figure 12A, lane 4). It is feasible to speculate that high level of SREBP1c protein may partly stimulate lipogenic gene expression even in the presence of RNF20 overexpression. On the other hand, overexpression of RNF20 did not significantly alter the mRNA level of other SREBP isoforms, including SREBP1a and 2 (Figure 12A). Moreover, in primary hepatocytes, RNF20 overexpression decreased intracellular lipid accumulation as determined by Oil Red O staining (Figure 12B). These data indicate that RNF20 can indeed downregulate lipogenic gene expression by suppressing SREBP1c.

Suppression of RNF20 enhances hepatic lipid metabolism via SREBP1c.

To determine whether endogenous RNF20 influences lipogenic activity, I investigated the effect of RNF20 suppression via siRNA on lipogenic gene expression in primary hepatocytes. When the level of RNF20 was decreased (by approximately 25%), the mRNA levels of SREBP1c and its target genes, including

Figure 11. RNF20 suppresses the transcriptional activity of SREBP1c. **(A)** HEK293T cells were co-transfected with luciferase reporter plasmids containing the FASN or Acrp30 promoter along with pRSV-β-gal, Myc-SREBP1c and/or Myc-RNF20 expression vectors. Total cell lysates were subjected to luciferase and β-galactosidase assays. The values presented are representative data from three independent experiments carried out in triplicate. Each bar represents the mean ± SD of three individual samples. $^{\#}P < 0.05$ vs. negative control; $^{\#\#}P < 0.01$ vs. negative control; $^{*}P < 0.05$; RLU, relative luminescence units. **(B)** Mouse primary hepatocytes were infected with adenovirus containing GFP alone (Ad-Mock), Flag-SREBP1c (Ad-SREBP1c) and/or Myc-RNF20 (Ad-RNF20) as indicated. After infection for 12 hours, total cell lysates were subjected to SDS-PAGE followed by western blotting analyses with the indicated antibodies. nSREBP1, nuclear SREBP1. **(C)** Mouse primary hepatocytes were infected with Ad-Mock or Ad-RNF20 for 12 hours. Subsequently, the culture media were replaced with fresh media and 24 hours. And then the cells were incubated for 12 hours with or without insulin (100 nM) and T0901317 (3 μM). Total cell lysates were subjected to SDS-PAGE followed by western blotting analyses with the indicated antibodies. pSREBP1, precursor SREBP1; nSREBP1, nuclear SREBP1.

Figure 11

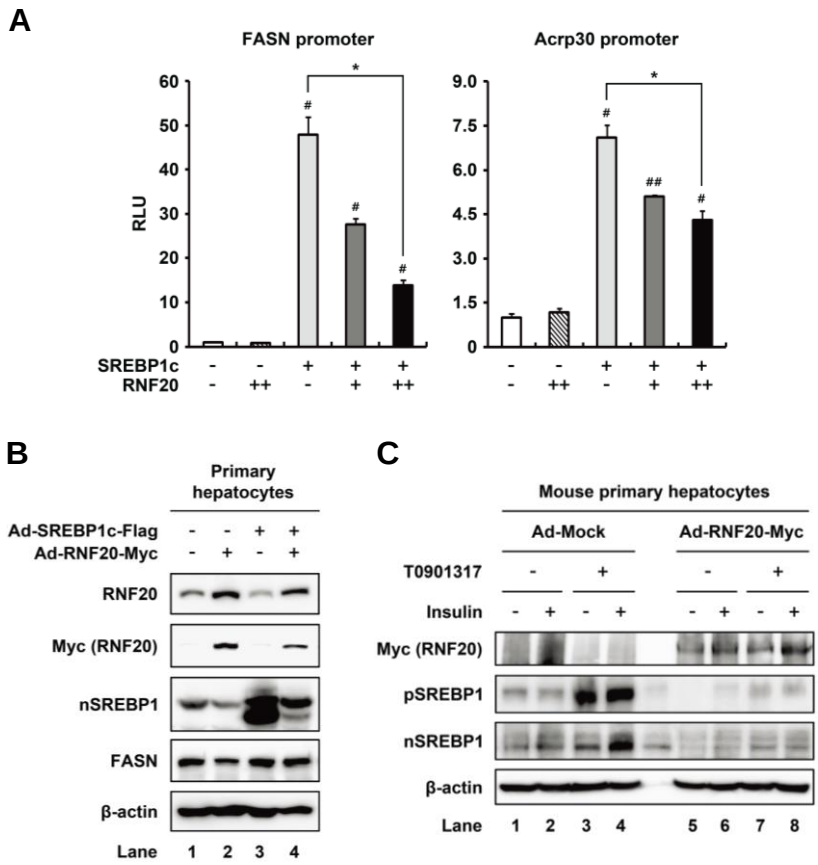
A
FASN promoter
Acrp30 promoter
RLU
SREBP1c
RNF20
B
Primary hepatocytes
Ad-SREBP1c-Flag
Ad-RNF20-Myc
RNF20
Myc (RNF20)
nSREBP1
FASN
β-actin
Lane
C
Mouse primary hepatocytes
Ad-Mock
Ad-RNF20-Myc
T0901317
Insulin
Myc (RNF20)
pSREBP1
nSREBP1
β-actin
Lane

Figure 12. RNF20 downregulates the expression of SREBP1c and its target genes. (A) Mouse primary hepatocytes were infected with Ad-SREBP1c and/or Ad-RNF20. After infection for 12 hours, the culture media were replaced with fresh media and subsequently incubated for 36 hours. The relative mRNA levels were measured using qRT-PCR. The relative values were normalized to the level of GAPDH mRNA. Each bar represents the mean ± SD of three individual samples. $^{\#}P < 0.05$ vs. negative control; $^{\#\#}P < 0.01$ vs. negative control; $*P < 0.05$; $**P < 0.01$. **(B)** Mouse primary hepatocytes were transduced with Ad-SREBP1c and/or Ad-RNF20 adenoviruses. After incubation for 48 hours, intracellular lipid droplets were visualized by Oil Red O staining, and the cells were photographed. Microscopic views of cells at a magnification of ×200 are shown. Scale bar, 100 μm.

Figure 12

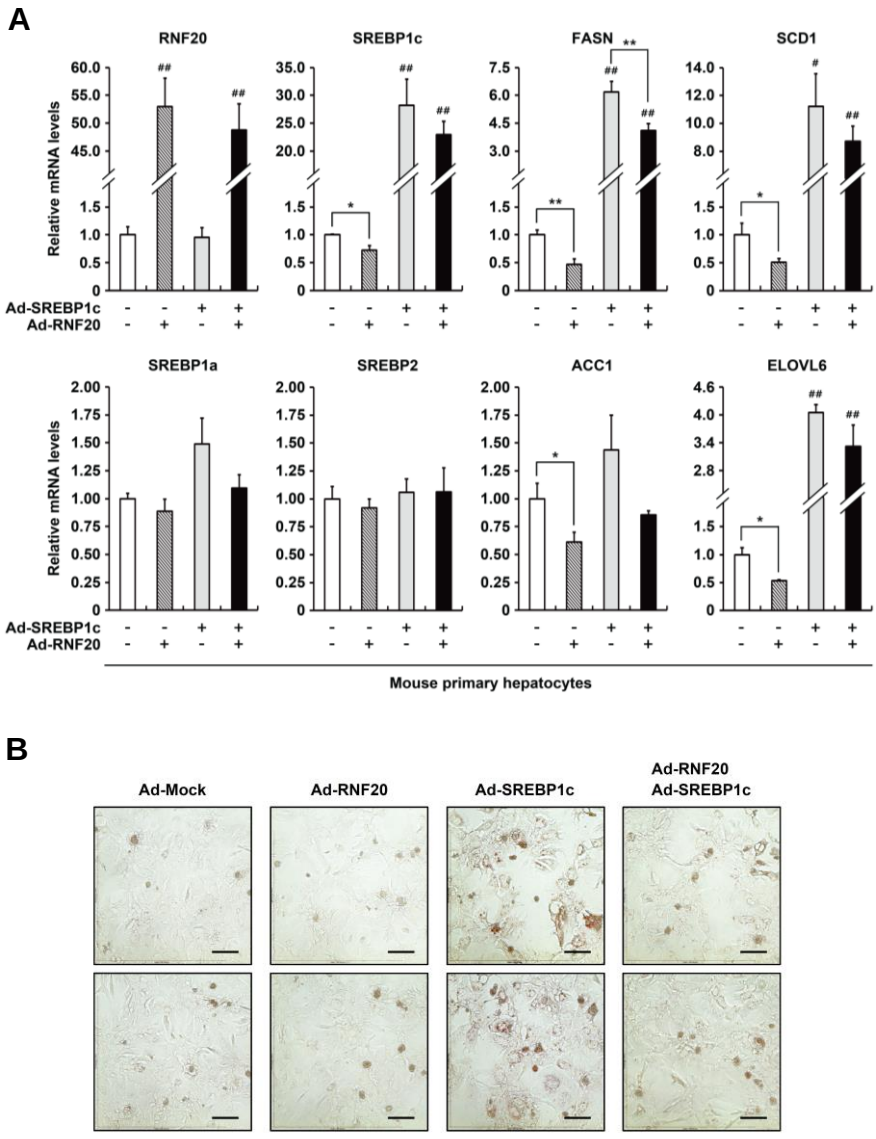
A
RNF20
SREBP1c
FASN
SCD1
SREBP1a
SREBP2
ACC1
ELOVL6
Relative mRNA levels
Ad-SREBP1c
Ad-RNF20
Mouse primary hepatocytes
B
Ad-Mock
Ad-RNF20
Ad-SREBP1c
Ad-RNF20
Ad-SREBP1c

FASN and *ELOVL6*, were significantly elevated (Figure 13A). On the contrary, the mRNA levels of other SREBP isoforms, including SREBP1a and 2, were not altered by RNF20 suppression (Figure 13A), whereas the level of SREBP1c mRNA was upregulated, probably, through an auto-regulatory mechanism (Amemiya-Kudo et al., 2000; Dif et al., 2006). Consistently, suppression of RNF20 with siRNA in primary hepatocytes increased the level of endogenous SREBP1 protein (both precursor and nuclear forms) (Figure 13B) and promoted intracellular neutral lipid accumulation as determined by Oil Red O staining (Figure 14A). Additionally, RNF20-suppressed hepatocytes stored more intracellular cellular triglycerides than control primary hepatocytes (Figure 14B). On the contrary, the mRNA expression levels of other lipogenic transcription factors, such as peroxisome proliferator-activated receptor-gamma (PPARγ), liver X receptor-alpha (LXRα), and carbohydrate responsive element-binding protein (ChREBP), were not altered by RNF20 suppression (Figure 13A and 14C). Besides, the mRNA levels of fatty acid oxidation pathway genes, including peroxisome proliferator-activated receptor-alpha (*PPARα*), carnitine palmitoyltransferase 1A (*CPT1A*), medium-chain acyl-CoA dehydrogenase (*MCAD*) and aconitase 1 (*ACO1*), were not changed by RNF20 suppression in primary hepatocytes (Figure 14C), implying that RNF20 can selectively downregulate lipogenic gene expression via SREBP1c in hepatocytes.

Hepatic RNF20 is regulated by nutritional changes.

Nutritional and hormonal changes coordinate energy homeostasis, including lipid and glucose metabolism. Thus, I examined whether the nutritional status might modulate hepatic RNF20 expression. In the liver of fasted mice, the

Figure 13. Suppression of RNF20 enhances hepatic lipid metabolism via SREBP1c. (A) Mouse primary hepatocytes were transfected with siControl or siRNF20, and relative mRNA levels were determined using qRT-PCR. The level of each mRNA was normalized to the mRNA level of the TATA-binding protein (TBP) gene. Each bar represents the mean ± SD of three individual samples. **P* < 0.05 and ***P* < 0.01 were considered significant. SQS, squalene synthetase; LDLR, low-density lipoprotein receptor. **(B)** Mouse primary hepatocytes were transfected with siControl or siRNF20. After isolating nuclear extracts, western blotting analyses were performed with the indicated antibodies. Relative amounts of RNF20 and nuclear SREBP1 proteins were calculated using Labworks software (UVP Bioimaging System) and normalized to Lamin B1. The western blots shown are representative of three independent experiments. pSREBP1, precursor SREBP1; nSREBP1, nuclear SREBP1.

Figure 13

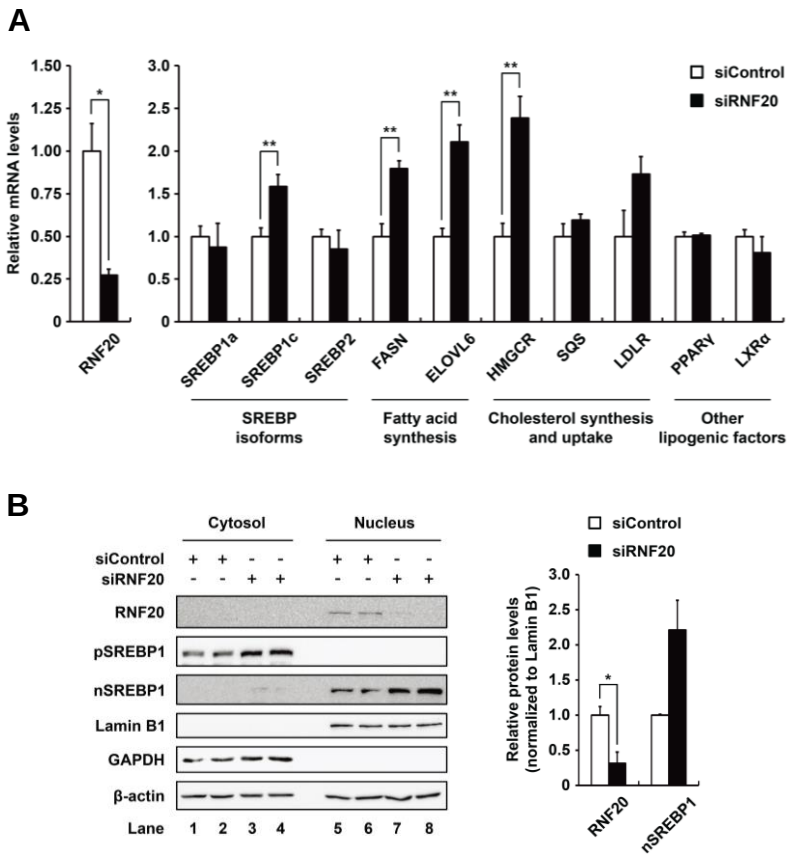
A
Relative mRNA levels
siControl
siRNF20
RNF20
SREBP1a
SREBP1c
SREBP2
FASN
ELOVL6
HMGCR
SQS
LDLR
PPARγ
LXRα
SREBP isoforms
Fatty acid synthesis
Cholesterol synthesis and uptake
Other lipogenic factors
B
Cytosol
Nucleus
siControl
siRNF20
RNF20
pSREBP1
nSREBP1
Lamin B1
GAPDH
β-actin
Lane
Relative protein levels (normalized to Lamin B1)
nSREBP1

Figure 14. RNF20 negatively regulates hepatic lipogenesis. (A) Mouse primary hepatocytes were transfected with siControl or siRNF20. After incubation for 48 hours, intracellular lipid droplets were visualized by Oil Red O staining, and the cells were photographed. Microscopic views of cells at a magnification of ×200 are shown. Scale bar, 100 μm. **(B)** Intracellular triglyceride contents were measured biochemically. **(C)** Mouse primary hepatocytes were transfected with siControl or siRNF20. Relative mRNA levels of PPARα, ChREBP and their target genes were determined using qRT-PCR. The level of each mRNA was normalized to the mRNA level of the TATA-binding protein (TBP) gene.

Figure 14

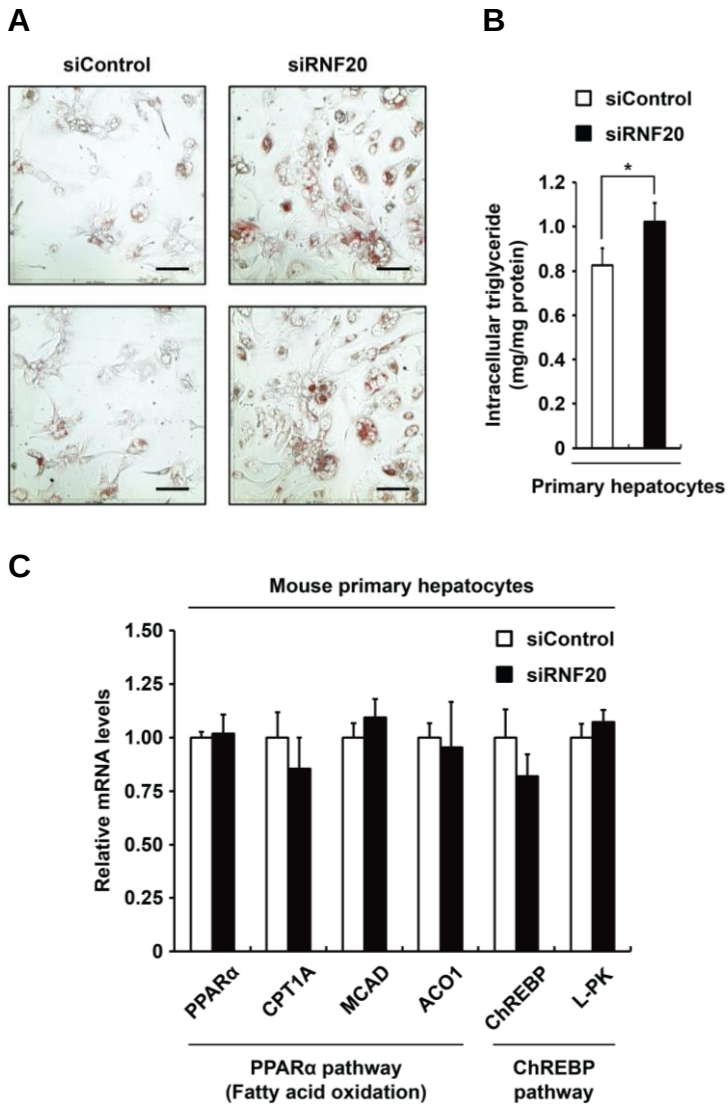
A
siControl
siRNF20
B
siControl
siRNF20
*
Intracellular triglyceride (mg/mg protein)
1.2
1.0
0.8
0.6
0.4
0.2
0
Primary hepatocytes
C
Mouse primary hepatocytes
siControl
siRNF20
Relative mRNA levels
1.50
1.25
1.00
0.75
0.50
0.25
0
PPARα
CPT1A
MCAD
ACO1
ChREBP
L-PK
PPARα pathway
(Fatty acid oxidation)
ChREBP
pathway

expression of RNF20 mRNA was significantly increased (Figure 15A), whereas that of SREBP1c and FASN mRNA was decreased. These observations indicate that the change in RNF20 expression might be associated with the regulation of SREBP1c during nutritional changes. In contrast, the mRNA level of FBXW7, an E3 ligase of SREBP proteins, was unchanged by either feeding or fasting conditions (Figure 15A). Upon fasting, glucagon stimulates the PKA cascade to regulate lipid and glucose metabolism to accomplish catabolic responses (Girard et al., 1994; Jitrapakdee, 2012). Thus, to address the question of whether RNF20 expression might be regulated by PKA activation, I examined the level of RNF20 mRNA in hepatocytes with or without forskolin. Notably, forskolin increased the level of RNF20 mRNA, whereas it decreased SREBP1c and SCD1 mRNA levels (Figure 15B). Furthermore, in primary hepatocytes, both glucagon and forskolin increased the RNF20 protein level and decreased the nuclear SREBP1 protein level (Figure 15C). Next, to determine whether cytosolic or nuclear RNF20 is regulated upon PKA activation, cytosolic and nuclear extracts were isolated from hepatoma cells with or without forskolin treatment. As shown in Figure 15D, forskolin enhanced the nuclear RNF20 protein level and reduced the nuclear SREBP1 protein level. However, unlike RNF20, FBXW7 expression was not altered by forskolin (Figure 15B). In addition, I investigated the mRNA levels of SREBP1c target genes in RNF20-suppressed hepatocytes treated with forskolin. As shown in Figure 16A, the mRNA levels of lipogenic genes such as *SREBP1c*, *FASN*, and *SCD1* were decreased by forskolin, whereas RNF20 suppression via siRNA restored the expression of lipogenic genes, even in the presence of forskolin (Figure 16A). To understand whether RNF20 is involved in the PKA-dependent

Figure 15. Expression of hepatic RNF20 is nutritionally regulated. (A) The levels of each mRNA in the livers of fed and fasted mice were determined by qRT-PCR analysis. The TBP mRNA level was used for normalization. The fed control (Fed) was allowed free access to food, and the fasted groups (Fast) were denied access to food for 24 hours. The refed group (Refed) was allowed free access to food for 7 hours after 24 hours of fasting. $n = 4$ for each group. $*P < 0.05$ and $**P < 0.01$ were considered significant. **(B)** Mouse primary hepatocytes were incubated with or without forskolin (+ indicates 10 μM forskolin and ++ indicates 100 μM forskolin) for 6 hours. Each relative mRNA level was determined using qRT-PCR and normalized to the TBP mRNA level. As a positive control, the expression of G6Pase mRNA was greatly enhanced by forskolin. Each bar represents the mean ± SD of three individual samples. $*P < 0.05$ and $**P < 0.01$ were considered significant. N.D., not detected. **(C)** Mouse primary hepatocytes were incubated with glucagon (100 nM) or forskolin (50 μM) for 4 hours. Total cell lysates were subjected to western blotting analyses with the indicated antibodies. nSREBP1, nuclear SREBP1. **(D)** H4IIE rat hepatoma cells were incubated with forskolin (50 μM) for 5 hours. Cytosolic and nuclear extracts were subjected to western blotting analyses with the indicated antibodies. The results are representative of three independent experiments.

Figure 15

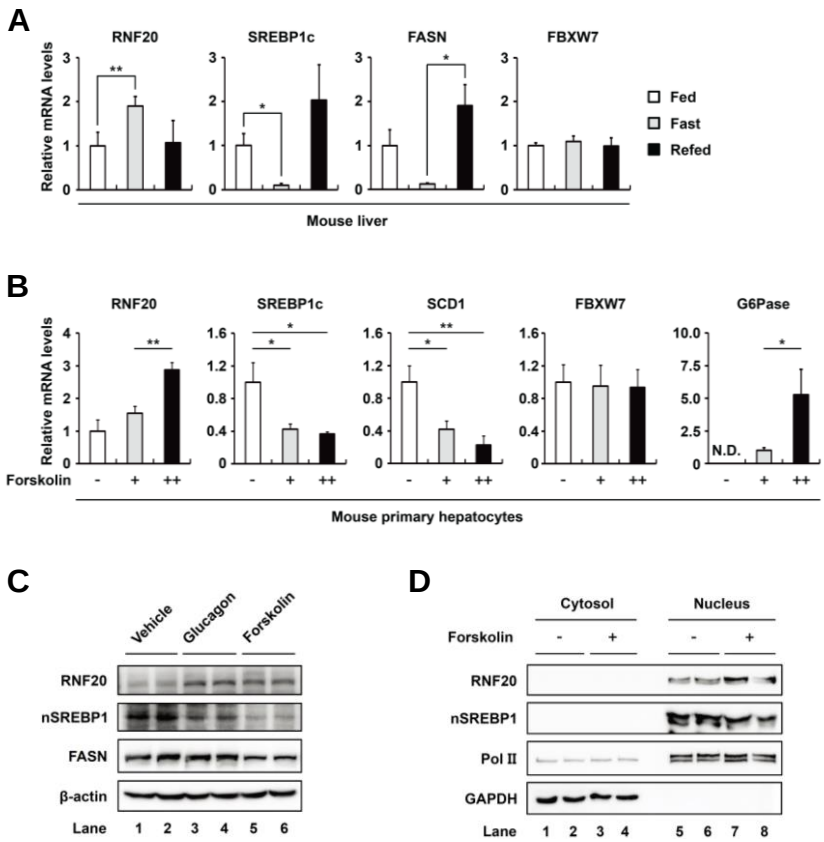
A
RNF20
SREBP1c
FASN
FBXW7
Relative mRNA levels
Fed
Fast
Refed
Mouse liver
B
RNF20
SREBP1c
SCD1
FBXW7
G6Pase
Relative mRNA levels
N.D.
Forskolin
Mouse primary hepatocytes
C
Vehicle
Glucagon
Forskolin
RNF20
nSREBP1
FASN
β-actin
Lane
D
Cytosol
Nucleus
Forskolin
RNF20
nSREBP1
Pol II
GAPDH
Lane

Figure 16. RNF20 is a negative regulator of SREBP1c and the lipogenic program upon PKA activation. (A) Mouse primary hepatocytes transfected with siControl or siRNF20 were incubated with forskolin (10 μM) for 6 hours. The level of each mRNA was determined using qRT-PCR and normalized to the TBP mRNA level. Each bar represents the mean ± SD of experiments carried out in triplicate. $*P < 0.05$ and $**P < 0.01$ were considered significant. **(B)** COS-1 cells were co-transfected with DNA plasmids and siRNAs as indicated. After incubation for 36 hours, the cells were incubated with MG132 (10 μM) for 12 hours and subsequently treated with forskolin (20 μM) for 4 hours. Then, the cells were treated with or without forskolin (20 μM) for another 3 hours. Total cell lysates were isolated and subjected to cell-based ubiquitination assays. IP, immunoprecipitation; IB, immunoblotting; IgG, immunoglobulin G.

Figure 16

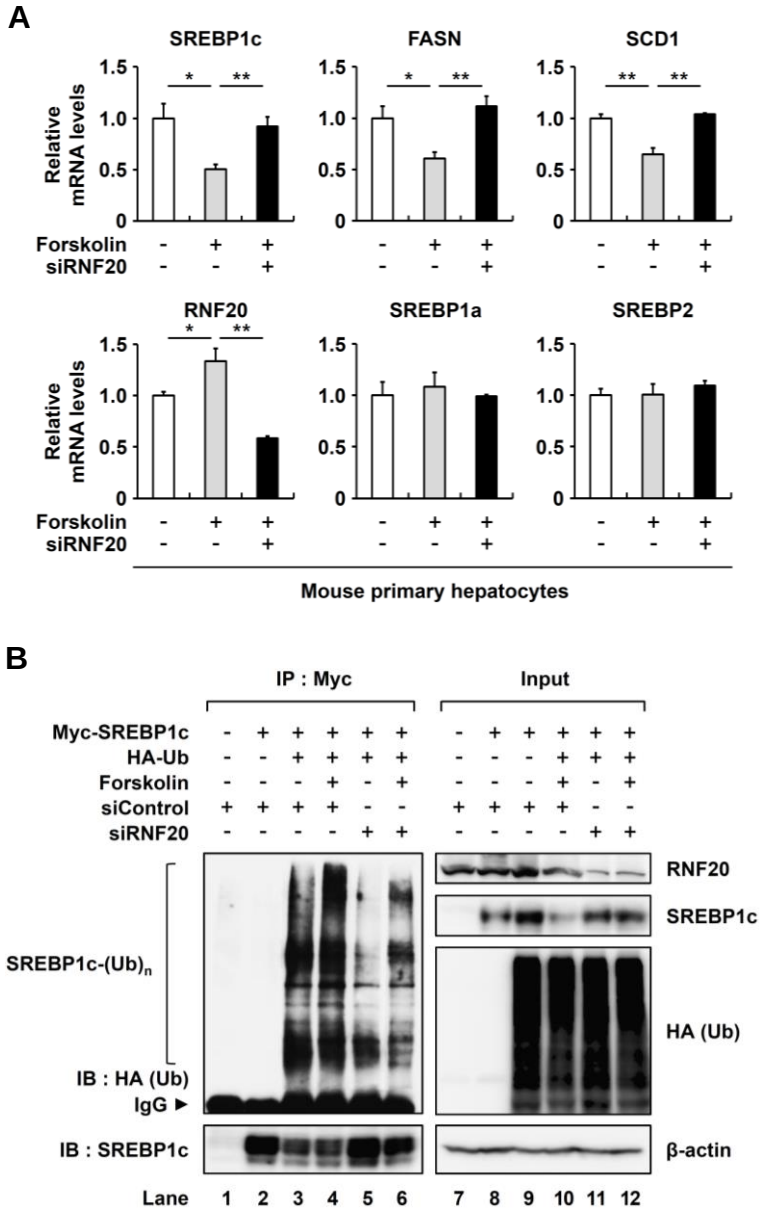
A
SREBP1c
FASN
SCD1
RNF20
SREBP1a
SREBP2
Relative mRNA levels
1.5
1.0
0.5
0
*
**
Forskolin
siRNF20
Mouse primary hepatocytes
B
IP : Myc
Input
Myc-SREBP1c
HA-Ub
Forskolin
siControl
siRNF20
SREBP1c-(Ub)n
IB : HA (Ub)
IgG ►
IB : SREBP1c
RNF20
SREBP1c
HA (Ub)
β-actin
Lane
1 2 3 4 5 6 7 8 9 10 11 12

SREBP1c ubiquitination, I examined the level of SREBP1c ubiquitination upon PKA activation with RNF20 suppression. As shown in Figure 16B, knockdown of RNF20 with siRNA successfully decreased the level of PKA-mediated SREBP1c ubiquitination, implying that PKA-dependent SREBP1c degradation would require for RNF20. These data strongly indicate that RNF20 is a negative regulator of SREBP1c and the lipogenic program upon PKA activation in hepatocytes.

RNF20 represses hepatic lipid metabolism *in vivo*.

To further examine whether RNF20 confers hepatic lipid metabolism via SREBP1c *in vivo*, adenovirus expressing RNF20 was intravenously injected into wild-type mice. In agreement with the above data, *in vivo* RNF20 overexpression decreased the level of hepatic SREBP1 protein (Figure 17A). Consistently, the hepatic triglyceride level was decreased by RNF20 overexpression (Figure 17B). To confirm the possibility that the decrease in hepatic lipid metabolism is mediated by RNF20-dependent SREBP1c suppression, I tested FASN promoter activity *in vivo*. As shown in Figure 17C, optical *in vivo* imaging analyses revealed that adenoviral RNF20 overexpression repressed FASN promoter activity compared with control mice. In addition, I found that the expression of lipogenic genes such as *SREBP1c*, *FASN*, *SCD1*, and *ELOVL6* was significantly attenuated in the liver of RNF20-overexpressing mice (Figure 17D). However, hepatic RNF20 over-expression did not significantly alter the mRNA level of other SREBPs such as SREBP1a and 2 (Figure 17D). Moreover, adenovirally ovevexpressed RNF20 *in vivo* did not change the mRNA levels of other lipogenic transcription factors, including PPARγ, LXRα and ChREBP, and fatty acid oxidation pathway genes in

Figure 17. RNF20 overexpression inhibits the hepatic lipogenic program *in vivo*. (A) Ten-week-old male C57BL/6 mice were infected through the tail vein with adenovirus encoding GFP (Ad-Mock) as the control or mouse RNF20 (Ad-RNF20) (adenoviral dose of 1×10^{10} viral particles per mouse). After 7 days of adenoviral injection, the mice were sacrificed in fed states. The expression levels of RNF20, nSREBP1 and FASN protein in the livers of mice infected with Ad-Mock or Ad-RNF20 were monitored by western blotting analyses. nSREBP1, nuclear SREBP1. **(B)** The hepatic triglyceride level was measured from 100 mg liver tissue as described in "Materials and Methods". $*P < 0.05$ was considered significant (vs. the Ad-Mock control group). **(C)** Live imaging of *in vivo* FASN-luciferase (FASN-luc) activity in response to RNF20 overexpression in C57BL/6 mice. *In vivo* luminescence was measured 7 days post-adenoviral infection as described in "Materials and Methods". **(D)** In C57BL/6 mouse liver injected Ad-Mock or Ad-RNF20, the effects of adenoviral RNF20 overexpression on lipogenic gene expression were determined by qRT-PCR analyses. The level of TBP mRNA was used for normalization. Each mRNA level is shown as a ratio relative to the Ad-Mock control group. $*P < 0.05$ was considered significant (vs. the Ad-Mock control group). $n = 3$ for each group in panel A, and $n = 4$ for each group in all other panels.

Figure 17

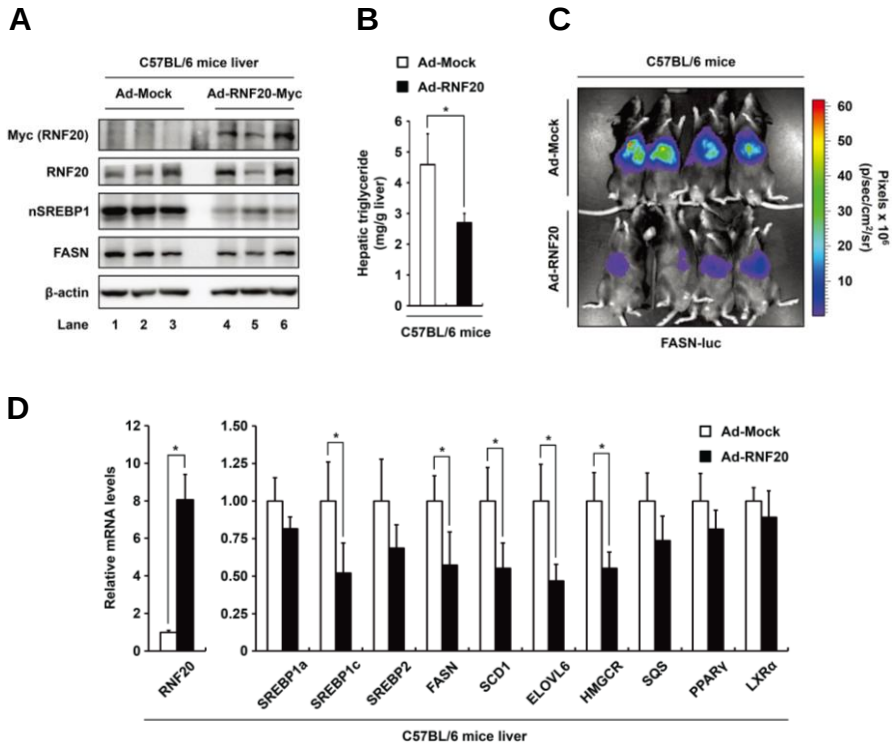
A
C57BL/6 mice liver
Ad-Mock
Ad-RNF20-Myc
Myc (RNF20)
RNF20
nSREBP1
FASN
β-actin
Lane 1 2 3 4 5 6
B
Ad-Mock
Ad-RNF20
Hepatic triglyceride (mg/g liver)
C57BL/6 mice
C
C57BL/6 mice
Ad-Mock
Ad-RNF20
Pixels x 10⁶ (p/sec/cm²/sr)
FASN-luc
D
Relative mRNA levels
Ad-Mock
Ad-RNF20
RNF20
SREBP1a
SREBP1c
SREBP2
FASN
SCD1
ELOVL6
HMGCR
SQS
PPARγ
LXRα
C57BL/6 mice liver

liver (Figure 17D). Thus, these *in vivo* data confirm the notion that RNF20 plays an important role in the regulation of hepatic lipogenesis via SREBP1c.

RNF20 alleviates hepatic steatosis in *db*/*db* mice.

Several obese rodent animals, including *db*/*db* mice, exhibit hepatic steatosis with enhanced SREBP1c and lipogenic activity (Li et al., 2005; Marchesini et al., 2001; Muoio and Newgard, 2006). To investigate whether RNF20 overexpression might alleviate fatty liver through the regulation of SREBP1c, RNF20 was overexpressed by adenovirus in the liver of *db*/*db* mice. In *db*/*db* mice, adenoviral overexpression of RNF20 did not cause major differences in body weight and fasting blood glucose (Figures 18A and 18B). Similar to lean mice, hepatic RNF20 overexpression decreased both precursor and nuclear forms of SREBP1 protein in *db*/*db* mice (Figure 19A). In accordance with reduced SREBP1 expression, hepatic steatosis was alleviated by RNF20 overexpression in *db*/*db* mice (Figures 19B and 19C). Furthermore, hepatic RNF20 overexpression in *db*/*db* mice significantly lowered FASN promoter activity (Figure 19D) and reduced the expression of lipogenic genes (Figure 20A). However, similar to lean mice, hepatic RNF20 overexpression in *db*/*db* mice did not alter the mRNA levels fatty acid oxidation pathway genes (Figure 20B), indicating that hepatic RNF20 overexpression would alleviate hepatic steatosis by suppression of SREBP1c and lipogenic gene expression. Next, to investigate whether hepatic RNF20 might be involved in glucose homeostasis in diabetic *db*/*db* mice, oral glucose tolerance tests were examined. As shown in Figure 20C, RNF20 overexpression improved glucose intolerance in *db*/*db* mice. Together, these data propose the idea that hepatic

Figure 18. In *db*/*db* mice, RNF20 overexpression did not cause differences in body weight and fasting blood glucose. Nine-week-old male *db*/*db* mice were infected through the tail vein with adenovirus encoding GFP or RNF20 (adenoviral dose of 2×10^{10} viral particles per mouse). After 7 days of adenoviral injection, the mice were sacrificed. **(A)** Body weight (grams) of Ad-Mock or Ad-RNF20 injected *db*/*db* mice. **(B)** Fasting glucose levels (mg/dL) of Ad-Mock or Ad-RNF20 injected *db*/*db* mice after 12 hours of fasting.

Figure 18

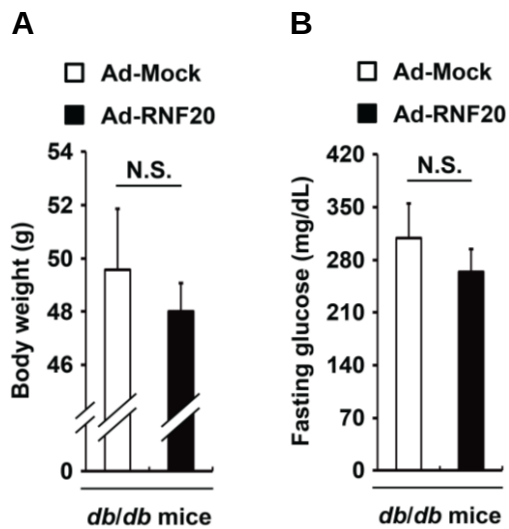
A
Ad-Mock
Ad-RNF20
N.S.
54
52
50
48
46
0
Body weight (g)
db/db mice
B
Ad-Mock
Ad-RNF20
N.S.
420
350
280
210
140
70
0
Fasting glucose (mg/dL)
db/db mice

Figure 19. RNF20 overexpression alleviates hepatic steatosis in *db*/*db* mice. **(A)** Nine-week-old male *db*/*db* mice were infected through the tail vein with adenovirus encoding GFP or RNF20 (adenoviral dose of 2×10^{10} viral particles per mouse). After 7 days of adenoviral injection, the mice were sacrificed in fed states. The liver tissue was then subjected to SDS-PAGE followed by western blotting analyses with the indicated antibodies. $n = 3$ for each group. **(B)** The level of hepatic triglycerides was measured from 100 mg liver tissue in *db*/*db* mice infected with each adenovirus. $n = 5$ for each group. $^*P < 0.05$ was considered significant (vs. the Ad-Mock control group). **(C)** Representative hematoxylin and eosin (H&E) and Oil Red O staining of liver sections of *db*/*db* mice infected with Ad-Mock or Ad-RNF20. Scale bar, 100 μm. **(D)** Live imaging of *in vivo* FASN-luciferase (FASN-luc) activity in response to RNF20 overexpression in *db*/*db* mice. $n = 2$ for each group.

Figure 19

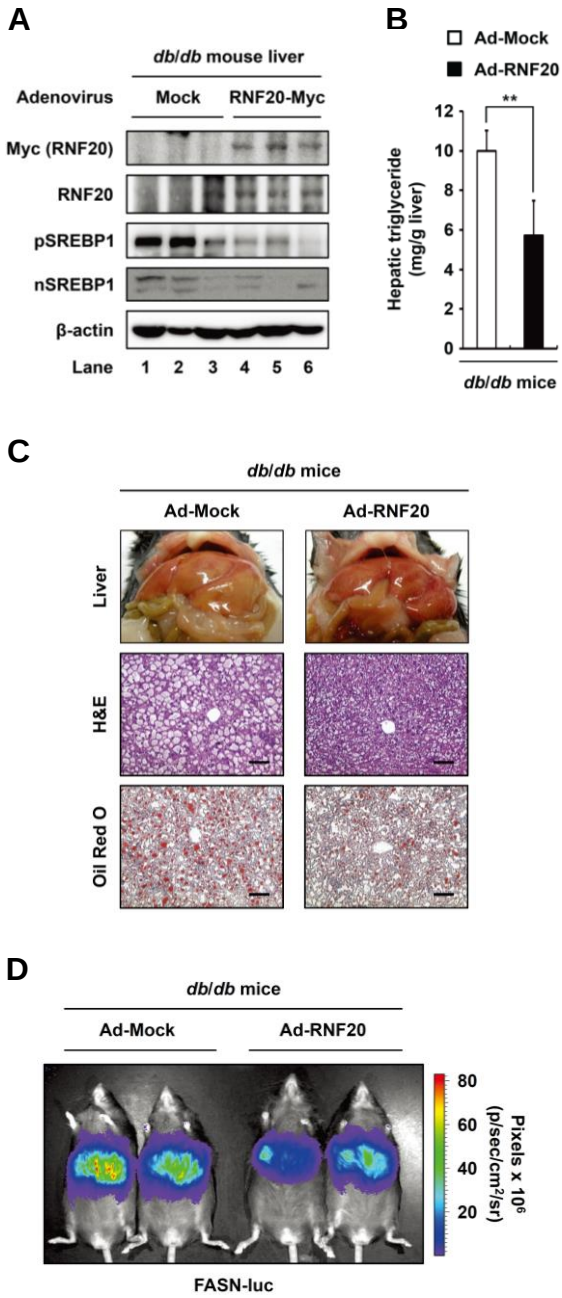
A
db/db mouse liver
Adenovirus
Mock
RNF20-Myc
Myc (RNF20)
RNF20
pSREBP1
nSREBP1
β-actin
Lane 1 2 3 4 5 6
B
Ad-Mock
Ad-RNF20
**
Hepatic triglyceride (mg/g liver)
12
10
8
6
4
2
0
db/db mice
C
db/db mice
Ad-Mock
Ad-RNF20
Liver
H&E
Oil Red O
D
db/db mice
Ad-Mock
Ad-RNF20
80
60
40
20
Pixels x 10^6 (p/sec/cm²/sr)
FASN-luc

Figure 20. RNF20 overexpression improved glucose intolerance in *db*/*db* mice. Nine-week-old male *db*/*db* mice were infected through the tail vein with adenovirus encoding GFP or RNF20 (adenoviral dose of 2×10^{10} viral particles per mouse). **(A)** The relative mRNA levels of various lipogenic genes in the livers of *db*/*db* mice infected with Ad-Mock or Ad-RNF20. Each mRNA level was determined by qRT-PCR analyses and normalized to the TBP mRNA level. Each relative mRNA level is presented as a ratio relative to the Ad-Mock-infected *db*/*db* control group. $n = 3$ for each group. $^{*}P < 0.05$ and $^{**}P < 0.01$ were considered significant (vs. the Ad-Mock control group). **(B)** The relative mRNA levels of PPARα and ChREBP pathway genes in the livers of *db*/*db* mice infected with Ad-Mock or Ad-RNF20. Each mRNA level was determined by qRT-PCR analyses and normalized to the TBP mRNA level. $n = 3$ for each group. **(C)** *db*/*db* mice were infected with Ad-Mock or Ad-RNF20 and subjected to oral glucose tolerance test. $n = 5$ at each time point. $^{*}P < 0.05$ and $^{**}P < 0.01$ were considered significant (vs. the Ad-Mock control group). And this result was confirmed by area-under-the-curve (AUC) analysis.

Figure 20

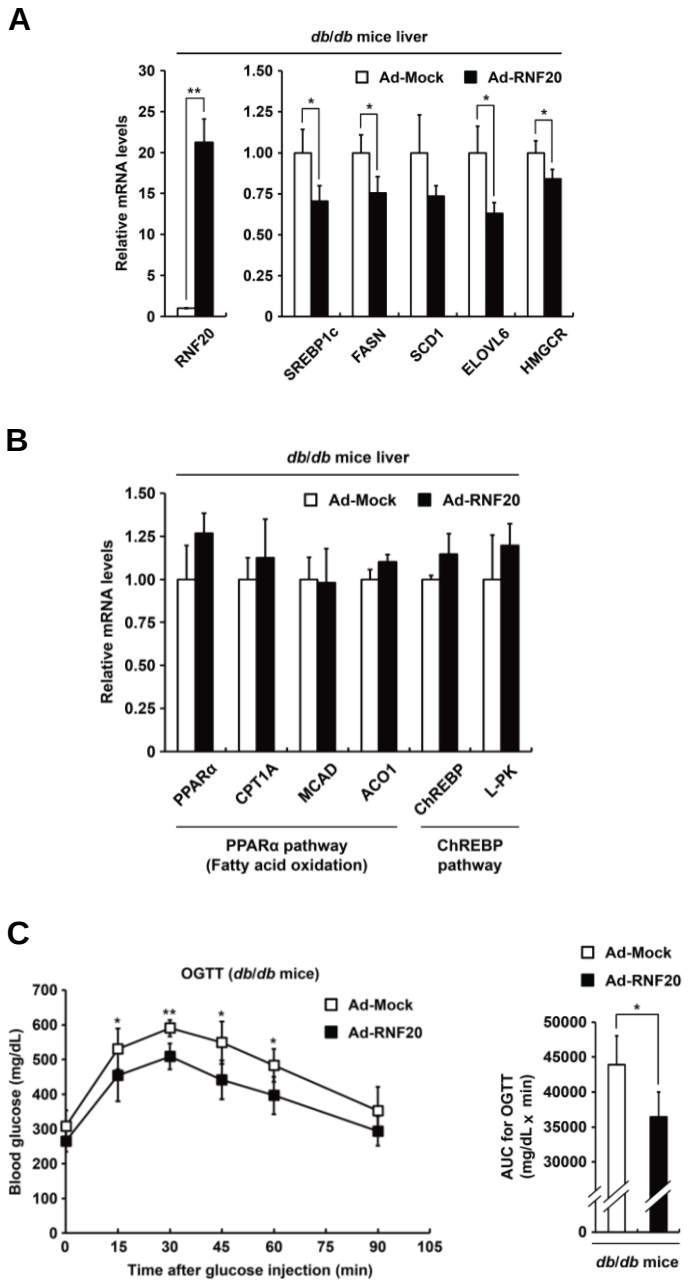
A
db/db mice liver
Ad-Mock
Ad-RNF20
Relative mRNA levels
RNF20
SREBP1c
FASN
SCD1
ELOVL6
HMGCR
B
db/db mice liver
Ad-Mock
Ad-RNF20
Relative mRNA levels
PPARα
CPT1A
MCAD
ACO1
ChREBP
L-PK
PPARα pathway
(Fatty acid oxidation)
ChREBP
pathway
C
OGTT (db/db mice)
Ad-Mock
Ad-RNF20
Blood glucose (mg/dL)
Time after glucose injection (min)
AUC for OGTT
(mg/dL x min)
db/db mice

RNF20 might also affect the regulation of whole body energy metabolisms such as lipid and glucose.

Discussion

Due to its key roles in lipid metabolism, several metabolic diseases are associated with SREBP1c dysregulation. Both animal models and human subjects with obesity and diabetes mellitus often suffer from hepatic steatosis and hyperlipidemia, accompanied by elevated SREBP1c (Li et al., 2005; Marchesini et al., 2001; Muoio and Newgard, 2006). Thus, elucidation of the molecular mechanisms of SREBP1c function and its lipogenic activity under physiological conditions is important. SREBP1c is controlled by several different mechanisms, including transcriptional regulation, proteolytic maturation and post-translational modifications (Giandomenico et al., 2003; Hirano et al., 2003; Hirano et al., 2001; Kim et al., 2004; Li et al., 2011; Ponugoti et al., 2010; Sundqvist et al., 2005). It has been reported that PKA, one of the fasting-induced kinases, phosphorylates SREBP1c and consequently suppresses lipogenic activity (Lu and Shyy, 2006). However, the factors that are involved in SREBP1c degradation under fasting conditions are poorly understood. Here, I demonstrated that SREBP1c protein is ubiquitinated and degraded by an E3 ubiquitin ligase concurrent with PKA activation during fasting (Figure 21).

RNF20 was first identified as yeast Bre1 and possesses a RING finger domain that primarily functions as an E3 ligase for histone H2B monoubiquitination, which regulates transcription of certain genes (Hwang et al., 2003; Kim et al., 2005; Wood et al., 2003). In addition, it has been reported that knockdown of RNF20 leads to abrogation of H2B monoubiquitination and elevated expression of several proto-oncogenes for tumorigenesis, indicating that RNF20 could act as a tumor suppressor protein (Shema et al., 2011; Shema et al., 2008).

Figure 21. Model illustrating the regulatory pathway for RNF20-mediated degradation of SREBP1c upon PKA activation. RNF20 physically interacts with SREBP1c, leading to degradation of SREBP1c via ubiquitination. RNF20 represses SREBP1c activity and turns off the expression of lipogenic program in hepatocytes. Furthermore, PKA activation enhances the expression of RNF20 and potentiates the ubiquitination of SREBP1c. Taken together, RNF20-induced SREBP1c ubiquitination downregulates hepatic lipogenic activity upon PKA activation.

Figure 21

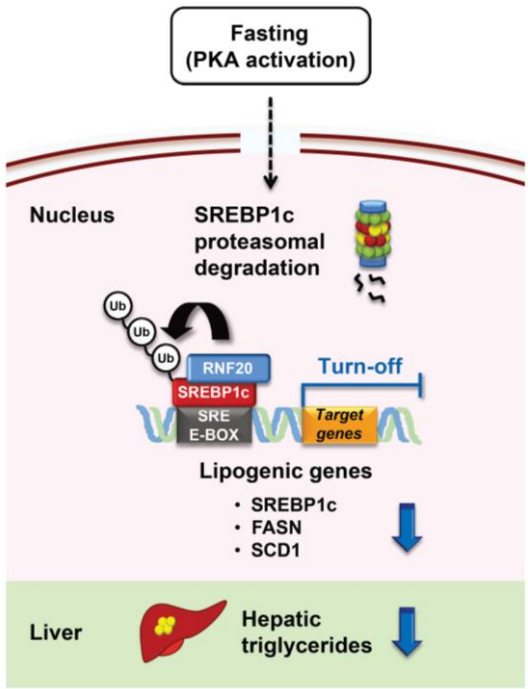
Fasting
(PKA activation)
Nucleus
SREBP1c
proteasomal
degradation
Ub
Ub
Ub
RNF20
SREBP1c
SRE
E-BOX
Turn-off
Target
genes
Lipogenic genes
• SREBP1c
• FASN
• SCD1
Liver
Hepatic
triglycerides

However, to date, there is no report that RNF20 could selectively regulate hepatic lipid metabolism. In this work, I have identified that RNF20 would act as a negative regulator of hepatic lipid metabolism in a SREBP1c-dependent pathway. Several lines of evidence from *in vitro* and *in vivo* data support the above idea. First, ectopic expression of RNF20 repressed SREBP1c and lipogenic gene expression in primary hepatocytes (Figure 12A) and the mouse liver (Figures 17D and 20A). Second, the level of nuclear SREBP1 protein and the expression of its target genes were increased by RNF20 knockdown in primary hepatocytes, accompanied by augmentation of intracellular lipid accumulation (Figures 13 and 14). Moreover, the mRNA levels of other lipogenic factors, such as PPARγ, LXRα and ChREBP, and fatty acid oxidation pathway genes were not significantly altered by RNF20-overexpressing or suppressing conditions (Figures 13A, 14C, 17D, and 20B), indicating that RNF20 would control hepatic lipid metabolism through SREBP1c modulation.

In order to examine the effect of RNF20 on other SREBP isoforms such as SREBP1a and 2, I have tested the effect of RNF20 on degradation of SREBP1a and 2. As shown in Figure 22, RNF20 was also able to induce the degradation of nuclear SREBP1a and 2, implying that RNF20 may regulate the stability of all isoforms of SREBP proteins, at least, *in vitro* cell culture system. Although RNF20 may influence hepatic lipid metabolism via SREBP1a, 1c and/or 2, several current *in vitro* and *in vivo* data supported the idea that hepatic lipid metabolism would be primarily regulated by SREBP1c rather than 1a or 2 (Figures 12A, 13A, 16A, and 17D). Nevertheless, future studies are necessary to clarify whether RNF20 might be involved in the regulation of other SREBP isoforms *in vivo*.

Figure 22. RNF20 regulates the stability of all isoforms of SREBP proteins. HEK293T cells were co-transfected with Myc-SREBP1a, Myc-SREBP1c, Myc-SREBP2 and/or Flag-RNF20 expression vectors. Total cell lysates were subjected to SDS-PAGE followed by western blotting analyses with the indicated antibodies.

Figure 22

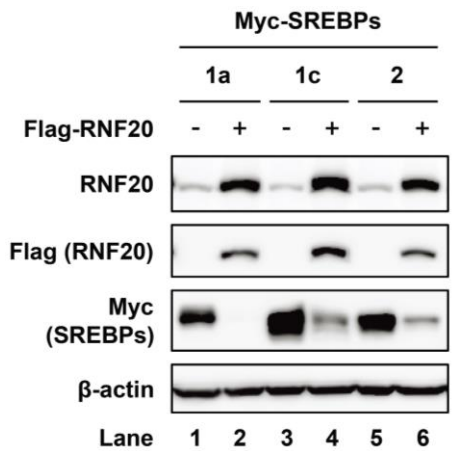
Myc-SREBPs
1a
1c
2
Flag-RNF20
- + - + - +
RNF20
Flag (RNF20)
Myc
(SREBPs)
β-actin
Lane 1 2 3 4 5 6

Next, to test the possibility that the expression of hepatic RNF20 might be altered in pathophysiological conditions, I have examined the mRNA level of hepatic RNF20 by comparison with *db*/+ vs. *db*/*db* and normal-chow diet vs. high-fat diet fed mice. Although the levels of lipogenic genes such as *SREBP1c*, *FASN*, and *SCD1* were increased in the liver of insulin-resistant mouse models, the level of hepatic RNF20 was not significantly altered (Figures 23A and 23B). Thus, it is likely that RNF20 might regulate lipogenic activity upon hormonal changes in normal conditions rather than pathophysiological conditions. However, since overexpression of hepatic RNF20 markedly improved glucose intolerance in diabetic *db*/*db* mice (Figure 20C), I cannot exclude the possibility that hepatic RNF20 might affect glucose metabolism *in vivo*. Further studies are required to understand the detail mechanisms for the role of RNF20 in whole body energy homeostasis.

Recently, it has been demonstrated that SREBP1c is dynamically modified by various post-translational modifications. For example, SIRT1 promotes the deacetylation-mediated ubiquitination of SREBP1c and represses lipogenic activity during fasting (Ponugoti et al., 2010; Walker et al., 2010). Additionally, another study showed that fasting-induced cyclin-dependent kinase 8 (CDK8) phosphorylates and sequentially degrades SREBP1c (Zhao et al., 2012). Although it is unknown whether RNF20-mediated ubiquitination of SREBP1c might be required for prerequisite post-translational modifications under catabolic conditions, I cannot exclude the possibility that any modification of SREBP1c might change the association with an E3 ligase activity of RNF20 during fasting.

Figure 23. The expression of RNF20 is not altered in mouse liver under obese and diabetic conditions. (A) Ten-week-old male *db*/+ and *db*/*db* mice were sacrificed and isolated the liver tissues in fed states. The mRNA levels of RNF20, SREBP1c, FASN, and SCD1 were determined by qRT-PCR analyses. The level of cyclophilin mRNA was used for normalization. $n = 3$ for each group. $*P < 0.05$ and $**P < 0.01$ were considered significant. **(B)** Eight-week-old male C57BL/6 mice were fed normal chow diet (NCD) and then were administered a 60% high-fat diet (HFD) for ten weeks. Then, on the day of sacrifice, all of the HFD-fed mice were compared to age-matched NCD-fed mice. In the mouse liver, the mRNA levels of RNF20, SREBP1c, SCD1, and IL-6 were determined by qRT-PCR analyses. The level of cyclophilin mRNA was used for normalization. $n = 2$ for each group. $*P < 0.05$ and $**P < 0.01$ were considered significant. IL-6, interleukin-6.

Figure 23

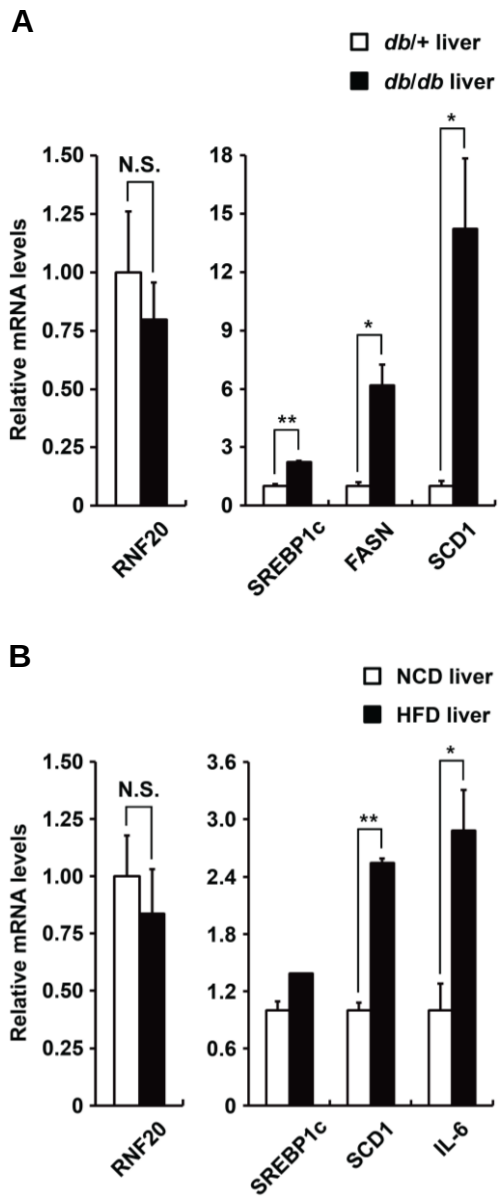
A
db/+ liver
db/db liver
Relative mRNA levels
1.50
1.25
1.00
0.75
0.50
0.25
0
N.S.
18
15
12
9
6
3
0
**
*
*
RNF20
SREBP1c
FASN
SCD1
B
NCD liver
HFD liver
Relative mRNA levels
1.50
1.25
1.00
0.75
0.50
0.25
0
N.S.
3.6
3.0
2.4
1.8
1.2
0.6
0
**
*
RNF20
SREBP1c
SCD1
IL-6

In addition to RNF20, FBXW7 is another E3 ubiquitin ligase for SREBP1 (Sundqvist et al., 2005). FBXW7-dependent SREBP1 degradation requires for GSK-3β-mediated phosphorylation of SREBP1 (Kim et al., 2004; Sundqvist et al., 2005). It is of interest to note that RNF20 would induce the ubiquitination and degradation of SREBP1c upon PKA activation. In contrast, the expression level of FBXW7 was not altered by nutritional states such as feeding and fasting (Figure 15A). Furthermore, PKA activation did not change the level of FBXW7. Given that PKA plays a crucial role in immediate catabolic responses, PKA activation with forskolin significantly decreased lipogenic gene expression with an increase in RNF20 in primary hepatocytes, whereas suppression of RNF20 reversed the effect of forskolin on lipogenic gene expression (Figure 16A), indicating that RNF20 might mediate the PKA signaling cascade to downregulate hepatic lipid metabolism via SREBP1c degradation. Additionally, it has been reported that suppression of FBXW7 *in vivo* causes fatty liver through the induction of PPARγ rather than SREBP1c (Kumadaki et al., 2011). On the contrary, RNF20 overexpression did not affect the protein levels of PPARγ and LXRα (Figure 24), implying that RNF20 functions as a "turn-off" switch in hepatic lipogenesis through the regulation of SREBP1c, but not PPARγ, protein stability. Therefore, these data clearly support the hypothesis that RNF20 acts as a negative regulator of SREBP1c and hepatic lipogenesis under catabolic conditions.

Here, I have elucidated a novel mechanism of ubiquitination and degradation of SREBP1c by RNF20 during nutritional deprivation (Figure 21). It is plausible to speculate that RNF20 is a suppressor of hepatic lipogenesis through the downregulation of SREBP1c upon PKA activation. Furthermore, these data

Figure 24. RNF20 overexpression did not affect the protein levels of PPARγ and LXRα. HEK293T cells were co-transfected with Myc-PPARγ, Myc-LXRα and/or Flag-RNF20 expression vectors. Total cell lysates were subjected to SDS-PAGE followed by western blotting analyses with the indicated antibodies.

Figure 24

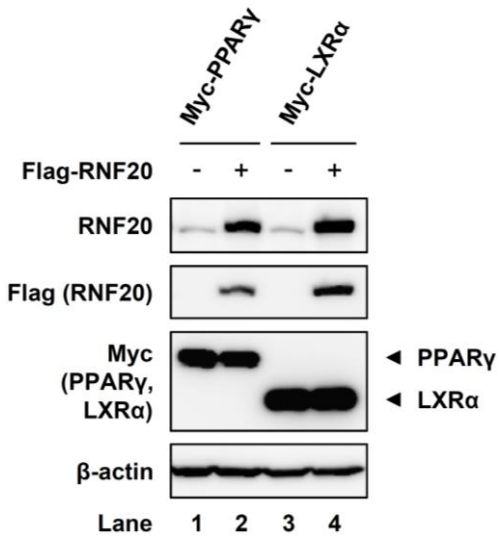
Myc-PPARγ
Myc-LXRα
Flag-RNF20
- + - +
RNF20
Flag (RNF20)
Myc
(PPARγ,
LXRα)
◄ PPARγ
◄ LXRα
β-actin
Lane 1 2 3 4

provide a clue to understand how SREBP1c is rapidly regulated by fasting signals to prevent excess lipid metabolism. Because there is a positive correlation between lipogenic activity and metabolic complications such as obesity, non-alcoholic fatty liver disease (NAFLD), and certain cancers, it is likely that treatments that activate RNF20 might be useful tools for ameliorating metabolic disorders associated with increased lipid metabolism.

CHAPTER TWO:

Ring finger protein 20 downregulation promotes tumorigenesis by sterol regulatory element-binding protein 1c-mediated lipogenesis and cell cycle regulation in clear cell renal cell carcinoma

Abstract

In cancer cells, elevated lipid metabolism plays an important role by providing building blocks for tumor growth. Particularly, clear cell renal cell carcinoma (ccRCC), the most common subtype of kidney cancers, is characterized by ectopic intracellular lipid accumulation. However, the relationship between lipid metabolism and tumorigenesis in ccRCC has not been thoroughly elucidated. Here I demonstrate that ring finger protein 20 (RNF20) acts as a tumor suppressor in ccRCC. In ccRCC tumor tissues, RNF20 is downregulated, accompanied with sterol regulatory element-binding protein 1c (SREBP1c) activation and poor prognosis. In ccRCC cells, RNF20 overexpression repressed lipogenesis and cell proliferation by inhibiting SREBP1c. Notably, SREBP1c regulates cell cycle progression by inducing pituitary tumor-transforming gene 1 (*PTTG1*) as a novel SREBP1c target gene. Moreover, suppression of SREBP1 by either knockdown or small-molecule inhibitor betulin attenuated cell proliferation with decreased expression of PTTG1 and several cell-cycle regulators in ccRCC cells. Furthermore, xenograft studies showed that ectopic RNF20 expression reduced tumor growth and lipid storage. Taken together, these data suggest that RNF20 suppresses tumorigenesis in ccRCC by regulating SREBP1c-dependent lipogenesis and PTTG1 axes.

Introduction

Increased demands for building blocks and membrane biogenesis during excessive cell proliferation of cancer cells are satisfied by complex metabolic reprogramming (DeBerardinis et al., 2008; Schulze and Harris, 2012). Especially, most lipid metabolites are derived from *de novo* lipogenesis in cancer cells rather than from extracellular lipid uptake (Medes et al., 1953; Ookhtens et al., 1984). Moreover, it has been reported that lipogenesis and lipid accumulation are upregulated in various cancers (Kuhajda, 2000; Menendez and Lupu, 2007). Ectopic lipid accumulation is a hallmark of clear cell renal cell carcinoma (ccRCC), which is the most common subtype of kidney cancers (Rezende et al., 1999; Valera and Merino, 2011). To date, the primary etiology of ccRCC follows the loss or inactivation of von Hippel-Lindau (*VHL*) and a consequent activation of hypoxia-inducible factor (HIF) (Kaelin, 2008; Shen and Kaelin, 2013). Recently, it has been reported that HIF2α-selective antagonist, PT2399, effectively suppresses tumorigenesis in ccRCC (Chen et al., 2016; Cho et al., 2016). Although lipid and glucose metabolic pathways are frequently dysregulated in ccRCC (Linehan and Ricketts, 2013; Qiu et al., 2015), the underlying tumorigenic mechanisms that lead to aberrant lipogenesis in ccRCC remain poorly understood.

Ring finger protein 20 (RNF20) is an E3 ubiquitin ligase that plays various roles in transcription regulation, DNA damage responses, stem cell differentiation, and lipid metabolism (Lee et al., 2014b; Nakamura et al., 2011; Shema et al., 2008). RNF20 promotes the monoubiquitination of histone H2B, which regulates the transcription of a subset of genes and contributes to chromatin remodeling (Minsky et al., 2008; Shema et al., 2008). Moreover, it has been suggested that RNF20 acts

as a tumor suppressor in inflammation-associated cancer (Tarcic et al., 2016).

I demonstrated that hepatic RNF20 is an E3 ubiquitin ligase for sterol regulatory element-binding protein 1c (SREBP1c), which is a key transcription factor in *de novo* lipogenesis (Brown and Goldstein, 1997; Tontonoz et al., 1993). RNF20 promotes polyubiquitination and degradation of SREBP1c upon PKA activation, thereby suppressing hepatic lipid metabolism (Lee et al., 2014b). In mammals, SREBP1a and SREBP1c are encoded by the *SREBF1* gene, whereas SREBP2 is encoded by the *SREBF2* gene (Brown and Goldstein, 1997; Horton et al., 2002). SREBP1 primarily activates genes that are involved in fatty acid synthesis, including fatty acid synthase (*FASN*), stearoyl-CoA desaturase 1 (*SCD1*), and long-chain fatty acid elongase (*ELOVL6*), whereas SREBP2 mainly promotes the expression of genes for cholesterol homeostasis, such as HMG-CoA reductase (*HMGCR*) (Brown and Goldstein, 1997; Horton et al., 2002). It has been reported that activated SREBP1c upregulates lipogenic genes and enhances lipogenesis in certain cancers (Griffiths et al., 2013; Guo et al., 2014). In addition, SREBP1c promotes lipid metabolism and tumor development, potentiating progression, migration, and leading to poor prognosis for several cancers (Guo et al., 2009; Huang et al., 2012). However, the molecular mechanisms by which SREBP1c promotes cancer cell proliferation are not clearly understood.

In this study, I uncover that RNF20 suppressed ccRCC tumorigenesis by inhibiting SREBP1c, and RNF20 downregulation stimulated SREBP1c-mediated lipogenesis and cell proliferation. In accordance with these data, genetic and pharmacologic inhibition of SREBP1 decreased lipogenesis and cell growth in ccRCC cells. Notably, downregulation of RNF20 in ccRCC cells augmented cell

cycle progression by activating SREBP1c-mediated pituitary tumor-transforming gene 1 (PTTG1). Together, these findings suggest that RNF20 functions as a tumor suppressor by inhibiting SREBP1c-dependent lipogenesis and PTTG1 signaling in ccRCC.

Materials and Methods

Cell culture and reagents

ACHN, A498, HEK293, Caki-2, and human primary renal cortical epithelial (HRCE) cells were obtained from American Type Culture Collection (ATCC). ACHN and A498 cells were grown in in Eagle's minimum essential medium (MEM; HyClone, Logan, UT; #SH30024.01) supplemented with 10% fetal bovine serum (FBS; HyClone; #SH30919.03) and penicillin (100 U/ml)-streptomycin (100 μg/ml). HEK293 and Caki-2 cells were grown in Dulbecco's modified Eagle medium (DMEM; HyClone; #SH30243.01) supplemented with 10% FBS and penicillin-streptomycin. HRCE cells were cultured in renal epithelial cell basal medium (ATCC; #PCS-400-030) with the following supplements: 0.5% FBS, 10 nM triiodothyronine, 10 ng/ml epidermal growth factor, 100 ng/ml hydrocortisone, 5 μg/ml insulin, 1 μM epinephrine, 5 μg/ml transferrin, 2.4 mM L-Alanyl-L-Glutamine, and penicillin-streptomycin. All cells were cultured at 37℃ in a 5% CO_2 incubator. Betulin and BODIPY 493/503 were purchased from Sigma-Aldrich (St. Louis, MO; #B8936 and #D3922, respectively). C75 and TOFA were obtained from Abcam (Cambridge, MA; #ab141397 and #ab141578, respectively). Propodium iodide was provided by BD Biosciences (San Jose, CA; #51-66211E).

Human ccRCC samples

Fresh frozen human ccRCC and matched normal kidney tissue samples were obtained from the Seoul National University Hospital (SNUH). The Institutional Review Board at SNUH approved this study (approval number:

H-1501-011-636). Informed consent documents from patients were not required due to the retrospective nature of the study.

TCGA RNA-Seq analysis

RNA sequencing data, *VHL* mutation status, and clinicopathological data for 533 ccRCC and 72 normal kidney samples were downloaded from TCGA ccRCC project (http://cancergenome.nih.gov) in September 2015. Box and whisker plots are presented with 1–99th percentiles (bars), 25–75th percentiles (box), and median values (line in box).

Survival analysis

Available patient survival data were obtained from TCGA ccRCC project. Patients were ranked on tumor expressions of the genes shown in TCGA RNA-Seq data. The top half of ranked patients was defined as the 'high' group, and the lower half were defined as the 'low' group. Overall survival curves were estimated using Kaplan–Meier survival analyses, and survival outcomes between the two groups were compared using the Log-rank test.

Tissue arrays and immunohistochemistry

Immunohistochemistry was performed on tissue microarrays of ccRCC and normal kidney tissue sections (SuperBioChips Laboratories, South Korea; #CL2) according to the supplier's protocol (Ventana Medical Systems; #760-700). Briefly, the streptavidin–biotin complex method was used to detect RNF20 and

SREBP1 in immunohistochemistry analyses with corresponding primary antibodies from Abcam (#ab32629; 1:30) and BD Biosciences (#557036; 1:25), respectively.

Preparation of recombinant adenovirus

Adenovirus plasmids were constructed as previously described (Lee et al., 2014b). Briefly, nuclear rat SREBP1c encoding amino acids 1–403, and full-length mouse RNF20 cDNAs were incorporated into the AdTrack-CMV shuttle vector and recombinant vectors were generated using Ad-Easy adenoviral vector systems. An adenovirus encoding GFP only was used as a negative control in all experiments. Adenoviruses were amplified in HEK293A cells and were purified using CsCl gradient centrifugation as described previously (Becker et al., 1994).

Lentivirus production and viral transduction

Full-length RNF20 or nuclear SREBP1c cDNAs with Flag-tags were incorporated into the lentiviral vector pLVX-EF1α-AcGFP1-N1 (Clontech, Mountain View, CA; #631983). Lentiviruses were then transfected into HEK293T cells with the indicated expression vectors, pAX2 (Addgene, Cambridge, MA; #35002) and pMD2.G (Addgene; #12259) using Lipofectamine 2000 Reagent (Invitrogen, Grand Island, NY; #11668-027). At 48 hours after transfection, viruses were harvested and filtered through 0.45-μm filters. Subsequently, ACHN cells were incubated with medium containing virus and 8 μg/ml polybrene (Sigma-Aldrich; #107689) for 18 hours. Infected cells were then allowed to recover for 48 hours before selection of puromycin resistant colonies for experiments.

Western blot analysis

Cells and tissues were lysed on ice in modified radioimmunoprecipitation assay (RIPA) buffer containing 150 mM NaCl, 50 mM Tris-HCl (pH 7.4), 1% NP-40, 0.25% Na-deoxycholate, 1 mM EDTA, 1 mM PMSF, and protease inhibitor cocktail (GeneDEPOT, Katy, TX; #P3100). Equal amounts of protein from each sample were separated on SDS-PAGE gels and were then transferred to polyvinylidene difluoride membranes (Merck Millipore, Germany; #IPVH00010). After transfer, membranes were blocked with 5% non-fat milk or 3% bovine serum albumin in TBS containing 0.1% Tween-20 (TBST) and were probed with primary antibodies against RNF20 (Abcam; #ab32629; 1:1,000), SREBP1 (BD Biosciences; #557036; 1:1,000), FASN (Cell Signaling, Danvers, MA; #3180; 1:1,000), SCD1 (Santa Cruz Biotechnology, Dallas, TX; #SC-58420; 1:500), PTTG1 (Thermo Fisher Scientific, Waltham, MA; #MS-1511-P0; 1:1,000), Cyclin B1 (Santa Cruz Biotechnology; #SC-752; 1:500), Cyclin E (Santa Cruz Biotechnology; #SC-198; 1:500), Myc-tag (Cell Signaling; #2276; 1:1,000), Flag-tag (Sigma-Aldrich; #F1804; 1:1,000), or β-actin (Sigma-Aldrich; #A5316; 1:2,000). Subsequently, membranes were incubated with horseradish peroxidase-conjugated secondary anti-rabbit IgG or anti-mouse IgG antibodies (Sigma-Aldrich; #A0545 and #A9044, respectively), and protein bands were visualized using enhanced chemiluminescence with a LuminoImager (LAS-3000).

RNA isolation and quantitative RT-PCR

Total RNA was isolated using TRIzol Reagent (Thermo Fisher Scientific; #15596026). Subsequently, equal amounts of RNA were subjected to cDNA

synthesis using RevertAid reverse transcriptase (Thermo Fisher Scientific; #EP0441), and relative mRNA expression was evaluated using a CFX Real-Time System (Bio-Rad Laboratories, Hercules, CA) and was normalized to GAPDH or cyclophilin mRNA expression. The primer sequences used for quantitative real-time PCR (qRT-PCR) analyses are listed in Table 3.

siRNA transfection

Small-interference RNA (siRNA) duplexes for RNF20, SREBP1, PTTG1, and FASN were synthesized by Bioneer (South Korea). The sequence information for siRNAs is provided in Table 4. ACHN cells were transfected using Lipofectamine RNAiMAX Reagent (Invitrogen; #13778-150) according to the manufacturer's protocol.

Cell proliferation assays with CCK-8 reagent

Cell proliferation rates were determined using a Cell Counting Kit-8 (CCK-8) reagent as described previously (Kim et al., 2010). Briefly, cell growth curves were generated using the sensitive colorimetric assay for viable cells according to the manufacturer's protocol (Dojindo Molecular Technologies, Rockville, MD; #CK04-11).

Colony formation assays

ACHN cells with lentiviral RNF20 and/or SREBP1c overexpression were seeded on 6-well plates (5,000 cells/well). Cells were cultured at 37℃ in 5% CO_2

Table 3. Primers sequences for qRT-PCR

Species	Gene	Sequence (5' to 3')	Direction
Human	RNF20	**CACAGGAGAGCCAAAAGGAG**	Forward
		GCATCCTCATCAGCCATTTT	Reverse
	SREBP1c	**CCATGGATTGCACTTTCGAA**	Forward
		CCAGCATAGGGTGGGTCAAA	Reverse
	FASN	**GCCTACACCCAGAGCTACCG**	Forward
		GCCATGGTACTTGGCCTTG	Reverse
	ACC1	**CAACGAGATTTCACTGTGGCT**	Forward
		TTCTGCATTGGCTTTAAGGTCT	Reverse
	SCD1	**ACAAACCTGGCTTGCTGATG**	Forward
		CCACAGCTCCAAGTGAAACC	Reverse
	ELOVL6	**CTCTGGTCTCTGACCCTTGC**	Forward
		CTCCTAGTTCGGGTGCTTTG	Reverse
	SREBP2	**CAAGCTTCTAAAGGGCATCG**	Forward
		GGCTCATCTTTGACCTTTGC	Reverse
	HMGCR	**ATTTGGCAGCTCAGCCATT**	Forward
		TGAGGAGAAGGATCAGCTATCC	Reverse
	PCNA	**CATGGGCGTGAACCTCACC**	Forward
		CACAGCTGTACTCCTGTTCTGG	Reverse
	Cyclin A	**CCTTAGGGAAATGGAGGTTAAA**	Forward
		CCAAATGCAGGGTCTCATTC	Reverse
	Cyclin D1	**TTCCTCTCCAAAATGCCAGA**	Forward
		CAGTCCGGGTCACACTTGAT	Reverse
	Cyclin E	**TCAGTGGTGCGACATAGAGAA**	Forward
		TGTCCAGCAAATCCAAGCTG	Reverse
	PTTG1	**GGGTCTGGACCTTCAATCAA**	Forward
		GGCAGGAACAGAGCTTTTTG	Reverse
	GAPDH	**TTCACCACCATGGAGAAGG**	Forward
		CTAAGCAGTTGGTGGTGCAG	Reverse
	Cyclophilin	**TGCTGGACCCAACACAAATG**	Forward
		GTCCACAGTCAGCAATGGTG	Reverse
Mouse	SREBP1c	**GGAGCCATGGATTGCACATT**	Forward
		CAGGAAGGCTTCCAGAGAGG	Reverse
	PTTG1	**GGCATCTAAGGATGGGTTGA**	Forward
		GGGGTTTGCCAGTCTTCATA	Reverse
	TBP	**GGGAGAATCATGGACCAGAA**	Forward
		CCGTAAGGCATCATTGGACT	Reverse

Table 4. Sequences of siRNA oligos

Species	Gene	Sequence (5' to 3')	Direction
Human	RNF20	**GGAUAAAGAGAAAGGCAAA**	Sense
		UUUGCCUUUCUCUUUAUCC	Antisense
	SREBP1	**CCACCGUUUCUUCGUGGAU**	Sense
		AUCCACGAAGAAACGGUGG	Antisense
	PTTG1	**CUCAGAUGAAUGCGGCUGU**	Sense
		ACAGCCGCAUUCAUCUGAG	Antisense
	FASN	**UCAACCUGGACAGCUCACU**	Sense
		AGUGAGCUGUCCAGGUUGA	Antisense

for 7 days, and colonies were then fixed with formaldehyde and were stained with crystal violet.

Cell cycle analysis

Trypsinized cells were washed with phosphate-buffered saline (PBS) and were then fixed in 70% ethanol at 4℃ for 30 minutes. Fixed cells were washed with PBS twice and incubated with propodium iodide (PI) solution containing 0.1% Nonidet P-40, 100 μg/ml RNase, and 2.5 μg/ml PI for 30 minutes. Stained cells were then analyzed by flow cytometry using a FACS Canto II instrument (BD Biosciences), and numbers of cells in each stage were calculated using the ModFit LT^{TM} cell cycle analysis program (Verity Software House) according to the manufacturer's instructions.

Intracellular triglyceride measurements

Intracellular triglycerides were determined in cell lysates using a colorimetric assay, and were expressed as mg of lipid per mg of cellular protein as described previously (Lee et al., 2014b). Briefly, total cell contents were extracted using 5% Triton X-100 and were incubated in a water bath at 80℃ and subsequently cooled to room temperature twice. After centrifugation at 12,000 rpm for 5 minutes at room temperature, supernatants were collected and intracellular triglycerides were assayed using Infinity Triglycerides Reagent (Thermo Fisher Scientific; #TR22321). Values were normalized to total protein contents, which were estimated using a BCA Protein Assay Kit that is compatible with reducing agents (Thermo Fisher Scientific; #23250).

BODIPY staining

ACHN cells were treated with or without betulin (10 μM) for 24 hours, were rinsed twice with PBS, and were then fixed in 4% paraformaldehyde for 10 minutes. Subsequently, fixed cells were washed twice with PBS containing Tween-20, and were stained with fluorescein isothiocyanate (FITC)-conjugated BODIPY 493/503 (Thermo Fisher Scientific; #D3922) for 1 hour in the dark at room temperature. Samples were then stained with a Vectashield solution (Vector Laboratories, Burlingame, CA; #H-1200) containing 4',6-diamidino-2-phenylindole (DAPI) and were observed using a Zeiss LSM 700 confocal microscope (Carl Zeiss, Germany).

PTTG1 reporter and luciferase assays

The PTTG1 luciferase reporter containing −908 to +25 nucleotides from the transcription start site of the human PTTG1 promoter was cloned into a pGL3-basic vector (Promega, Madison, WI; #E1751). HEK293 cells were transiently transfected with various DNA plasmids using the calcium-phosphate method as described previously (Jang et al., 2016). After incubation for 36 hours, transfected cells were harvested and extracted using lysis buffer containing 25 mM Tris-phosphate (pH 7.8), 10% glycerol, 2 mM EDTA, 2 mM DTT, and 1% Triton X-100, and luciferase and β-galactosidase activities were measured according to the manufacturer's protocol (Promega; #E1500). Relative luciferase activity was normalized to β-galactosidase activity in each sample.

Xenograft studies

Subcutaneous xenograft experiments were approved by the Institutional Animal Care and Use Committee (IACUC) of SNUH (IACUC number: 13-0080). Five female BALB/c athymic nude mice (Central Lab Animal, South Korea) were subcutaneously injected in both flanks with 1×10^7 vector control ACHN cells or ACHN cells stably expressing RNF20. Before injections, cells were resuspended in 200 μl of PBS and were mixed with equal volumes of matrigel (Corning, NY; #354234). Following establishment of palpable tumors, tumor sizes were measured once a week using calipers, and tumor volumes were calculated according to the following formula: volume (mm^3) = (length × $width^2$) × $\pi/6$. After transplantation for 5 weeks, mice were killed by CO_2 inhalation, and xenograft tumors were dissected and weighed.

Xenograft tissue samples were fixed in 4% paraformaldehyde, equilibrated in 30% sucrose, and then embedded in OCT (Scigen Scientific, Gardena, CA; #4583). Sections (10 μm) were then cut stained with Hematoxylin and eosin (H&E) and Oil Red O as previously described (Ham et al., 2016). Immunohistochemistry analyses of xenograft tumor sections were performed according to the supplier's protocol (SuperBioChips Laboratories). Briefly, Ki67 and TUNEL proteins were detected using the streptavidin–biotin complex method with primary antibodies against Ki67 (Abcam; #ab66155) and TUNEL (R&D Systems; #4810-30-K). Images were obtained using an EVOS ORIGINAL microscope (Thermo Fisher Scientific; Advanced Microscopy Group) and a Nikon TMS inverted microscope.

Statistical analysis

All results reported in the main and Supplementary figures are presented as mean ± SD or mean ± SEM (for Figures 46B and 46C). Multiple comparisons were performed using one-way analysis of variance (ANOVA), and two-way ANOVA when two conditions were involved. Statistical significance was assessed by the two-tailed Student's *t*-test. Statistical analyses were performed using Prism (GraphPad Software), and differences were considered significant when $P < 0.05$.

Results

RNF20 is downregulated in ccRCC.

Ectopic lipid accumulation is profoundly upregulated in ccRCC (Rezende et al., 1999; Valera and Merino, 2011). Because RNF20 reportedly acts as a negative regulator of *de novo* lipogenesis by inhibiting SREBP1c (Lee et al., 2014b), I investigated whether RNF20 might be dysregulated in ccRCC tumors. As shown in Figure 25A, RNF20 mRNA expression was greatly downregulated in ccRCC tumors compared with that in patient-matched normal kidney tissues. Similarly, RNA-Seq data from the Cancer Genome Atlas (TCGA) show significant reductions in RNF20 mRNA expression in ccRCC tumors (Figure 25B) and indicate that low RNF20 expression is closely correlated with advanced tumor stages (Figure 25C). Furthermore, immunohistochemistry (IHC) analyses showed that RNF20 protein expression was lower in ccRCC tumors than adjacent normal kidney tissues (Figure 25D). In agreement, RNF20 staining data from patient-matched normal kidney and tumor tissues revealed decreased RNF20 expression in ccRCC (Figure 25E). RNF20 expression was also decreased in ccRCC cell lines A498, Caki-2, and ACHN compared with that in human primary renal cortical epithelial (HRCE) and HEK293 normal kidney cells (Figure 25F). In a previous study, the promoter region of RNF20 was selectively hypermethylated in breast cancer tissues (Shema et al., 2008). Thus, to determine whether hypermethylation of RNF20 promoter might downregulate RNF20 expression in ccRCC, I inhibited DNA methyltransferases (DNMTs) using the inhibitor RG108 and determined the expression levels of RNF20 mRNA in ccRCC cells. Treatment with RG108 elevated RNF20 expression in ccRCC cells without affecting HEK293 non-cancer

Figure 25. RNF20 is downregulated in ccRCC. (A) qRT-PCR analyses of RNF20 in patient-matched ccRCC tumor ($n = 9$) and normal kidney ($n = 9$) samples. RNF20 mRNA expression was normalized to those in matched normal kidney samples. **(B)** Normalized RNA-Seq reads of RNF20 in ccRCC tumors ($n = 533$) and normal kidney ($n = 72$) samples. RNA-Seq data were obtained from TCGA ccRCC project. **(C)** RNF20 expression in ccRCC tumors was analyzed according to tumor stages. RNA-Seq data were obtained from TCGA. $^{\#\#}P < 0.01$ versus normal kidney; $^{\#\#\#}P < 0.001$ versus normal kidney. **(D)** Immunohistochemistry (IHC) staining of a representative ccRCC tissue microarray with an RNF20 antibody. **(E)** IHC staining of matched ccRCC tumor and adjacent normal kidney tissues. Representative tissue sections with RNF20 staining. Scale bar, 100 μm. **(F)** RNF20 protein expression in normal kidney cell lines such as human primary renal cortical epithelial (HRCE) and HEK293, and ccRCC cell lines including ACHN, A498, and Caki-2 were determined using western blot analyses.

Figure 25

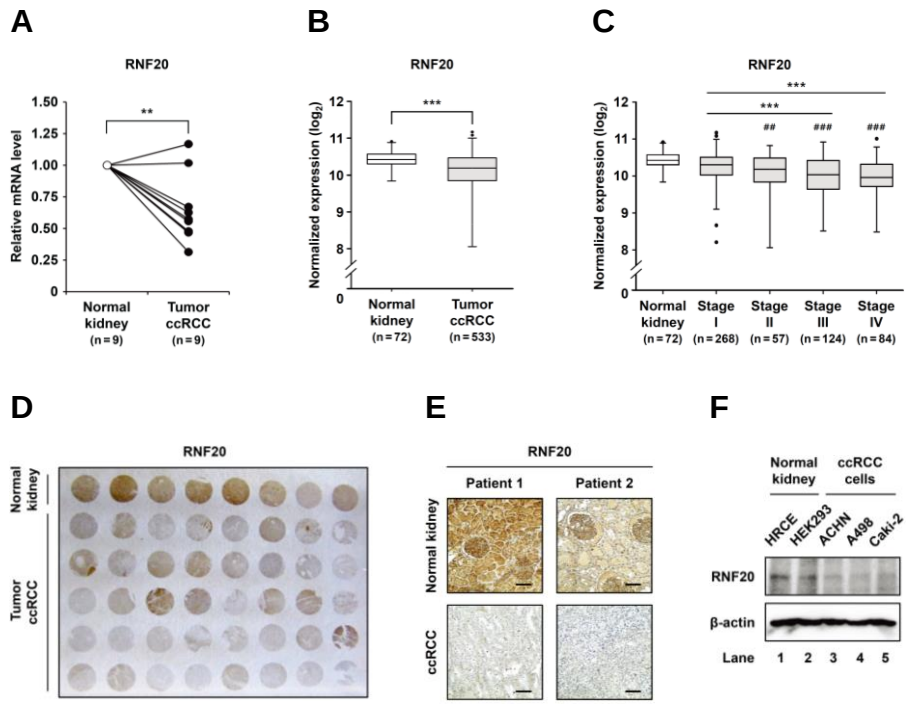
A
RNF20
Relative mRNA level
1.50
1.25
1.00
0.75
0.50
0.25
0
**
Normal kidney (n = 9)
Tumor ccRCC (n = 9)
B
RNF20
Normalized expression (log2)
12
11
10
9
8
0
***
Normal kidney (n = 72)
Tumor ccRCC (n = 533)
C
RNF20
Normalized expression (log2)
***
***
##
###
###
Normal kidney (n = 72)
Stage I (n = 268)
Stage II (n = 57)
Stage III (n = 124)
Stage IV (n = 84)
D
RNF20
Normal kidney
Tumor ccRCC
E
RNF20
Patient 1
Patient 2
Normal kidney
ccRCC
F
Normal kidney
ccRCC cells
HRCE
HEK293
ACHN
A498
Caki-2
RNF20
β-actin
Lane 1 2 3 4 5

Figure 26. The DNA methyltransferase inhibitor RG108 leads to an increase in RNF20 expression in ccRCC cells. (A) ACHN ccRCC cells were treated with or without RG108 (+; 250 μM or ++; 1 mM). After incubation for 48 hours, relative mRNA levels were determined using qRT-PCR. RNF20 mRNA level was normalized to that of cyclophilin gene and is presented relative to that in the vehicle group. Data are presented as mean ± SD of three individual samples. *$P < 0.05$. **(B)** HEK293 cells were incubated with or without RG108 (+; 250 μM or ++; 1 mM) for 48 hours, and relative mRNA levels were determined using qRT-PCR. RNF20 mRNA level was normalized to that of cyclophilin gene and is presented relative to that in the vehicle group. Data are presented as means ± SD of three individual samples. n.s., not significant.

Figure 26

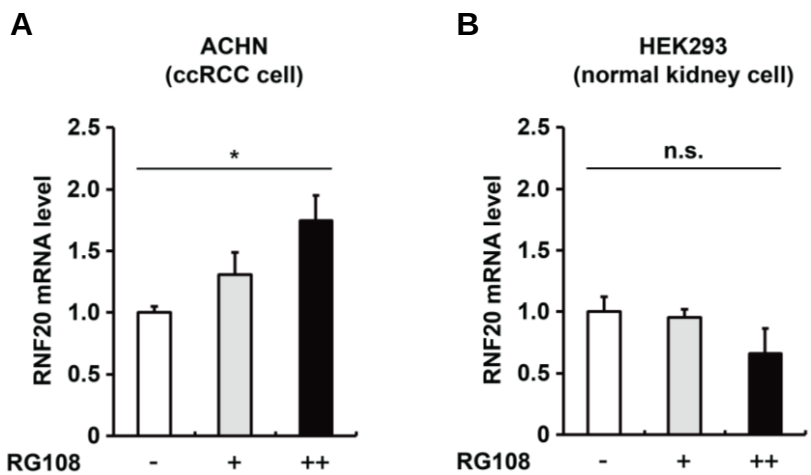
A
ACHN
(ccRCC cell)
RNF20 mRNA level
2.5
2.0
1.5
1.0
0.5
0
*
RG108
-
+
++
B
HEK293
(normal kidney cell)
RNF20 mRNA level
2.5
2.0
1.5
1.0
0.5
0
n.s.
RG108
-
+
++

cells (Figures 26A and 26B). Subsequently, I explored the relationship between RNF20 expression and clinical outcomes, and showed that low expression of RNF20 is significantly correlated with poor survival (Figure 27A). This close correlation between RNF20 and poor prognosis was observed in *VHL* wild-type and in *VHL* mutant ccRCC patients (Figures 27B and 27C). Thus, to evaluate tumorigenic consequences of low RNF20 expression, I determined whether RNF20 might affect cell proliferation in *VHL* wild-type ACHN and *VHL*-depleted A498 ccRCC cells. In these experiments, overexpression of RNF20 suppressed cell proliferation in ACHN and A498 ccRCC cells (Figures 28A and 28B). Conversely, siRNA-mediated suppression of RNF20 increased cell growth in ccRCC cell lines, including ACHN and A498 cells (Figures 28C and 28D). In contrast, neither overexpression nor siRNA-mediated knockdown of RNF20 affected the growth of HRCE and HEK293 normal kidney cells, which have high levels of RNF20 (Figure 29, A-D). These data indicate that RNF20 would act as a tumor suppressor in ccRCC cells independently of *VHL* mutation status.

SREBP1 and lipogenic genes are upregulated in ccRCC and are negatively correlated with RNF20 expression.

Several types of tumors such as glioblastoma, hepatic, prostate, and pancreatic cancers express high levels of SREBP1 and lipogenic genes, which are also positively correlated with malignant progression and worse outcomes (Griffiths et al., 2013; Guo et al., 2014; Guo et al., 2009; Huang et al., 2012). However, it remains unclear whether SREBP1 and lipogenic genes might be

Figure 27. Low expression of RNF20 is correlated with poor survival in ccRCC patients regardless of *VHL* mutation status. (A) Kaplan–Meier survival curves of 532 ccRCC patients enrolled in TCGA database. Patients were divided into two groups according to median RNF20 mRNA levels, and differences were identified using the Log-rank test. **(B** and **C)** Survival analyses were stratified according to *VHL* mutation status.

Figure 27

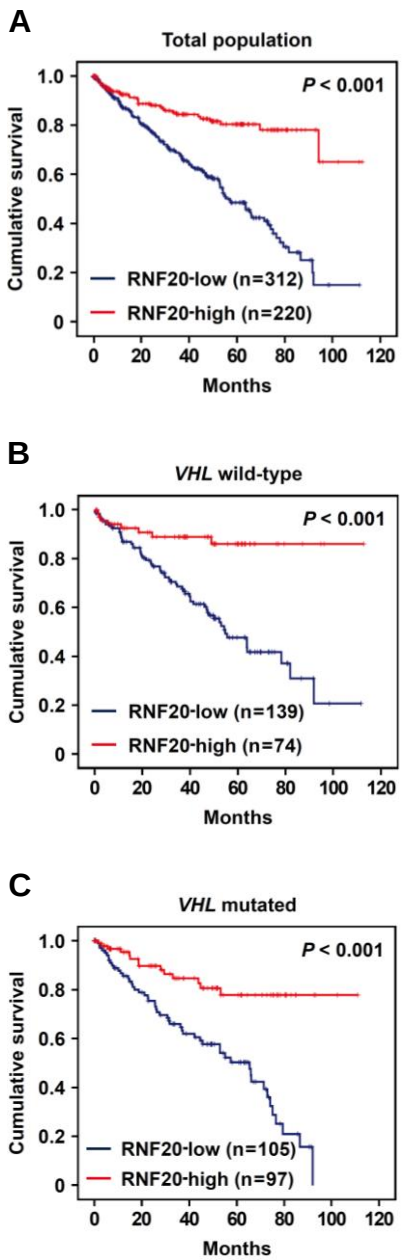
A
Total population
P < 0.001
Cumulative survival
1.0
0.8
0.6
0.4
0.2
0
RNF20-low (n=312)
RNF20-high (n=220)
0 20 40 60 80 100 120
Months
B
VHL wild-type
P < 0.001
Cumulative survival
1.0
0.8
0.6
0.4
0.2
0
RNF20-low (n=139)
RNF20-high (n=74)
0 20 40 60 80 100 120
Months
C
VHL mutated
P < 0.001
Cumulative survival
1.0
0.8
0.6
0.4
0.2
0
RNF20-low (n=105)
RNF20-high (n=97)
0 20 40 60 80 100 120
Months

Figure 28. RNF20 exhibits tumor-suppressive roles in ccRCC. (A) ACHN and A498 ccRCC cells were infected with adenovirus containing GFP alone (Mock) or Myc-RNF20. After infection for 24 hours, total cell lysates were subjected to SDS-PAGE and western blotting analyses with indicated antibodies. **(B)** ACHN and A498 human ccRCC cell lines were infected with adenovirus containing GFP alone (Mock) or RNF20, and proliferation rates were monitored using CCK-8 assays. Data are presented as mean ± SD of five individual samples. **(C)** ACHN and A498 ccRCC cells were transfected with nonspecific control siRNA (siControl) or RNF20-specific siRNA (siRNF20), and RNF20 expression was determined in western blotting analyses. **(D)** ACHN and A498 ccRCC cells were transfected with siControl or siRNF20, and relative growth rates were measured using CCK-8 assays. CCK-8, Cell Counting Kit-8; *$P < 0.05$; **$P < 0.01$.

Figure 28

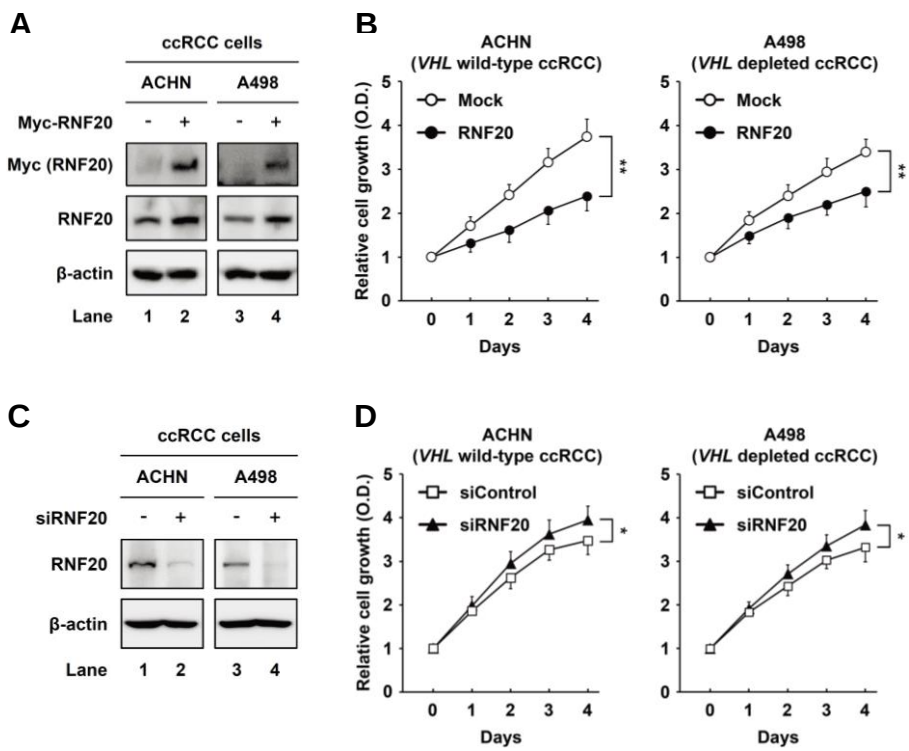
A
ccRCC cells
ACHN
A498
Myc-RNF20
- + - +
Myc (RNF20)
RNF20
β-actin
Lane 1 2 3 4
B
ACHN
(VHL wild-type ccRCC)
Mock
RNF20
Relative cell growth (O.D.)
Days
**
A498
(VHL depleted ccRCC)
Mock
RNF20
Days
**
C
ccRCC cells
ACHN
A498
siRNF20
- + - +
RNF20
β-actin
Lane 1 2 3 4
D
ACHN
(VHL wild-type ccRCC)
siControl
siRNF20
Relative cell growth (O.D.)
Days
*
A498
(VHL depleted ccRCC)
siControl
siRNF20
Days
*

Figure 29. RNF20 does not affect proliferation of normal kidney cells with high basal RNF20 expression. (A) Human primary renal cortical epithelial (HRCE) and HEK293 cells were infected with adenovirus containing Mock or Myc-RNF20, and cell lysates were examined using western blotting analyses. **(B)** HRCE and HEK293 cells were infected with adenoviral RNF20, and cell proliferation rates were monitored using CCK-8 assays. Data are presented as means ± SD of five individual samples. **(C)** HRCE and HEK293 cells were transfected with siControl or siRNF20, and cell lysates were then analyzed using western blotting. **(D)** HRCE and HEK293 cells were transfected with siRNF20, and relative cell growth rates were measured using CCK-8 assays. CCK-8, Cell Counting Kit-8. n.s., not significant.

Figure 29

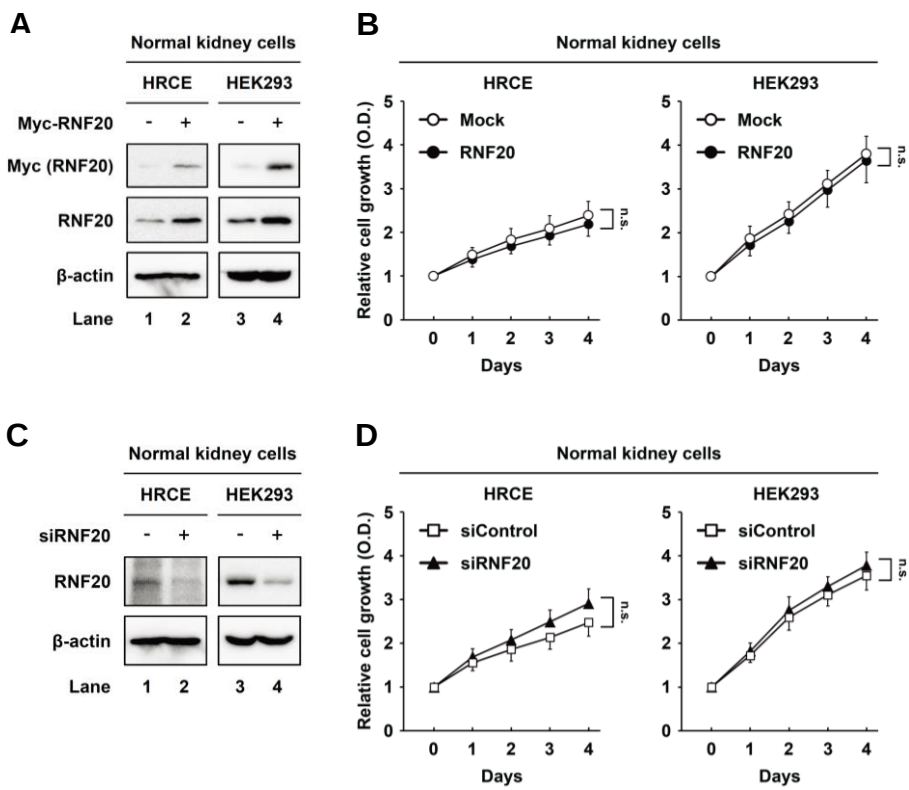
A
Normal kidney cells
HRCE
HEK293
Myc-RNF20
- + - +
Myc (RNF20)
RNF20
β-actin
Lane 1 2 3 4
B
Normal kidney cells
HRCE
HEK293
Mock
RNF20
Relative cell growth (O.D.)
Days
n.s.
C
Normal kidney cells
HRCE
HEK293
siRNF20
- + - +
RNF20
β-actin
Lane 1 2 3 4
D
Normal kidney cells
HRCE
HEK293
siControl
siRNF20
Relative cell growth (O.D.)
Days
n.s.

associated with ectopic lipid storage in ccRCC. Thus, I analyzed the expression patterns of lipogenic genes in normal kidney and ccRCC tumor tissues. As shown in Figure 30A, SREBP1c mRNA was significantly upregulated in ccRCC tumors compared with that in patient-matched normal samples. In addition, TCGA RNA-Seq data revealed that SREBP1 was upregulated in ccRCC tumors (Figure 30B) and was positively associated with advanced tumor stages (Figure 30C). In accordance with these data, mRNA levels of the SREBP1 target genes for *FASN* and *SCD1* were elevated in ccRCC tumors (Figure 30, D-I). Moreover, protein expression of SREBP1 and the lipogenic enzymes FASN and SCD1 were concurrently increased in ccRCC tumors compared with those in patient-matched normal kidney tissues, whereas RNF20 protein was downregulated (Figure 31A). Next, I examined the relationship between RNF20 and SREBP1 expression using IHC staining in matched normal kidney and tumor tissue sections from the same ccRCC patient. RNF20 signal intensity was reduced in ccRCC tumor tissues, whereas SREBP1 signals were increased (Figure 31B). Subsequent TCGA analyses revealed an inverse correlation between RNF20 and SREBP1 expression in ccRCC tumor tissues (Figure 31C). Accordingly, mRNA expression of RNF20 was inversely correlated with that of SREBP1c target genes *ELOVL6* and *FASN* (Figures 31D and 31E), and FASN mRNA expression was positively correlated with poor survival (Figure 31F). In contrast, qRT-PCR and TCGA RNA-Seq analyses showed that the mRNA levels of SREBP2 and its target gene *HMGCR*, the rate-limiting enzyme of cholesterol synthesis, were decreased in ccRCC tumors (Figure 32, A-D). Together, these results imply that elevated SREBP1 levels might enhance lipogenic activation and poor clinical outcomes in ccRCC.

Figure 30. SREBP1 and lipogenic genes are upregulated in ccRCC. (A) qRT-PCR analysis of SREBP1c in patient-matched ccRCC tumor and normal kidney samples. SREBP1c mRNA expression was normalized to those of matched normal kidney samples. **(B)** Normalized RNA-Seq reads of SREBP1 in ccRCC tumors and normal kidney samples. RNA-Seq data were obtained from TCGA ccRCC project. **(C)** ccRCC tumors were analyzed for SREBP1 expression according to tumor stages. **(D)** qRT-PCR analysis of FASN in patient-matched ccRCC tumor and normal kidney samples. FASN mRNA expression was normalized to those in matched normal kidney samples. **(E)** Normalized RNA-seq reads of FASN in ccRCC tumors and normal kidney samples. **(F)** FASN expression was analyzed in ccRCC tumors according to tumor stages. **(G)** qRT-PCR analysis of SCD1 mRNA level in matched ccRCC tumor and normal kidney samples. SCD1 mRNA expression was normalized to those in matched normal kidney samples. **(H)** Normalized RNA-seq reads of SCD1 in ccRCC tumors and normal kidney samples. **(I)** SCD1 expression was determined in ccRCC tumors of various tumor stages. $^{\#}P < 0.05$ versus normal kidney; $^{\#\#\#}P < 0.001$ versus normal kidney; $^{***}P < 0.001$.

Figure 30

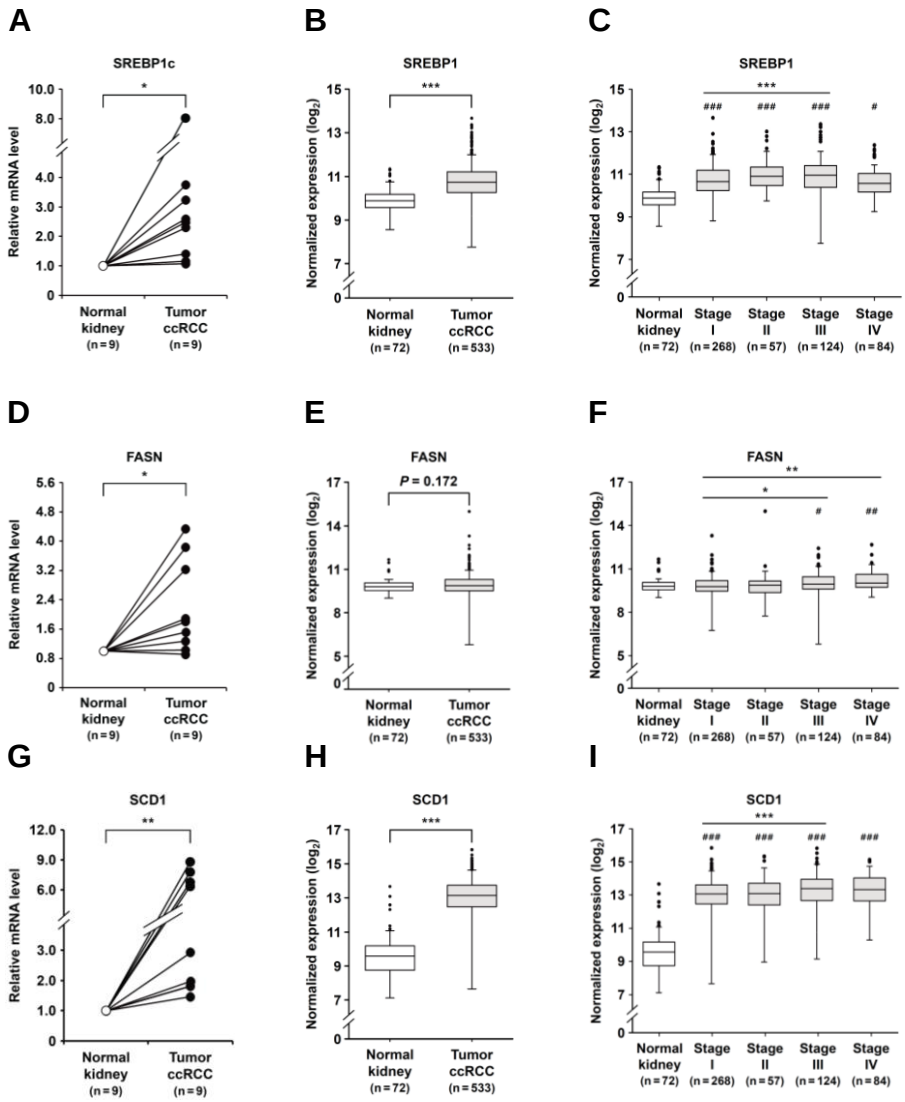
A
SREBP1c
*
Relative mRNA level
10.0
8.0
4.0
3.0
2.0
1.0
0
Normal kidney (n = 9)
Tumor ccRCC (n = 9)
B
SREBP1
***
Normalized expression (log2)
15
13
11
9
7
0
Normal kidney (n = 72)
Tumor ccRCC (n = 533)
C
SREBP1
***
###
###
###
#
Normalized expression (log2)
15
13
11
9
7
0
Normal kidney (n = 72)
Stage I (n = 268)
Stage II (n = 57)
Stage III (n = 124)
Stage IV (n = 84)
D
FASN
*
Relative mRNA level
5.6
4.8
4.0
3.2
2.4
1.6
0.8
0
Normal kidney (n = 9)
Tumor ccRCC (n = 9)
E
FASN
P = 0.172
Normalized expression (log2)
17
14
11
8
5
0
Normal kidney (n = 72)
Tumor ccRCC (n = 533)
F
FASN
**
*
#
##
Normalized expression (log2)
17
14
11
8
5
0
Normal kidney (n = 72)
Stage I (n = 268)
Stage II (n = 57)
Stage III (n = 124)
Stage IV (n = 84)
G
SCD1
**
Relative mRNA level
12.0
9.0
6.0
3.0
2.0
1.0
0
Normal kidney (n = 9)
Tumor ccRCC (n = 9)
H
SCD1
***
Normalized expression (log2)
17
15
13
11
9
7
0
Normal kidney (n = 72)
Tumor ccRCC (n = 533)
I
SCD1
***
###
###
###
###
Normalized expression (log2)
17
15
13
11
9
7
0
Normal kidney (n = 72)
Stage I (n = 268)
Stage II (n = 57)
Stage III (n = 124)
Stage IV (n = 84)

Figure 31. Lipogenic enzymes are upregulated in ccRCC and are inversely correlated with RNF20 expression. (A) Protein levels in matched ccRCC tumor and normal kidney samples were determined using western blotting analyses. Total cell lysates were subjected to SDS-PAGE followed by western blotting analyses with indicated antibodies. **(B)** IHC staining of matched ccRCC tumors and adjacent normal kidney tissues. Representative tissue sections are shown with RNF20 and SREBP1 staining. Scale bar, 100 μm. **(C)** Correlations between RNF20 and SREBP1 mRNA levels in ccRCC tumor samples were identified in data from TCGA datasets using Pearson correlation tests. Numbers of cases (n), Pearson correlation coefficient (r), and P values (*P*) are indicated. **(D)** Correlations of RNF20 and ELOVL6 mRNA expression in ccRCC samples were identified in TCGA ccRCC datasets using Pearson correlation tests. **(E)** Correlation of RNF20 and FASN mRNA expression in ccRCC samples were determined in TCGA ccRCC datasets and were identified using Pearson correlation tests. **(F)** Kaplan–Meier survival analysis for ccRCC patients from low or high FASN expression groups. P values were calculated using the Log-rank test.

Figure 31

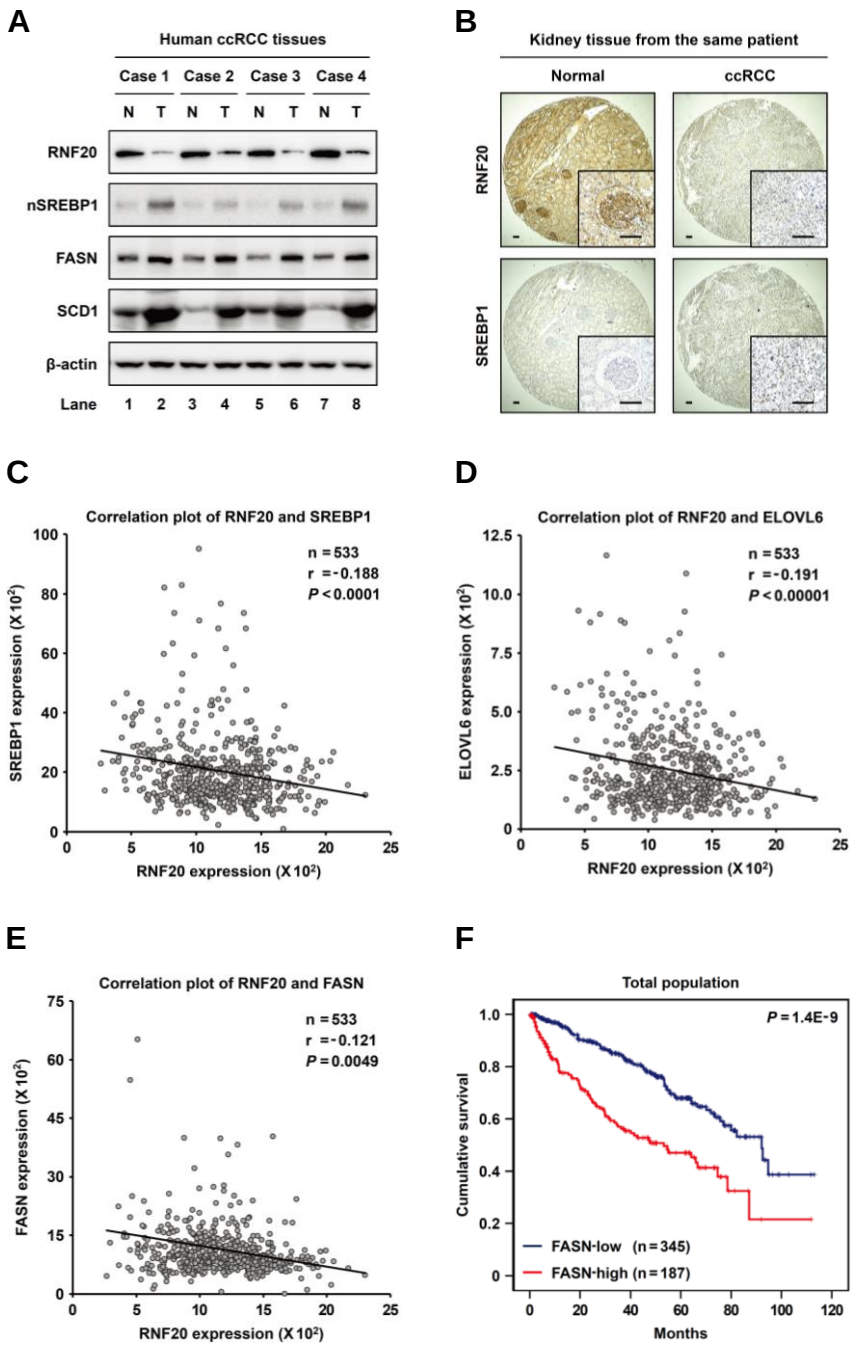
A
Human ccRCC tissues
Case 1
Case 2
Case 3
Case 4
N T N T N T N T
RNF20
nSREBP1
FASN
SCD1
β-actin
Lane 1 2 3 4 5 6 7 8
B
Kidney tissue from the same patient
Normal
ccRCC
RNF20
SREBP1
C
Correlation plot of RNF20 and SREBP1
n = 533
r = -0.188
P < 0.0001
SREBP1 expression (X 10²)
RNF20 expression (X 10²)
D
Correlation plot of RNF20 and ELOVL6
n = 533
r = -0.191
P < 0.00001
ELOVL6 expression (X 10²)
RNF20 expression (X 10²)
E
Correlation plot of RNF20 and FASN
n = 533
r = -0.121
P = 0.0049
FASN expression (X 10²)
RNF20 expression (X 10²)
F
Total population
P = 1.4E-9
Cumulative survival
FASN-low (n = 345)
FASN-high (n = 187)
Months

Figure 32. SREBP2 and its target gene HMGCR are decreased in ccRCC tumors. (A) qRT-PCR analysis of SREBP2 in matched ccRCC tumor and normal kidney samples. SREBP2 mRNA expression was normalized to that in matched normal kidney samples. **(B)** Normalized RNA-seq reads of SREBP2 in ccRCC tumors and normal kidney samples using TCGA ccRCC datasets. **(C)** qRT-PCR analysis of HMGCR in matched ccRCC tumor and normal kidney samples. HMGCR mRNA expression values were normalized to those in matched normal kidney samples. **(D)** Normalized RNA-seq reads of HMGCR in ccRCC tumors and normal kidney samples from TCGA ccRCC datasets; *$P < 0.05$; ***$P < 0.001$.

Figure 32

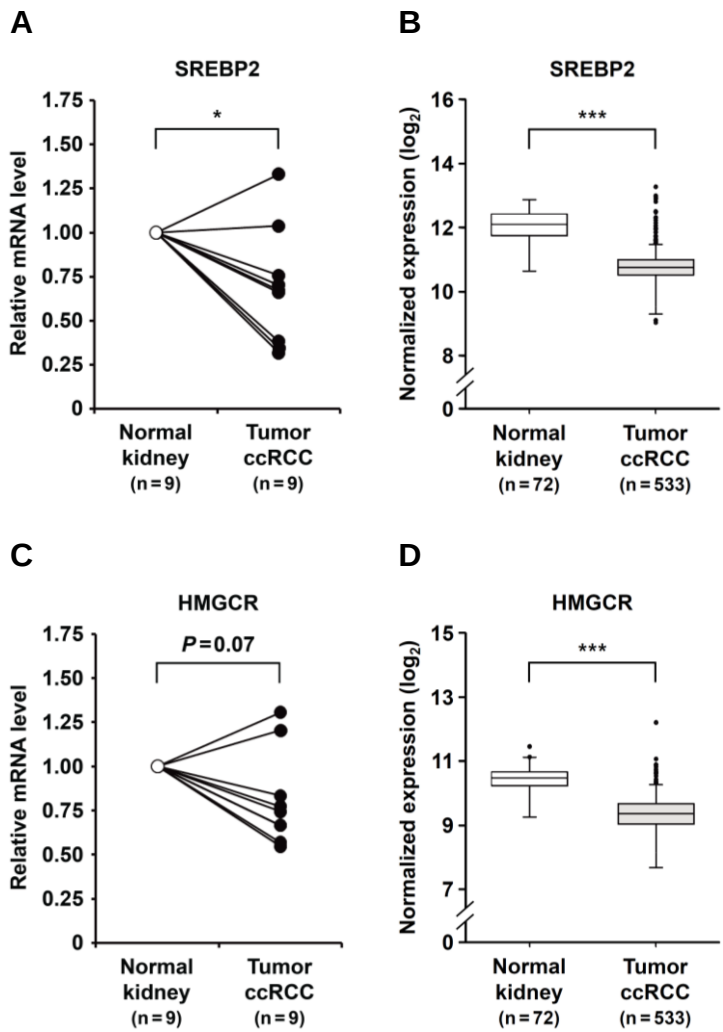
A
SREBP2
Relative mRNA level
1.75
1.50
1.25
1.00
0.75
0.50
0.25
0
*
Normal kidney (n = 9)
Tumor ccRCC (n = 9)
B
SREBP2
Normalized expression (log2)
16
14
12
10
8
0
***
Normal kidney (n = 72)
Tumor ccRCC (n = 533)
C
HMGCR
P = 0.07
Relative mRNA level
1.75
1.50
1.25
1.00
0.75
0.50
0.25
0
Normal kidney (n = 9)
Tumor ccRCC (n = 9)
D
HMGCR
Normalized expression (log2)
15
13
11
9
7
0
***
Normal kidney (n = 72)
Tumor ccRCC (n = 533)

RNF20 alleviates lipogenesis and cell proliferation by repressing SREBP1c in ccRCC cells.

I investigated the effects of RNF20 and/or SREBP1c overexpression in ccRCC cells. In *VHL* wild-type ACHN ccRCC cells, ectopic expression of RNF20 clearly suppressed both endogenous and ectopic nuclear SREBP1 proteins (Figure 33A). However, suppression of RNF20 using siRNA led to increased SREBP1c protein and mRNA expression (Figures 33B and 33C). In agreement, SREBP1c overexpression augmented mRNA levels of lipogenic genes including *FASN*, *ACC1*, *SCD1*, and *ELOVL6* in ACHN cells (Figure 34A), as shown in previous reports (Brown and Goldstein, 1997; Horton et al., 2002). In contrast, RNF20 potently inhibited mRNA expression of lipogenic genes in both control and SREBP1c-overexpressing ACHN cells (Figure 34A). However, suppression of RNF20 increased mRNA expression of lipogenic genes, and knockdown of both RNF20 and SREBP1 abolished the effects of RNF20 siRNA on the expression of lipogenic genes (Figure 34C). Accordingly, intracellular triglyceride accumulations were greater in SREBP1c-overexpressing ACHN cells than in control ACHN cells, whereas intracellular triglyceride levels were decreased by RNF20 overexpression (Figure 34B). Conversely, suppression of RNF20 increased intracellular triglyceride levels (Figure 34D). It has been reported that loss of SREBP1 markedly decreases glioma cell proliferation (Guo et al., 2009; Williams et al., 2013). In accordance with these, SREBP1c overexpression promoted mRNA expression of cell-cycle regulators including PCNA, cyclin A, D1, and E in ccRCC cells (Figure 35A), and concomitant RNF20 overexpression reduced the effects of overexpressed SREBP1c (Figure 35A). RNF20 knockdown also promoted cell

Figure 33. RNF20 suppresses the expression of SREBP1c in ccRCC cells. **(A)** ACHN ccRCC cells were infected with adenovirus containing Myc-RNF20 and/or Flag-SREBP1c. After infection, total cell lysates were subjected to SDS-PAGE followed by western blotting analyses with the indicated antibodies. nSREBP1, nuclear SREBP1. **(B)** ACHN ccRCC cells were transfected with siRNF20 and/or siSREBP1. After incubation for 48 hours, total cell lysates were subjected to SDS-PAGE and western blotting analyses with indicated antibodies. **(C)** RNF20 and/or SREBP1 were knocked down in ACHN ccRCC cells using siRNAs, and relative mRNA levels were determined using qRT-PCR. Subsequently, mRNA expression was normalized to that of the GAPDH gene, and is presented relative to those in the siControl group.

Figure 33

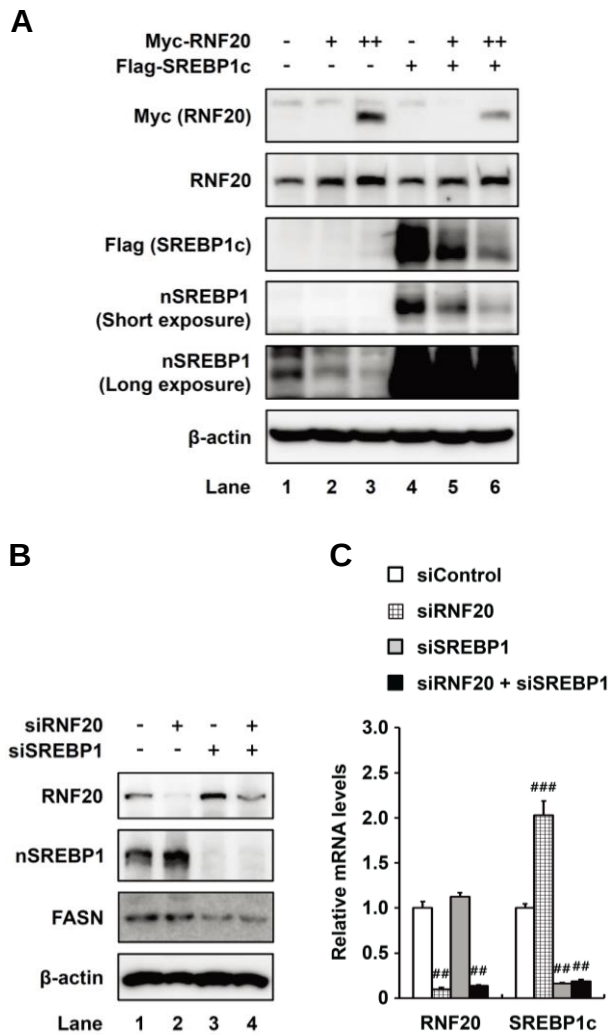
A
Myc-RNF20 - + ++ - + ++
Flag-SREBP1c - - - + + +
Myc (RNF20)
RNF20
Flag (SREBP1c)
nSREBP1
(Short exposure)
nSREBP1
(Long exposure)
β-actin
Lane 1 2 3 4 5 6
B
siRNF20 - + - +
siSREBP1 - - + +
RNF20
nSREBP1
FASN
β-actin
Lane 1 2 3 4
C
siControl
siRNF20
siSREBP1
siRNF20 + siSREBP1
Relative mRNA levels
3.0
2.5
2.0
1.5
1.0
0.5
0
###
##
##
##
###
RNF20
SREBP1c

Figure 34. In ccRCC cells, RNF20 represses lipogenic activity by inhibiting SREBP1c. (A) ACHN ccRCC cells were transduced with lentivirus for stable overexpression of RNF20 and/or SREBP1c. Relative mRNA levels were determined using qRT-PCR. The level of each mRNA was normalized to the mRNA level of the GAPDH gene. Each mRNA level is shown as a ratio relative to the Mock control group. **(B)** Intracellular triglyceride contents were measured in lentiviral RNF20 and/or SREBP1c overexpressing ACHN cells. **(C)** RNF20 and/or SREBP1 were knocked down in ACHN ccRCC cells using siRNAs, and relative mRNA levels were determined using qRT-PCR. Subsequently, mRNA expression was normalized to that of the GAPDH gene, and is presented relative to those in the siControl group. **(D)** ACHN ccRCC cells were transfected with siRNF20 and/or siSREBP1. Then, intracellular triglyceride contents were measured.

Figure 34

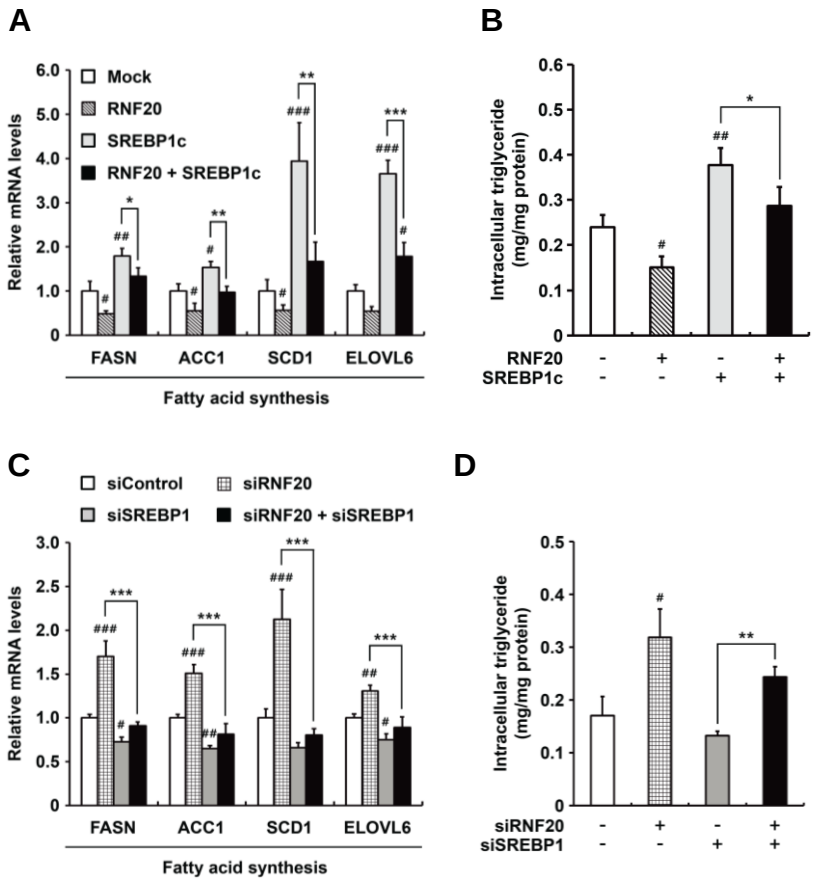
A
Mock
RNF20
SREBP1c
RNF20 + SREBP1c
Relative mRNA levels
FASN
ACC1
SCD1
ELOVL6
Fatty acid synthesis
B
Intracellular triglyceride (mg/mg protein)
RNF20
SREBP1c
C
siControl
siRNF20
siSREBP1
siRNF20 + siSREBP1
Relative mRNA levels
FASN
ACC1
SCD1
ELOVL6
Fatty acid synthesis
D
Intracellular triglyceride (mg/mg protein)
siRNF20
siSREBP1

cycle gene expression in ccRCC cells (Figure 35D). In contrast, RNF20 overexpression reduced colony formation whereas ectopic SREBP1c expression elevated colony formation in ACHN cells (Figure 35C). In addition, SREBP1c overexpression potentiated ccRCC cell proliferation (Figure 35B), and knockdown of SREBP1 reduced cell proliferation in both control and RNF20-suppressing cells (Figure 35E). These data propose that RNF20 would inhibit ccRCC cell proliferation by suppressing SREBP1c-induced lipogenesis and cell cycle progression.

PTTG1 is a novel target gene of SREBP1c in ccRCC cells.

As a transcriptional activator, it has been reported that SREBP1c stimulates fatty acid metabolism and cell cycle progression (Bengoechea-Alonso and Ericsson, 2006; Jeon et al., 2013; Williams et al., 2013). To identify further factor(s) that are involved in SREBP1c-induced cell cycle progression in ccRCC, I attempted to identify SREBP1c target genes that are involved in cell cycle regulation using RNA-Seq analyses in liver tissues of wild-type and *SREBP1c* deficient mice, and identified *PTTG1* as a novel target gene of SREBP1c (Figure 36A). As shown in Figure 36B, PTTG1 expression was remarkably reduced in kidney, liver, and adipose tissues of *SREBP1c* deficient mice compared with that in wild-type mice. Subsequently, I investigated PTTG1 expression in SREBP1c-overexpressing ACHN cells and found that ectopic SREBP1c expression increased PTTG1 mRNA expression, whereas RNF20 co-expression attenuated this effect (Figure 37A). However, under conditions of SREBP1 knockdown, RNF20 did not suppress PTTG1 mRNA (Figure 37B) or protein (Figure 37D) expression.

Figure 35. RNF20 inhibits ccRCC cell proliferation by cell cycle regulation. **(A)** ACHN ccRCC cells were transduced with lentivirus for stable overexpression of RNF20 and/or SREBP1c. Relative mRNA levels were determined using qRT-PCR. The level of each mRNA was normalized to the mRNA level of the GAPDH gene. Each mRNA level is shown as a ratio relative to the Mock control group. **(B)** ACHN ccRCC cells were transduced with RNF20 and/or SREBP1c lentivirus, and the cell proliferation rates were monitored by CCK-8 assay. **(C)** ACHN ccRCC cells were transduced with RNF20 and/or SREBP1c lentivirus, and their ability to form colonies was determined by crystal violet staining. **(D)** RNF20 and/or SREBP1 were knocked down in ACHN ccRCC cells using siRNAs, and relative mRNA levels were determined using qRT-PCR. Subsequently, mRNA expression was normalized to that of the GAPDH gene and is presented relative to those in the siControl group. **(E)** ACHN ccRCC cells were transfected with siRNF20 and/or siSREBP1, and relative cell growth rates were determined using CCK-8 assay. All experiments were repeated independently at least three times and representative results are shown. CCK-8, Cell Counting Kit-8; $^{\#}P < 0.05$ versus Control; $^{\#\#}P < 0.01$ versus Control; $^{\#\#\#}P < 0.001$ versus Control; $*P < 0.05$; $**P < 0.01$; $***P < 0.001$.

Figure 35

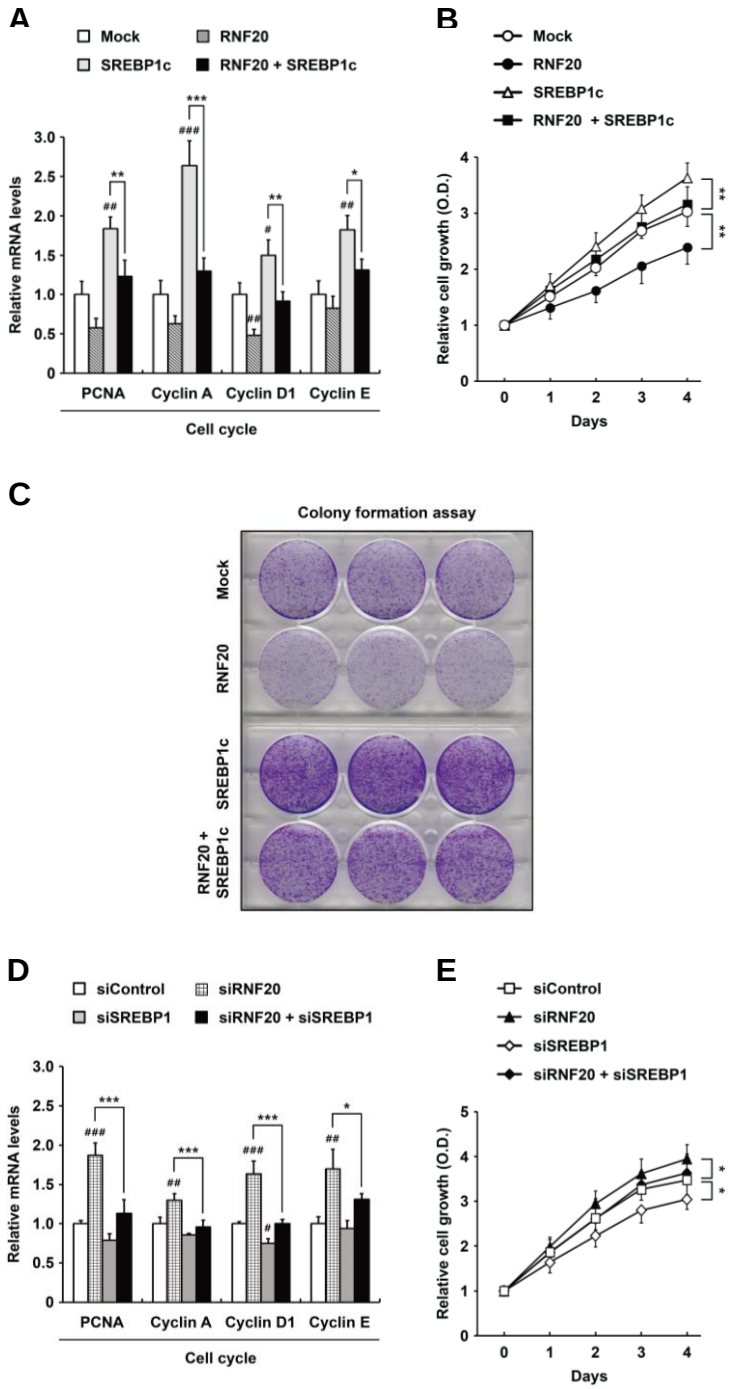
A
Mock
RNF20
SREBP1c
RNF20 + SREBP1c
Relative mRNA levels
PCNA
Cyclin A
Cyclin D1
Cyclin E
Cell cycle
B
Mock
RNF20
SREBP1c
RNF20 + SREBP1c
Relative cell growth (O.D.)
Days
C
Colony formation assay
Mock
RNF20
SREBP1c
RNF20 + SREBP1c
D
siControl
siRNF20
siSREBP1
siRNF20 + siSREBP1
Relative mRNA levels
PCNA
Cyclin A
Cyclin D1
Cyclin E
Cell cycle
E
siControl
siRNF20
siSREBP1
siRNF20 + siSREBP1
Relative cell growth (O.D.)
Days

Figure 36. PTTG1 is a novel target gene of SREBP1c using RNA-Seq analyses in *SREBP1c* deficient mice. (A) RNA-Seq analysis for transcriptome profiling of liver tissues from wild-type and *SREBP1c* deficient mice are presented as a scatter plot. **(B)** Kidney, liver, and adipose tissues were isolated from wild-type and *SREBP1c* deficient mice. Total RNA was extracted and relative mRNA levels were determined using qRT-PCR. Subsequently, mRNA expression values were normalized to that of the TATA-binding protein (TBP). EAT, epididymal adipose tissue; IAT, inguinal adipose tissue; BAT, brown adipose tissue; $^{**}P < 0.01$; $^{***}P < 0.001$.

Figure 36

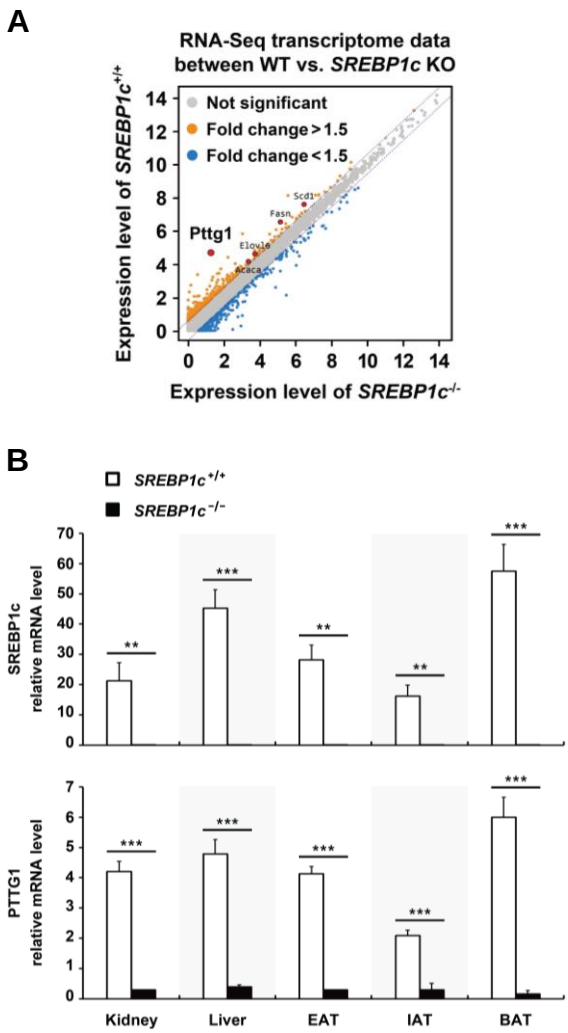
A
RNA-Seq transcriptome data
between WT vs. SREBP1c KO
Not significant
Fold change > 1.5
Fold change < 1.5
Pttg1
Scd1
Fasn
Elovl6
Acaca
Expression level of SREBP1c+/+
Expression level of SREBP1c-/-
B
SREBP1c+/+
SREBP1c-/-
SREBP1c relative mRNA level
PTTG1 relative mRNA level
Kidney
Liver
EAT
IAT
BAT

Accordingly, SREBP1c promoted PTTG1 protein expression in ccRCC cells (Figure 37C, lane 3). However, siRNA-mediated suppression of PTTG1 did not affect SREBP1c or FASN protein expression (Figure 37C, lane 4). To validate whether SREBP1c would regulate the transcription of PTTG1 directly, I analyzed putative sterol regulatory elements (SREs) and E-Box motifs, which are binding sites for SREBP1c (Kim et al., 1995; Shimano, 2001) in proximal promoter regions of *PTTG1* genes in human, monkey, dog, mouse, and rat (Figure 38A). In luciferase reporter assays with the human PTTG1 promoter, SREBP1c expression induced luciferase activity and co-expression of RNF20 suppressed SREBP1c-mediated PTTG1 promoter activation (Figure 38B). In ccRCC tumors, PTTG1 mRNA levels were significantly upregulated compared to those in patient-matched normal kidney tissues (Figure 39A). TCGA analyses also showed that PTTG1 mRNA levels were greatly enhanced in ccRCC tumor tissues (Figure 39B), and the expression of PTTG1 mRNA was positively associated with advanced tumor stages (Figure 39C). In addition, PTTG1 expression was inversely correlated with RNF20 expression in ccRCC tumor tissues (Figure 39D). Moreover, high expression of PTTG1 was associated with a poor survival of ccRCC patients (Figure 39E). Taken together, these data suggest that activated SREBP1c would induce high expression of the novel target gene *PTTG1* in ccRCC.

The SREBP inhibitor betulin inhibits cell proliferation of ccRCC cells.

Betulin is a pharmacological inhibitor that prevents proteolytic processing of SREBP proteins to achieve lipid-lowering effects (Soyal et al., 2015; Tang et al., 2011). In addition, betulin attenuates the growth of various cancers by inhibiting

Figure 37. PTTG1 is induced by SREBP1c in ccRCC cells. (A) ACHN ccRCC cells were transduced with RNF20 and/or SREBP1c lentivirus, and relative mRNA levels were determined using qRT-PCR. PTTG1 mRNA level was normalized to GAPDH and are shown relative to the negative control group. **(B)** ACHN ccRCC cells were transfected with siRNF20 and/or siSREBP1, and relative mRNA levels were determined using qRT-PCR. PTTG1 mRNA expression data were normalized to that of GAPDH, and all mRNA levels are presented relative to the negative control group. $^{\#}P < 0.05$ versus negative control; $^{\#\#}P < 0.01$ versus negative control; $^{*}P < 0.05$. **(C)** ACHN ccRCC cells were infected with SREBP1c adenovirus and were transfected with PTTG1 siRNA. After incubation for 48 hours, western blotting analyses were performed with indicated antibodies. **(D)** ACHN ccRCC cells were transfected with siControl or siRNF20. After incubation for 48 hours, western blotting analyses were performed with indicated antibodies. nSREBP1, nuclear SREBP1.

Figure 37

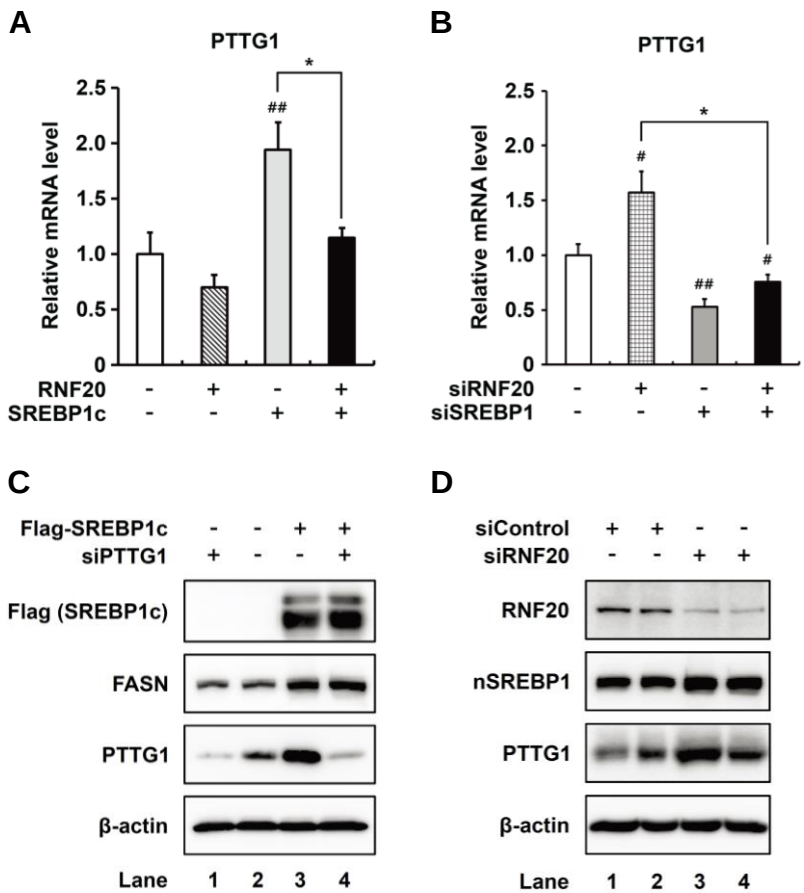
A
PTTG1
Relative mRNA level
2.5
2.0
1.5
1.0
0.5
0
##
*
RNF20 - + - +
SREBP1c - - + +
B
PTTG1
Relative mRNA level
2.5
2.0
1.5
1.0
0.5
0
#
##
#
*
siRNF20 - + - +
siSREBP1 - - + +
C
Flag-SREBP1c - - + +
siPTTG1 + - - +
Flag (SREBP1c)
FASN
PTTG1
β-actin
Lane 1 2 3 4
D
siControl + + - -
siRNF20 - - + +
RNF20
nSREBP1
PTTG1
β-actin
Lane 1 2 3 4

Figure 38. RNF20 suppresses SREBP1c-mediated PTTG1 promoter activation. **(A)** SRE motifs and E-Box sequences in PTTG promoters from several species. **(B)** HEK293 cells were co-transfected with luciferase reporter plasmids containing PTTG1 promoter and expression vectors for β-gal, RNF20, and/or SREBP1c. Total cell lysates were subjected to luciferase and β-galactosidase assays. Data are presented from three independent experiments performed in triplicate. RLU, relative luminescence units.

Figure 38

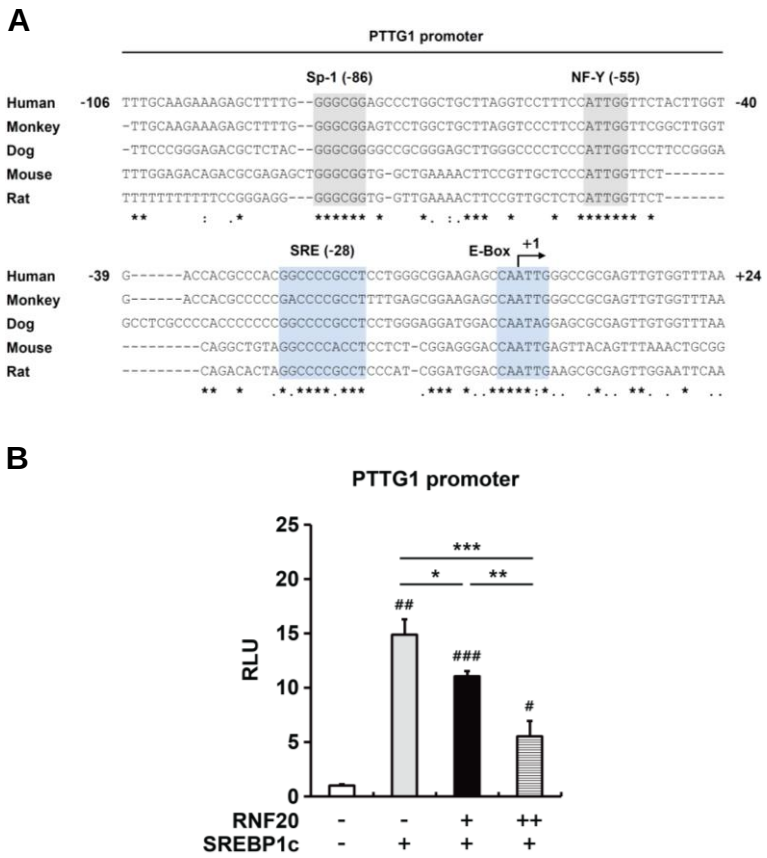
A
PTTG1 promoter
Sp-1 (-86)
NF-Y (-55)
Human -106 TTTGCAAGAAAGAGCTTTTG--GGGCGGAGCCCTGGCTGCTTAGGTCCTTTCCATTGGTTCTACTTGGT -40
Monkey -TTGCAAGAAAGAGCTTTTG--GGGCGGAGTCCTGGCTGCTTAGGTCCCTTCCATTGGTTCGGCTTGGT
Dog -TTCCCGGGAGACGCTCTAC--GGGCGGGGCCGCGGGAGCTTGGGCCCCTCCCATTGGTCCTTCCGGGA
Mouse TTTGGAGACAGACGCGAGAGCTGGGCGGTG-GCTGAAAACTTCCGTTGCTCCCATTGGTTCT-------
Rat TTTTTTTTTTTCCGGGAGG---GGGCGGTG-GTTGAAAACTTCCGTTGCTCTCATTGGTTCT-------
SRE (-28)
E-Box
+1
Human -39 G------ACCACGCCCACGGCCCCGCCTCCTGGGCGGAAGAGCCAATTGGGCCGCGAGTTGTGGTTTAA +24
Monkey G------ACCACGCCCCCGACCCCGCCTTTTGAGCGGAAGAGCCAATTGGGCCGCGAGTTGTGGTTTAA
Dog GCCTCGCCCCACCCCCCCGGCCCCGCCTCCTGGGAGGATGGACCAATAGGAGCGCGAGTTGTGGTTTAA
Mouse ---------CAGGCTGTAGGCCCCACCTCCTCT-CGGAGGGACCAATTGAGTTACAGTTTAAACTGCGG
Rat ---------CAGACACTAGGCCCCGCCTCCCAT-CGGATGGACCAATTGAAGCGCGAGTTGGAATTCAA
B
PTTG1 promoter
RLU
25
20
15
10
5
0
***
*
**
##
###
#
RNF20 - - + ++
SREBP1c - + + +

Figure 39. PTTG1 is upregulated in ccRCC, accompanied with poor prognosis. **(A)** qRT-PCR analysis of PTTG1 mRNA levels in patient-matched ccRCC tumors and normal kidney samples. PTTG1 mRNA expression was normalized to that in matched normal kidney samples. **(B)** Normalized RNA-Seq reads of PTTG1 in ccRCC tumors, and normal kidney samples were obtained from TCGA ccRCC project. **(C)** PTTG1 expression was analyzed in ccRCC according to tumor stages. RNA-Seq data were obtained from TCGA. $^{###}P < 0.001$ versus normal kidney; $***P < 0.001$. **(D)** Correlations between RNF20 and PTTG1 mRNA levels in ccRCC tumor samples were identified in data from TCGA using Pearson correlation tests. Numbers of cases (n), Pearson correlation coefficients (r), and the P values (*P*) are indicated. **(E)** Kaplan–Meier survival analyses of ccRCC patients were performed in low and high PTTG1 expression groups, and differences were identified using the Log-rank test.

Figure 39

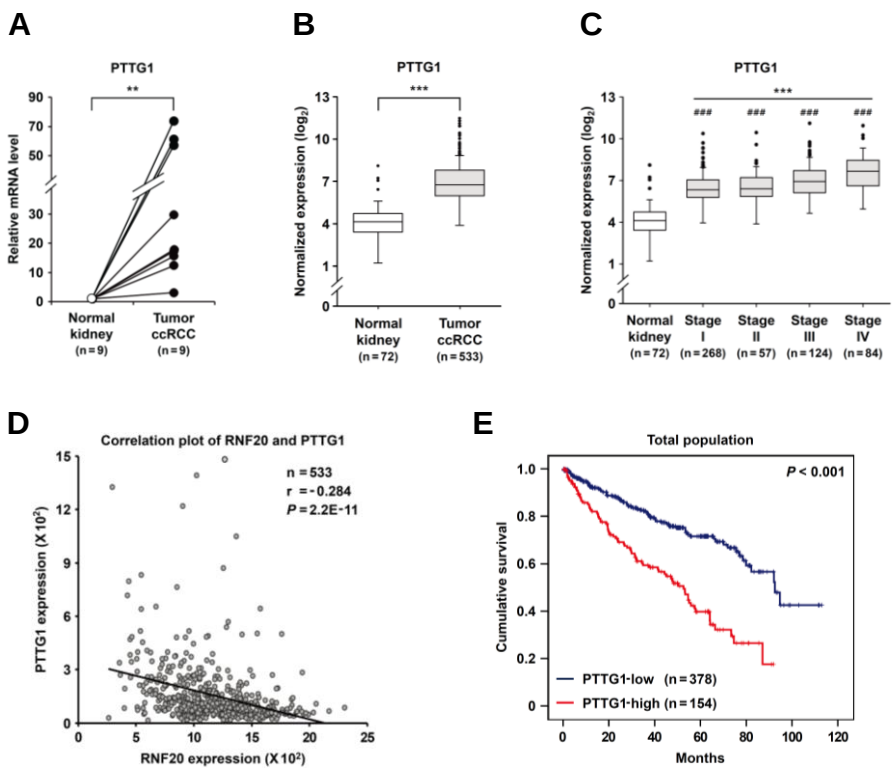
A
PTTG1
**
Relative mRNA level
90
70
50
30
20
10
0
Normal kidney (n=9)
Tumor ccRCC (n=9)
B
PTTG1
***
Normalized expression (log2)
13
10
7
4
1
0
Normal kidney (n=72)
Tumor ccRCC (n=533)
C
PTTG1
***
###
Normalized expression (log2)
Normal kidney (n=72)
Stage I (n=268)
Stage II (n=57)
Stage III (n=124)
Stage IV (n=84)
D
Correlation plot of RNF20 and PTTG1
n=533
r=-0.284
P=2.2E-11
PTTG1 expression (X10²)
RNF20 expression (X10²)
E
Total population
P<0.001
Cumulative survival
PTTG1-low (n=378)
PTTG1-high (n=154)
Months

multiple oncogenic factors, including cell-cycle regulators (Chintharlapalli et al., 2007; Li et al., 2014). Thus, I determined the effects of betulin on SREBP inhibition and assessed its anti-tumorigenic properties in ccRCC cells. Following treatment of *VHL* wild-type ACHN and *VHL*-depleted A498 ccRCC cells with betulin, nuclear SREBP1 protein was decreased in a dose-dependent manner, whereas the precursor form of SREBP1 was unaffected (Figure 40A), indicating that betulin represses SREBP1 processing. Simultaneously, protein levels of PTTG1 and cell-cycle regulators including cyclin B1 and E were decreased in betulin-treated ccRCC cells (Figure 40A). Moreover, betulin treatments led to decreased protein expression of the lipogenic enzymes FASN and SCD1 (Figure 40A). To explore whether betulin suppresses ccRCC cell growth, I measured its effects on cell proliferation in ACHN and A498 cells (Figures 40B and 40C) and showed dose dependent anti-proliferative effects. Subsequently, to determine whether enhanced ccRCC cell proliferation following RNF20 suppression might be required for activated SREBP, ccRCC cells were treated with betulin and RNF20 siRNA. Consistent with above data (Figure 28D), ccRCC cell proliferation was elevated in the presence of RNF20 siRNA, and betulin attenuated cell growth under these conditions (Figures 41A and 41B). Moreover, RNF20 suppression in ccRCC cells augmented the expression of several betulin-sensitive genes that are involved in lipogenesis and cell cycle regulation (Figures 41C and 41D). These data propose that the effects of RNF20 on cell growth and lipogenic and cell-cycle regulatory gene expression would be mediated by SREBP1c in ccRCC cells. These gene expression changes also corresponded with decreased intracellular lipid accumulation in betulin-treated ccRCC cells (Figure 42A).

Figure 40. The SREBP inhibitor betulin inhibits ccRCC cell proliferation. **(A)** ACHN and A498 ccRCC cells were treated with increasing concentrations of betulin for 12 hours, and total cell lysates were then subjected to SDS-PAGE and western blotting analyses with indicated antibodies. pSREBP1, precursor SREBP1; nSREBP1, nuclear SREBP1. **(B** and **C)** ACHN and A498 ccRCC cells were treated with or without betulin, and cell proliferation rates were determined using CCK-8 assays. Data are presented as means ± SD of five individual samples. CCK-8, Cell Counting Kit-8; *$P < 0.05$; **$P < 0.01$; ***$P < 0.001$.

Figure 40

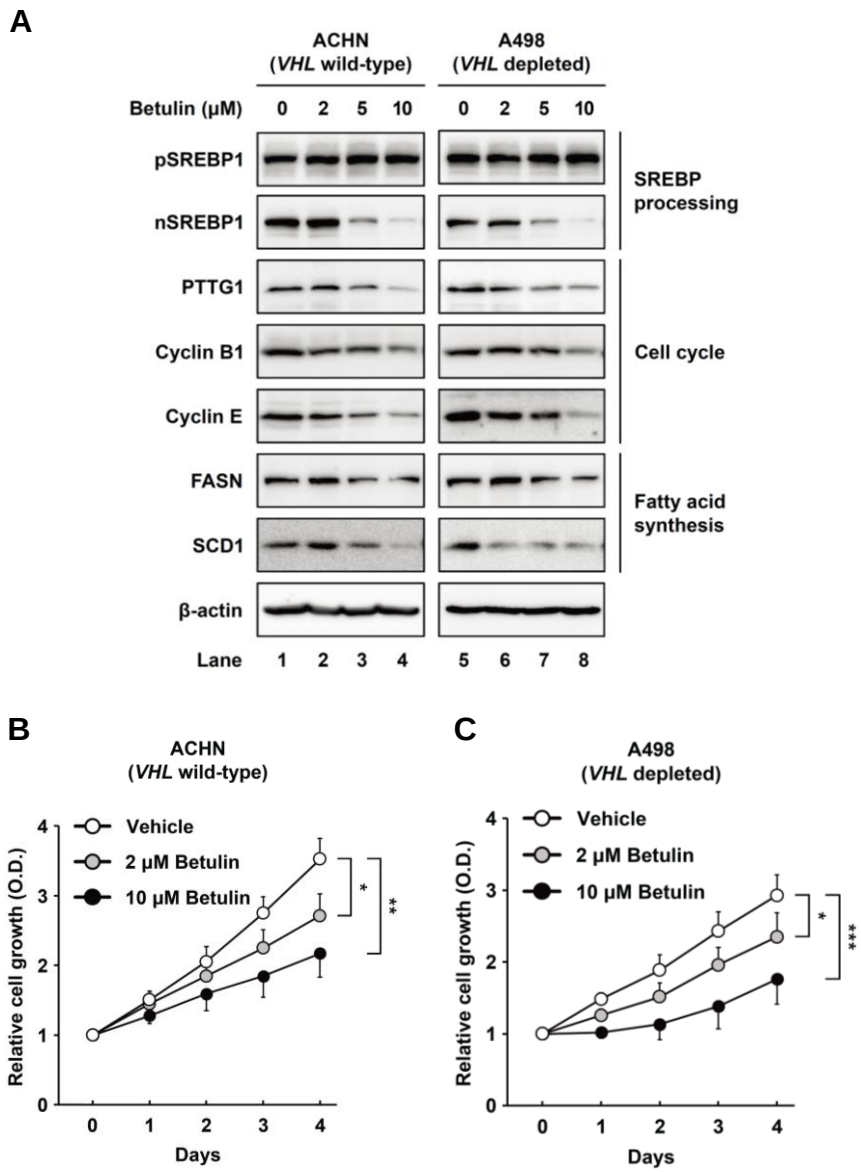
A
ACHN
(VHL wild-type)
A498
(VHL depleted)
Betulin (μM)
0 2 5 10 0 2 5 10
pSREBP1
nSREBP1
PTTG1
Cyclin B1
Cyclin E
FASN
SCD1
β-actin
SREBP processing
Cell cycle
Fatty acid synthesis
Lane
1 2 3 4 5 6 7 8
B
ACHN
(VHL wild-type)
Vehicle
2 μM Betulin
10 μM Betulin
Relative cell growth (O.D.)
Days
C
A498
(VHL depleted)
Vehicle
2 μM Betulin
10 μM Betulin
Relative cell growth (O.D.)
Days

Figure 41. Betulin efficiently inhibits cell proliferation in ccRCC cells with or without RNF20 suppression. (A and **B)** ACHN and A498 ccRCC cells were transfected with siControl or siRNF20. Then, cell proliferation rates were determined using CCK-8 assays. Data are presented as means ± SD of five individual samples. CCK-8, Cell Counting Kit-8; **P* < 0.05; ****P* < 0.001; n.s., not significant. **(C** and **D)** ACHN and A498 ccRCC cells were transfected with siControl or siRNF20. After transfection for 24 hours, cells were treated with betulin (10 μM) for 24 hours, and relative mRNA levels were determined using qRT-PCR. Subsequently, mRNA expression was normalized to that of the GAPDH gene. Data are presented as means ± SD of three individual samples. $^{\#}P$ < 0.05 versus negative control; $^{\#\#}P$ < 0.01 versus negative control; $^{\#\#\#}P$ < 0.001 versus negative control; ***P* < 0.01; ****P* < 0.001.

Figure 41

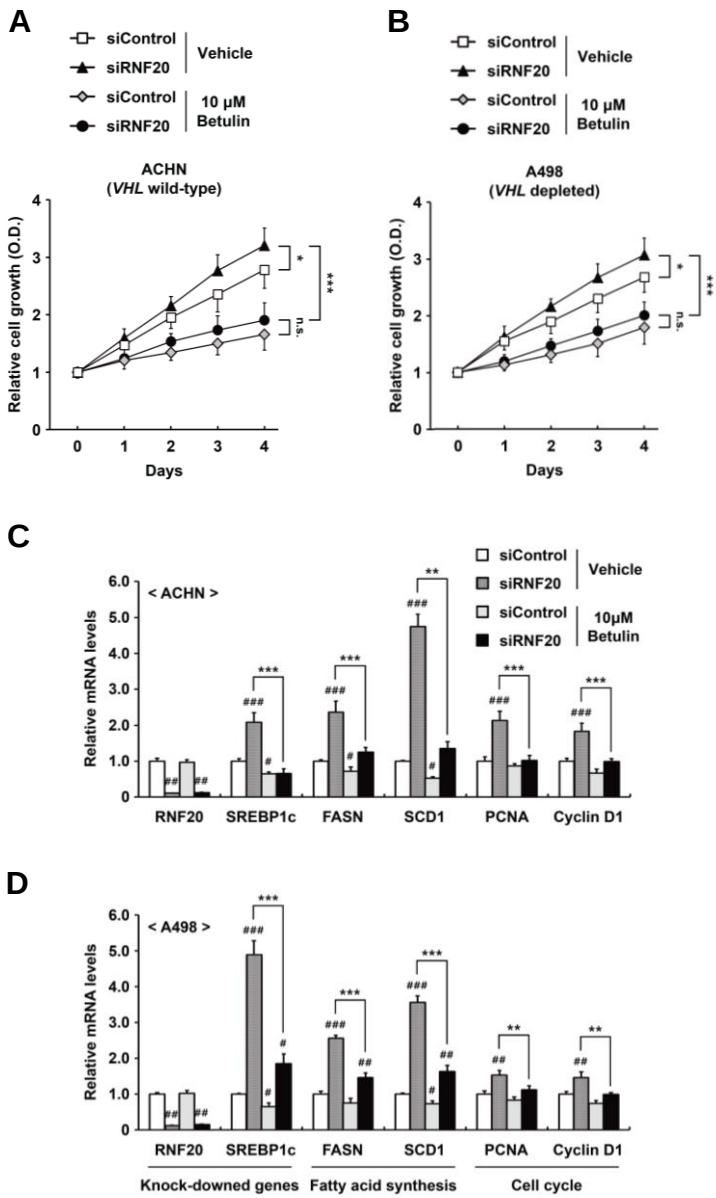
A
siControl
siRNF20
Vehicle
siControl
siRNF20
10 μM Betulin
ACHN
(VHL wild-type)
Relative cell growth (O.D.)
Days
B
A498
(VHL depleted)
C
< ACHN >
Relative mRNA levels
10μM Betulin
RNF20
SREBP1c
FASN
SCD1
PCNA
Cyclin D1
D
< A498 >
Knock-downed genes
Fatty acid synthesis
Cell cycle

In accordance with the reduced expression of cell-cycle regulatory genes, including *PTTG1* and certain cyclins (Figure 40A), betulin slightly but substantially increased numbers of ccRCC cells in the G_1 phase (Figure 42B). These data suggest that betulin would repress ccRCC cell proliferation by regulating SREBP1-dependent lipogenesis and cell cycle progression.

SREBP1c controls ccRCC cell growth through dual mode actions that affect cell cycle and lipid metabolism.

The present data suggest a relationship between PTTG1 and lipid metabolism during SREBP1c-dependent ccRCC cell proliferation. Thus, I investigated the effects of PTTG1 on lipid metabolism and/or cell proliferation in SREBP1c-overexpresing ccRCC cells (Figure 43A). PTTG1 suppression did not alter mRNA expression of SREBP1c or FASN (Figure 43B), whereas ectopic SREBP1c expression promoted mRNA expression of PTTG1 and cell-cycle regulators including PCNA, cyclin A, D1, and E in ccRCC cells (Figures 43B and 43C). In contrast, suppression of PTTG1 expression in ccRCC cells downregulated these cell-cycle proteins (Figure 43C). In addition, PTTG1 suppression inhibited cell proliferation in both control and SREBP1c-overexpressing ACHN cells (Figure 43D). Next, I determined PTTG1 expression and cell proliferation in the presence or absence of the ACC inhibitor TOFA or the FASN inhibitor C75 (Figure 43A). As shown in Figure 44A, TOFA and C75 treatments reduced intracellular triglyceride accumulation in ACHN cells. However, reductions in lipogenic activity by TOFA or C75 did not greatly effect mRNA expression of PTTG1 or cell-cycle regulators PCNA, Cyclin A, D1, and E (Figures 44B, 44D, and 44E). Similarly,

Figure 42. The SREBP inhibitor betulin represses lipogenesis and cell cycle progression in ccRCC cells. (A) ACHN ccRCC cells were treated with betulin (10 μM). After incubation for 24 hours, cells were fixed and stained with BODIPY (green) and DAPI (blue). Images were acquired using a confocal microscope. DAPI, 4',6-diamidino-2-phenylindole; Scale bar, 10 μm. **(B)** ACHN ccRCC cells were treated with betulin (10 μM) for 24 hours, were fixed and stained with propidium iodine, and DNA contents were analyzed using flow cytometry. Percentages of cells in each phase of the cell cycle are indicated.

Figure 42

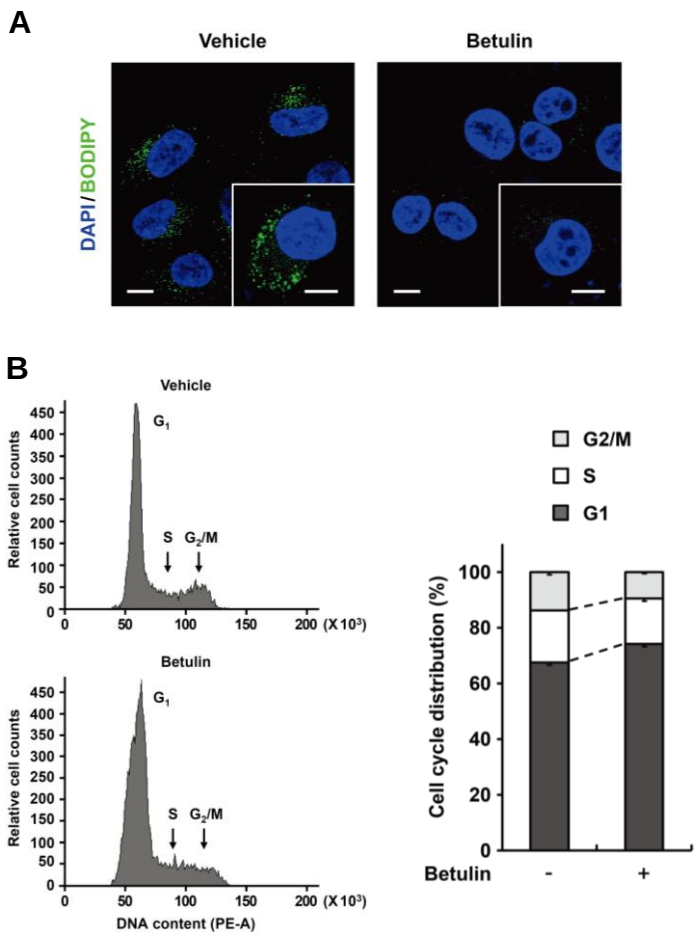
A
Vehicle
Betulin
DAPI/BODIPY
B
Vehicle
Relative cell counts
G1
S
G2/M
(X 10³)
Betulin
DNA content (PE-A)
G2/M
S
G1
Cell cycle distribution (%)
Betulin
-
+

Figure 43. SREBP1c controls ccRCC cell growth through coordinated regulation of cell cycle and fatty acid metabolism. (A) Experimental scheme to test the effects of siRNA-mediated suppression of PTTG1 or FASN, and pharmacological inhibition of lipogenic genes including *FASN* and *ACC*. **(B** and **C)** Lentivirus-mediated Mock (as a negative control) or SREBP1c overexpressing ACHN cells were transfected with PTTG1 siRNA for 48 hours. Relative mRNA levels were then determined using qRT-PCR and were normalized to that of GAPDH. Expression data are presented relative to the negative control as means ± SD of three individual samples. $^{\#}P < 0.05$ versus negative control; $^{\#\#}P < 0.01$ versus negative control. **(D)** Relative growth rates of cells described in Figures 43B and 43C were measured using CCK-8 assays. CCK-8, Cell Counting Kit-8; $*P < 0.05$; $**P < 0.01$; n.s., not significant.

Figure 43

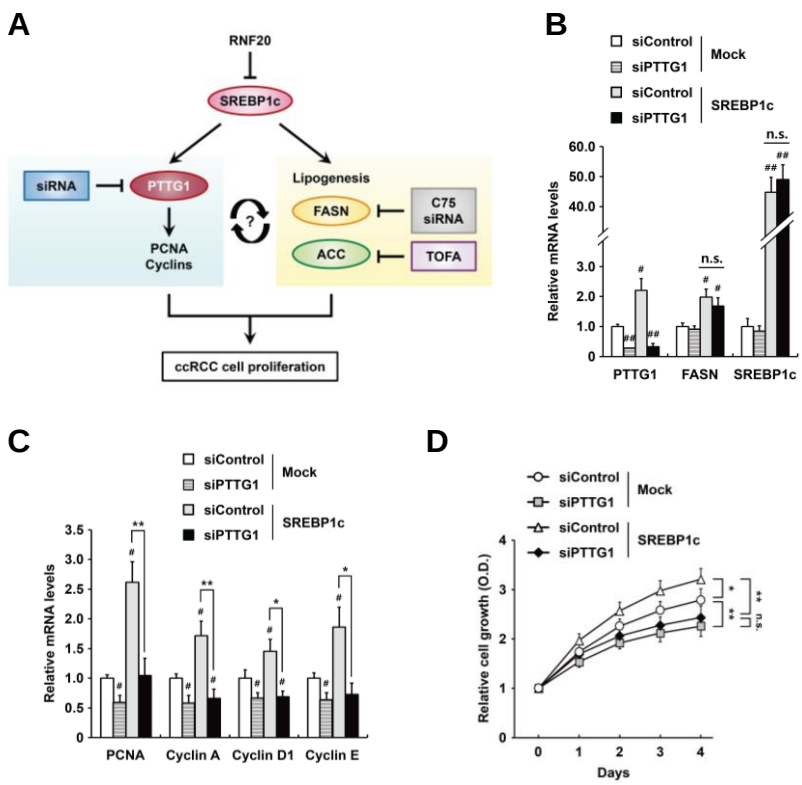
A
RNF20
SREBP1c
siRNA
PTTG1
PCNA
Cyclins
Lipogenesis
FASN
C75
siRNA
ACC
TOFA
ccRCC cell proliferation
B
siControl
siPTTG1
Mock
siControl
siPTTG1
SREBP1c
Relative mRNA levels
PTTG1
FASN
SREBP1c
n.s.
C
siControl
siPTTG1
Mock
siControl
siPTTG1
SREBP1c
Relative mRNA levels
PCNA
Cyclin A
Cyclin D1
Cyclin E
D
siControl
siPTTG1
Mock
siControl
siPTTG1
SREBP1c
Relative cell growth (O.D.)
Days
n.s.

Figure 44. Suppression of lipogenic activity does not change expression of PTTG1 and cell cycle genes. (A) ACHN ccRCC cells were treated with TOFA (10 μg/ml) or C75 (10 μg/ml) for 24 hours, and intracellular triglyceride contents were measured. **(B)** ACHN ccRCC cells were treated with TOFA (10 μg/ml) or C75 (10 μg/ml) for 24 hours, and relative mRNA expression levels were determined using qRT-PCR. PTTG1 mRNA levels are presented relative to those in the vehicle control group. n.s., not significant. **(C)** Relative growth rates of cells described in Figures 44A and 44B were measured using CCK-8 assays. CCK-8, Cell Counting Kit-8; $^{**}P < 0.01$; n.s., not significant. **(D** and **E)** ACHN ccRCC cells were treated with TOFA (10 μg/mL) or C75 (10 μg/mL) for 24 hours. Relative mRNA levels were normalized to that of the GAPDH gene, and are presented relative to those in the vehicle group. $^{*}P < 0.05$; $^{**}P < 0.01$.

Figure 44

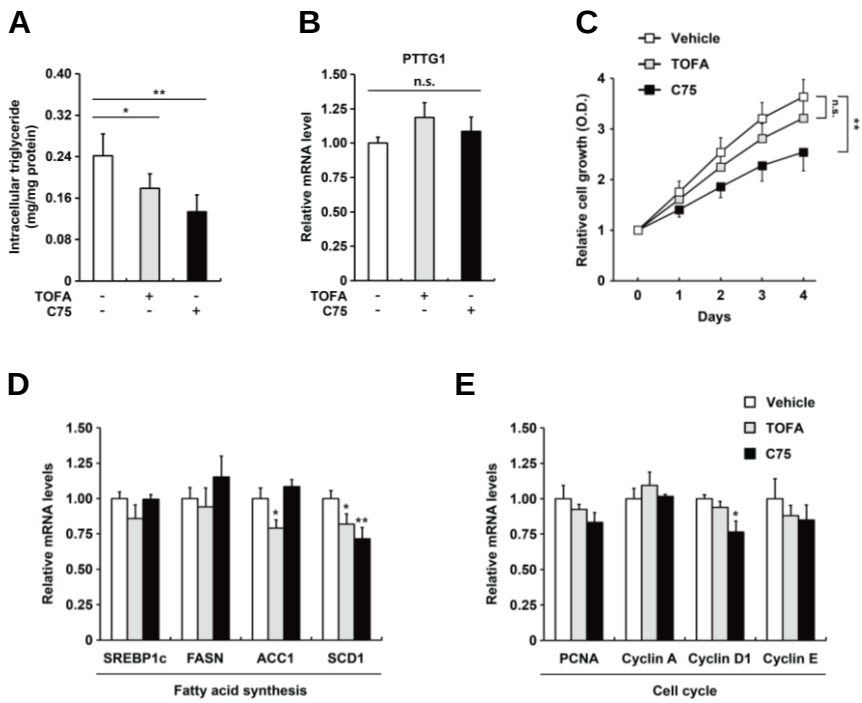
A
Intracellular triglyceride (mg/mg protein)
0.40
0.32
0.24
0.16
0.08
0
**
*
TOFA - + -
C75 - - +
B
PTTG1
n.s.
Relative mRNA level
1.50
1.25
1.00
0.75
0.50
0.25
0
TOFA - + -
C75 - - +
C
Vehicle
TOFA
C75
Relative cell growth (O.D.)
4
3
2
1
0
n.s.
**
0 1 2 3 4
Days
D
Relative mRNA levels
1.50
1.25
1.00
0.75
0.50
0.25
0
*
**
SREBP1c FASN ACC1 SCD1
Fatty acid synthesis
E
Vehicle
TOFA
C75
Relative mRNA levels
1.50
1.25
1.00
0.75
0.50
0.25
0
*
PCNA Cyclin A Cyclin D1 Cyclin E
Cell cycle

siRNA-mediated suppression of FASN did not greatly alter mRNA levels of PTTG1 and cell-cycle regulatory genes (Figures 45A and 45B). However, both C75-mediated pharmacological inhibition of FASN and siRNA-driven FASN knockdown led to significant decreases in ccRCC cell proliferation (Figures 44C and 45C). Furthermore, pharmacologic and genetic inhibition of FASN reduced the effects of SREBP1c overexpression on cell growth in ACHN cells, implying that inhibition of lipogenesis might attenuate ccRCC cell proliferation via SREBP1c-dependent pathways (Figures 45C and 45D). Taken together, these data show that PTTG1 and *de novo* lipogenic pathways in ccRCC cells are independently regulated by SREBP1c, which would influence cell proliferation via lipid metabolism and cell cycle regulation.

RNF20 overexpression attenuates tumor growth in ccRCC xenografts.

To validate the present roles of RNF20 in ccRCC tumor growth *in vivo*, I performed xenograft experiments in nude mice. In ACHN xenograft tumors, ectopic RNF20 expression significantly inhibited tumor growth rates (Figures 46A and 46B) and led to decreased tumor masses (Figure 46C), indicating that RNF20 could suppress ccRCC tumor growth. In addition, subsequent western blot analyses showed that ectopic expression of RNF20 inhibited protein expression of SREBP1, PTTG1, and FASN in xenograft tumors (Figure 46D). Moreover, RNF20 significantly attenuated mRNA expression of SREBP1c, cell-cycle regulators, and lipogenic genes in xenograft tumors (Figure 46E). In H&E staining experiments, ACHN tumors with elevated RNF20 expression exhibited reduced numbers of cells with clear cell morphology (Figure 47). Consistently, Oil Red O staining indicated

Figure 45. SREBP1c controls ccRCC cell growth through dual modes of action that affect cell cycle and lipid metabolism. (A and **B)** Lentivirus-mediated Mock (negative control) or SREBP1c overexpressing ACHN cells were transfected with FASN siRNA for 48 hours, and mRNA levels were determined using qRT-PCR. Relative mRNA expression was normalized to that of the GAPDH gene, and is shown relative to those in the negative control group. $^{\#}P < 0.05$ versus negative control; $^{\#\#}P < 0.01$ versus negative control; n.s., not significant. **(C)** Relative proliferation rates of cells described in Figures 45A and 45B were monitored using CCK-8 assays. CCK-8, Cell Counting Kit-8; $*P < 0.05$; $**P < 0.01$. **(D)** ACHN ccRCC cells stably overexpressing Mock or SREBP1c following lentiviral transduction. After treatment with C75, cell proliferation rates were monitored using CCK-8 assay. Data are representative of at least three independent experiments.

Figure 45

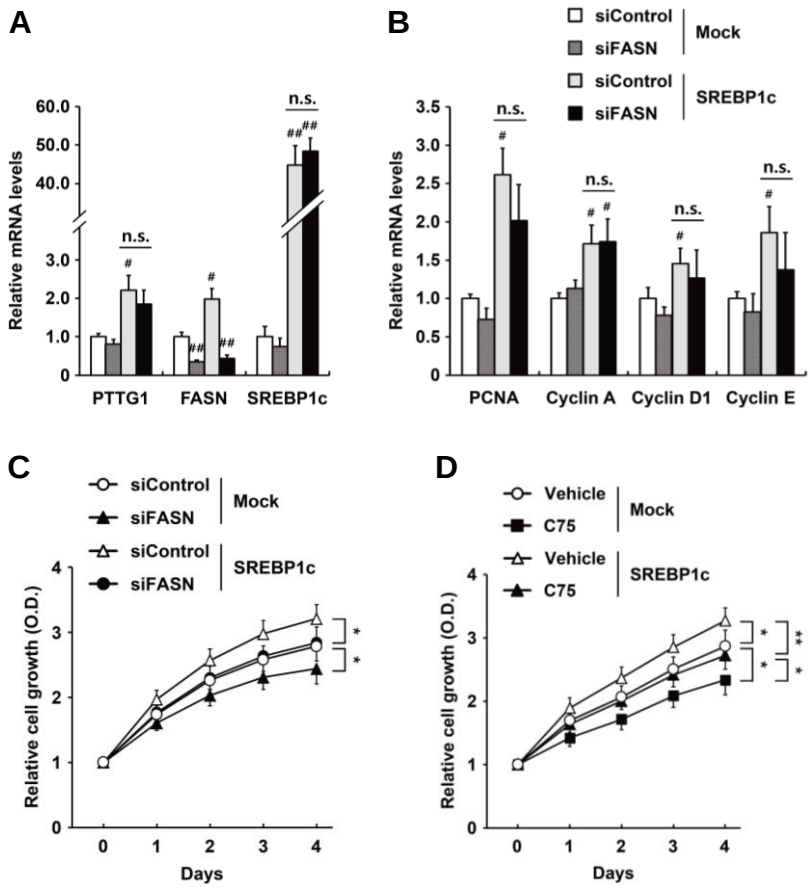
A
Relative mRNA levels
60.0
50.0
40.0
3.0
2.0
1.0
0
n.s.
n.s.
#
##
PTTG1
FASN
SREBP1c
B
siControl
siFASN
Mock
siControl
siFASN
SREBP1c
Relative mRNA levels
3.5
3.0
2.5
2.0
1.5
1.0
0.5
0
n.s.
PCNA
Cyclin A
Cyclin D1
Cyclin E
C
siControl
siFASN
Mock
siControl
siFASN
SREBP1c
Relative cell growth (O.D.)
Days
D
Vehicle
C75
Mock
Vehicle
C75
SREBP1c
Relative cell growth (O.D.)
Days

Figure 46. RNF20 overexpression attenuates tumor growth in xenograft mice. **(A)** Subcutaneous tumors of ACHN cells expressing either Mock or ectopic RNF20 were generated in female BALB/c nude mice (each group includes ten tumors from five mice). Representative images of tumors dissected at the end of the study showing the effect of RNF20 overexpression on the growth of *in vivo* xenograft tumors. Scale bar, 10 mm. **(B)** Xenograft tumor volumes (mm^3) of ACHN cells with or without ectopic RNF20 expression were determined over 35 days. The graph shows tumor volumes as mean ± SEM. **(C)** End-point xenograft tumor weights (mg) were measured and plotted. **(D)** Expression levels of RNF20, nSREBP1, PTTG1, and FASN protein in ACHN xenograft tumors were monitored using western blotting analyses. nSREBP1, nuclear SREBP1. **(E)** The effects of ectopic RNF20 expression on cell cycle, and lipogenic gene expression were determined using qRT-PCR analyses in ACHN xenograft tumors. Relative mRNA levels were normalized to GAPDH mRNA level and are shown relative to the Mock control group. $^{**}P < 0.01$; $^{***}P < 0.001$.

Figure 46

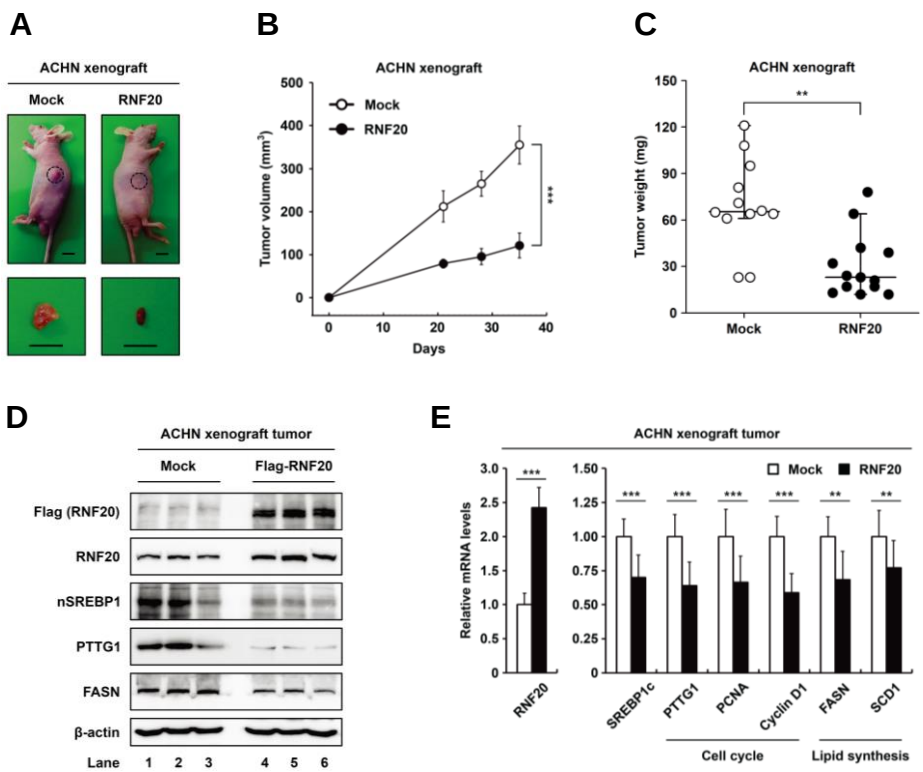
A
ACHN xenograft
Mock
RNF20
B
ACHN xenograft
Mock
RNF20
Tumor volume (mm³)
Days
***
C
ACHN xenograft
**
Tumor weight (mg)
Mock
RNF20
D
ACHN xenograft tumor
Mock
Flag-RNF20
Flag (RNF20)
RNF20
nSREBP1
PTTG1
FASN
β-actin
Lane 1 2 3 4 5 6
E
ACHN xenograft tumor
Mock
RNF20
Relative mRNA levels
RNF20
SREBP1c
PTTG1
PCNA
Cyclin D1
FASN
SCD1
Cell cycle
Lipid synthesis

that ectopic RNF20 expression reduced lipid accumulation (Figure 47). Furthermore, Ki67 staining analyses revealed that exogenous RNF20 reconstitution decreased cell proliferative properties in xenograft tumors (Figure 47). Moreover, terminal deoxynucleotidyl transferase dUTP nick end labeling (TUNEL) analyses showed that RNF20 overexpression induced apoptosis in xenograft tumors (Figure 47). I also observed increased mRNA expression of the pro-apoptotic genes including *Bax*, *Bid*, and *Caspase-3* following ectopic expression of RNF20, whereas mRNA expression of the anti-apoptotic genes *Bcl-2*, *cIAP-2*, and *XIAP* were reduced (Figure 48). These *in vivo* data suggest that RNF20 would act as a tumor suppressor by inhibiting SREBP1c-mediated lipogenesis and cell cycle regulation in ccRCC. In summary, the present data suggest that RNF20 downregulation in ccRCC allows for SREBP1c induction, which enhances the expression of PTTG1 and lipogenic genes that drive tumor growth and progression in ccRCC.

Figure 47. RNF20 overexpression reduces lipid storage and cell viability in ccRCC xenografts. Histologic analyses of xenograft tumors. Representative hematoxylin and eosin (H&E) and Oil Red O staining of Mock or RNF20-transduced ACHN xenograft tumors. IHC of xenograft tumors stained with Ki67 and TUNEL. TUNEL, terminal deoxynucleotidyl transferase dUTP nick end labeling; Scale bar, 100 μm.

Figure 47

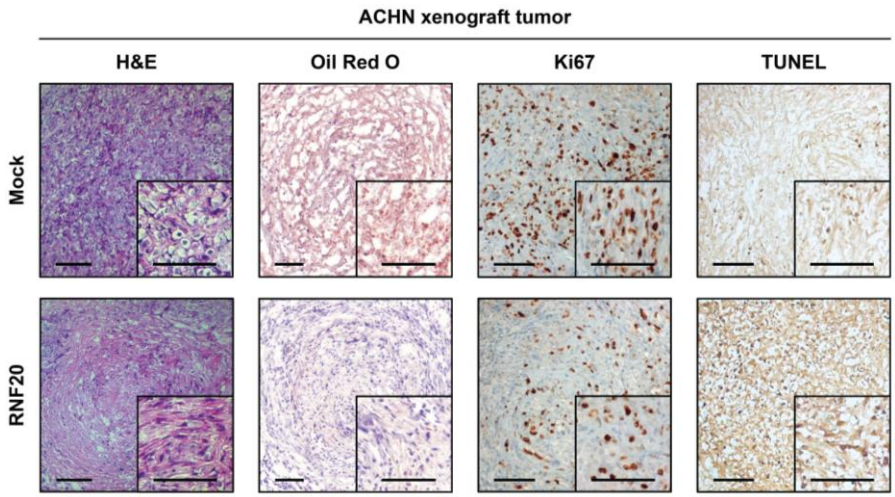

Figure 48. RNF20 regulates the expression of pro-apoptotic and anti-apoptotic genes in xenograft tumors. The effects of ectopic RNF20 expression on apoptotic gene expression in ACHN xenograft tumors were determined using qRT-PCR analyses. Relative mRNA expression was normalized to that of the GAPDH gene, and is presented relative to those in the Mock control group. $^{**}P < 0.01$; $^{***}P < 0.001$.

Figure 48

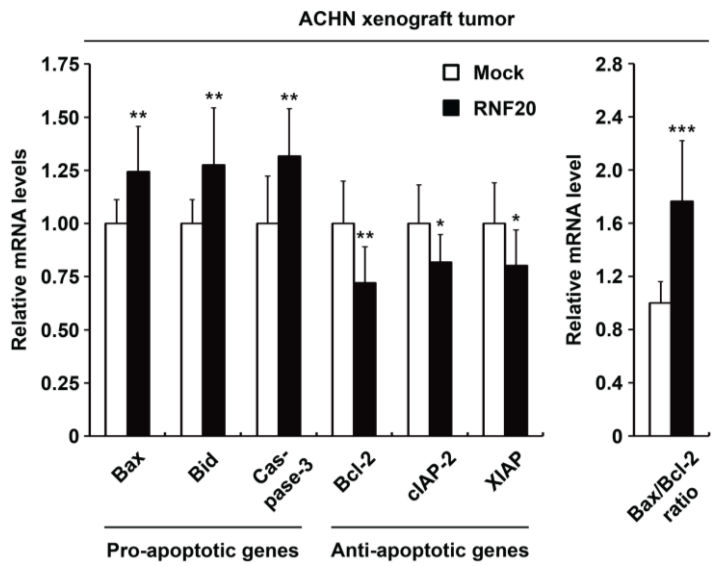
ACHN xenograft tumor
Mock
RNF20
Relative mRNA levels
1.75
1.50
1.25
1.00
0.75
0.50
0.25
0
**
**
**
**
*
*
Bax
Bid
Cas-pase-3
Bcl-2
cIAP-2
XIAP
Pro-apoptotic genes
Anti-apoptotic genes
Relative mRNA level
2.8
2.4
2.0
1.6
1.2
0.8
0.4
0
***
Bax/Bcl-2 ratio

Discussion

It is well established that constitutive activation of HIF due to the loss of *VHL* in ccRCC causes pathogenic metabolic alterations (Kaelin, 2008; Shen and Kaelin, 2013). However, kidney-specific *VHL* deficient mice did not exhibit ccRCC-like metabolic phenotypes (Rankin et al., 2006), suggesting additional mechanisms of ccRCC tumor formation. The present data demonstrate that RNF20 downregulation promotes ccRCC tumorigenesis by activating SREBP1c. In agreement, several lines of evidence support the idea that RNF20 would suppress ccRCC tumor growth. Among these, RNF20 expression was decreased in ccRCC tumors compared with normal kidney tissues (Figure 25, A-E) and was inversely correlated with SREBP1 and lipogenic gene expression (Figure 30, A-I; Figure 31, A-E). Accordingly, low RNF20 expression was strongly associated with poor survival in ccRCC patients regardless of *VHL* mutation status (Figure 27, A-C), indicating that RNF20 expression is inversely correlated with ccRCC progression. In agreement, ectopic expression of RNF20 repressed SREBP1c and cell proliferation in both *VHL* wild-type and depleted ccRCC cell lines (Figures 28B, 33A, and 35B), but did not affect proliferation of in HRCE and HEK293 normal kidney cells with high basal RNF20 expression (Figures 25F and 29B). Finally, RNF20 overexpression decreased tumor growth in ccRCC xenografts and was accompanied by reduced expression of SREBP1c and its target genes (Figure 46). Previous epigenetic studies have shown that several tumor suppressor genes play roles in ccRCC (Arai et al., 2009; Ricketts et al., 2012). For example, it has been reported that the RNF20 promoter contains prominent CpG islands and is hypermethylated in breast cancer tumors (Shema et al., 2008). Correspondingly,

treatment of ACHN ccRCC cells with the DNA methyltransferase inhibitor RG108 led to a substantial increase in RNF20 mRNA expression, but this was not observed in HEK293 cells (Figure 26B), implying that RNF20 promoter hypermethylation, at least partly, may serve to dampen RNF20 expression in ccRCC.

In agreement with previous observations of abundant lipid storage and increased lipogenesis in ccRCC (Drabkin and Gemmill, 2010; Li and Kaelin, 2011), the present data show upregulated SREBP1 and lipogenic activities (Figure 30, A-I; Figures 31A and 31B). However, mRNA levels of SREBP2 and its target gene, such as *HMGCR*, were decreased in ccRCC tumors (Figure 32, A-D), indicating that SREBP1 and *de novo* lipogenesis might play primary oncogenic roles. These observations warrant consideration of pharmacological inhibitors of lipogenesis as anti-cancer drugs for ccRCC. In accordance, the FASN inhibitor C75 and the SCD1 inhibitor A939572 potently inhibited tumor growth and invasiveness of ccRCC (Horiguchi et al., 2008; von Roemeling et al., 2013), and the SREBP inhibitor betulin repressed ccRCC cell proliferation by inhibiting SREBP1 and lipogenesis regardless of *VHL* gene mutations (Figure 40). In addition, betulin potently abolished the increases cell proliferation and lipogenic activity that followed suppression of RNF20 (Figure 41). Given the hyperactivation of SREBP1 and lipogenesis along with RNF20 downregulation in ccRCC (Figures 25, 30, and 31), unfettered SREBP1 may promote ccRCC tumor development via lipogenic activation. Therefore, it is plausible that SREBP1 and lipogenic pathways are exploitable therapeutic targets against ccRCC.

SREBP1c has been associated with *de novo* lipogenesis and cell cycle progression (Bengoechea-Alonso and Ericsson, 2006; Jeon et al., 2013; Williams et

al., 2013). Moreover, cyclin-dependent kinase 1 (CDK1)/cyclin B phosphorylates and activates SREBP1c during mitosis (Bengoechea-Alonso and Ericsson, 2006). Similarly, the SREBP-responsive miRNA miR-33 reportedly inhibited CDK6 and cyclin D1 expression, thereby reducing cell proliferation and cell cycle progression in certain cancer cells (Cirera-Salinas et al., 2012). In glioma and cervical cancers, suppression of SREBP1 represses tumor growth by inducing G_1 cell cycle arrest and apoptosis (Bengoechea-Alonso and Ericsson, 2006; Williams et al., 2013). In addition, it has been shown that betulin inhibits lung cancer cell proliferation by downregulating cell-cycle regulators such as cyclin B1, D, and E (Li et al., 2014). In this study, I showed that PTTG1 is also involved in cell cycle progression and tumorigenesis in ccRCC and acts as a novel target gene of SREBP1c. PTTG1 (also known as securin, EAP1, and TUTR1) is an anaphase inhibitor that prevents premature chromosome separation by inhibiting separase activity (Draviam et al., 2004; Jallepalli and Lengauer, 2001). Previous studies have suggested that PTTG1 participates in various pathways that modulate the cell cycle, proliferation, and survival. For example, PTTG1 has been shown to interact with p53 and prevent p53-dependent transcription and apoptosis (Bernal et al., 2002; Yu et al., 2000). Further, PTTG1 promotes the expression of several genes including *c-Myc*, *cyclin D3*, *FGF2*, and *MMP2*, potentially acting as a transcription factor (Dominguez et al., 1998; Tong and Eigler, 2009; Tong et al., 2007). In addition, it has been showed that PTTG1 is overexpressed in certain tumors including pituitary, thyroid, glioma, hepatic, colorectal, and renal cancers, and may drive tumorigenesis (Vlotides et al., 2007; Wondergem et al., 2012). In the present study, I found that high expression of PTTG1 was closely associated with advanced tumor stages and poor survival in

ccRCC patients (Figures 39D and 39E). Moreover, SREBP1c potently stimulated mRNA and protein expression of PTTG1 and several cell-cycle regulators, leading to cancer cell proliferation in ccRCC (Figures 35 and 37). In contrast, RNF20 overexpression repressed PTTG1 in both ccRCC cells and xenograft tumors (Figures 37A, 46D, and 46E), and RNF20 suppression led to increased mRNA and protein levels of PTTG1 (Figures 37B and 37D). Accordingly, PTTG1 expression was negatively associated with RNF20 expression, reflecting modulation of SREBP1c in ccRCC tumor tissues (Figure 39D) and suggesting that RNF20 downregulation would promote ccRCC development and progression, in part by upregulating PTTG1. In agreement, siRNA knockdown of PTTG1 led to decreased mRNA expression of cell-cycle regulatory genes without changing lipogenic activity (Figures 43B and 43C). Furthermore, PTTG1 suppression attenuated the effects of activated SREBP1c on ccRCC cell proliferation (Figure 43D). Therefore, it is likely that RNF20-SREBP1c-PTTG1 axis is central to ccRCC cell proliferation and tumorigenesis.

It is well established that SREBP1 regulates lipid metabolism, predominantly by increasing *de novo* lipogenesis. Thus, I tested whether lipogenesis is associated with PTTG1 expression in the presence of genetic and pharmacological inhibitors of *de novo* lipogenesis. In these experiments, mRNA expression of PTTG1 in ACHN ccRCC cells was not affected by pharmacological inhibition of lipogenesis using TOFA or C75 (Figure 44B) or by siRNA-mediated knockdown of FASN (Figure 45A), suggesting that SREBP1c would stimulate PTTG1 in a lipogenesis-independent manner. Thus, SREBP1c may affect lipid metabolism and cell cycle progression by regulating different set of genes, which

eventually coalesce to drive tumor development in ccRCC. Many studies have demonstrated that lipogenic inactivation by TOFA or C75 induces cell cycle arrest and apoptosis in several cancers, including lung, colorectal, and renal cancers (Horiguchi et al., 2008; Wang et al., 2009). Hence, future studies are required to clarify whether lipogenic pathways might affect PTTG1 and cell cycle progression in other tissues and/or cancers.

According to the present data, I propose a model in which RNF20 acts as a tumor suppressor by inhibiting SREBP1c-mediated lipogenesis and cell cycle regulation (Figure 49). Conversely, these data indicate that RNF20 downregulation promotes tumorigenesis by activating SREBP1c in ccRCC tumors. In addition, I identified a novel mechanism by which SREBP1c stimulates cell cycle progression by inducing PTTG1 in ccRCC, and I suggest that RNF20 could modulate the SREBP1c-lipogenesis axis and the SREBP1c-PTTG1 axis. Taken together, these findings implicate RNF20 as a novel tumor suppressor in ccRCC and suggest clinical benefits of therapeutic approaches that target components of the RNF20-SREBP1c pathway in cancer.

Figure 49. Proposed model illustrating tumor-suppressive functions of RNF20 against SREBP1-mediated lipogenesis and cell cycle progression in ccRCC. RNF20 downregulation and SREBP1 upregulation are associated with poor prognosis in ccRCC patients. Downregulation of RNF20 induces SREBP1 hyperactivation, leading to ccRCC tumorigenesis. SREBP1 controls cell cycle regulation by PTTG1 as a novel SREBP1c target gene. In addition, the small-molecule SREBP inhibitor betulin blocks cell proliferation by inhibiting lipogenesis and inducing G_1 cell cycle arrest. Taken together, RNF20 downregulation promotes tumorigenesis via SREBP1-mediated lipogenesis and cell cycle progression in ccRCC.

Figure 49

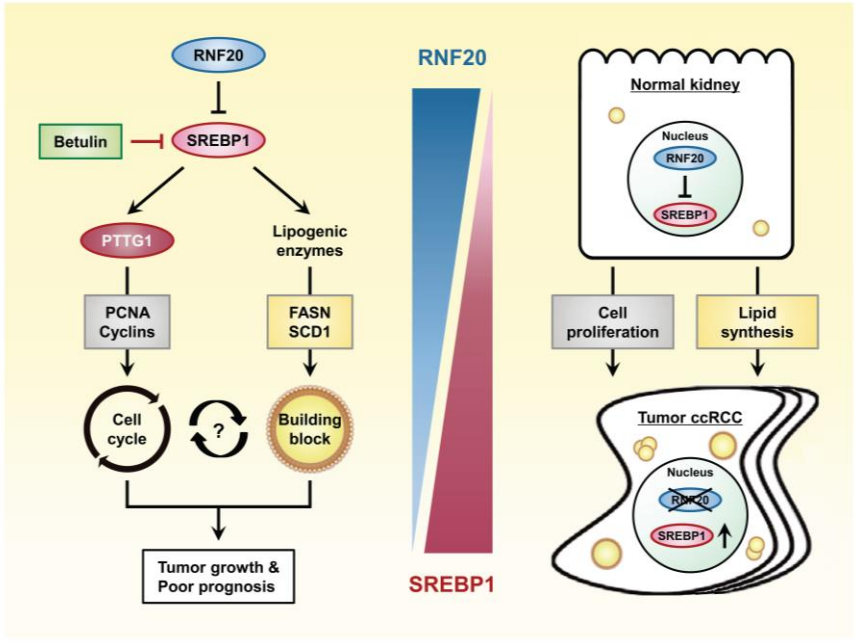
RNF20
Betulin
SREBP1
PTTG1
Lipogenic enzymes
PCNA Cyclins
FASN SCD1
Cell cycle
?
Building block
Tumor growth & Poor prognosis
RNF20
SREBP1
Normal kidney
Nucleus
RNF20
SREBP1
Cell proliferation
Lipid synthesis
Tumor ccRCC
Nucleus
RNF20
SREBP1

CONCLUSION & PERSPECTIVES

Lipid metabolism is essential for cell growth and survival. Thus, dysregulation of lipid metabolism is closely associated with metabolic disorders and tumorigenesis. SREBP1c is a key transcription factor for lipid metabolism. In last decades, enormous efforts have been made to elucidate the regulatory mechanisms and functions of SREBP1c in physiological and pathophysiological conditions. Nonetheless, the regulatory mechanisms that control SREBP1c turnover in response to fasting status are not thoroughly elucidated. To investigate which factors are involved in stability and activity of SREBP1c, I have tried to identify SREBP1c-interacting proteins. Through affinity purification and mass spectrometry analyses, RNF20 has been identified as an E3 ubiquitin ligase for SREBP1c. Furthermore, to investigate the pathophysiological roles of RNF20-SREBP1c axis on cell proliferation in cancers, I have attempted to identify SREBP1c target genes that might be involved in cell cycle regulation using RNA-Seq analyses with wild-type and *SREBP1c* deficient mice. As a novel target gene of SREBP1c, *PTTG1* regulate cell cycle genes and cell proliferation in ccRCC cells. Collectively, these data provide new insights to understand novel mechanism between lipid metabolism and cell cycle progression.

1. RNF20 is an E3 ubiquitin ligase for SREBP1c

SREBP1c governs *de novo* lipogenesis by stimulating its target genes, including *FASN*, *ACC*, *SCD1*, and *ELOVL6* (Eberle et al., 2004b; Kim and Spiegelman, 1996; Kumadaki et al., 2008). SREBP1c is sensitively regulated by

nutritional and hormonal changes to maintain energy homeostasis. SREBP1c is activated by insulin, whereas SREBP1c is suppressed by glucagon (Horton et al., 1998a; Kim et al., 1998). Although SREBP1c-mediated lipogenic program is rapidly repressed by nutritional deprivations, the factors that are involved in the suppression of SREBP1c activity during fasting have not been clearly identified. In the chapter one, I demonstrated that RNF20 is an E3 ubiquitin ligase for SREBP1c and acts as a negative regulator of hepatic lipid metabolism through PKA-dependent SREBP1c degradation.

RNF20 has been firstly identified as yeast Bre1 and possesses a RING finger domain that primarily functions as an E3 ligase for histone H2B monoubiquitination, which regulates expression of certain genes (Hwang et al., 2003; Kim et al., 2005; Wood et al., 2003). Also, RNF20 plays various roles in transcription, DNA damage responses, and stem cell differentiation (Cole et al., 2015; Shema et al., 2008). Moreover, it has been suggested that RNF20 acts as a tumor suppressor in breast and colorectal cancers (Shema et al., 2008; Tarcic et al., 2016). Nevertheless, it has not been thoroughly investigate whether RNF20 might be involved in lipid metabolism.

SREBP1c is very unstable and rapidly degraded by the proteasome (Hirano et al., 2003; Hirano et al., 2001). It has been reported that SREBP1c is phosphorylated by GSK-3β, which leads to F-box and WD repeat domain-containing 7 (FBXW7)-dependent ubiquitination of SREBP1c (Punga et al., 2006; Sundqvist et al., 2005). However, a recent *in vivo* study has been reported that inhibition FBXW7 does not alter the expression of SREBP1c or lipogenic genes in the liver (Kumadaki et al., 2011). It is of interest to note that RNF20 would induce

polyubiquitination and degradation of SREBP1c upon PKA activation, whereas PKA activation did not change the level of FBXW7. Given that PKA plays a crucial role in catabolic responses, PKA activation with forskolin decreased lipogenic gene expression with an increase in RNF20, whereas suppression of RNF20 reversed the effect of forskolin on lipogenic gene expression, implying that RNF20 might mediate PKA signaling cascade to downregulate hepatic lipid metabolism via SREBP1c degradation. Here, I found out a novel mechanism of SREBP1c regulation by RNF20 during nutritional deprivation. Knowledge regarding this process enhances the molecular mechanisms of how SREBP1c is able to turn off hepatic lipid metabolism during nutritional deprivation.

2. RNF20 is downregulated in ccRCC

In cancer cells, elevated lipid metabolism plays an important role by providing building blocks for tumor growth (DeBerardinis et al., 2008; Schulze and Harris, 2012). Particularly, ccRCC, the most common subtype of kidney cancers, is characterized by ectopic intracellular lipid accumulation (Rezende et al., 1999; Valera and Merino, 2011). Metabolic alteration and pathogenesis are characterized by constitutive activation of HIF due to loss of the *VHL* in 90% of ccRCC tumors (Kaelin, 2008; Shen and Kaelin, 2013). Nonetheless, kidney-specific *VHL* deficient mice fail to exhibit ccRCC-like metabolic phenotypes and tumor formation, implying that additional mechanisms might be present in ccRCC (Rankin et al., 2006). The finding that RNF20 acts as a negative regulator of *de novo* lipogenesis by inhibition of SREBP1c prompted me to test whether RNF20 might be dysregulated in ccRCC tumors.

In the chapter two, I have shown that RNF20 is downregulated and exhibits tumor-suppressive functions in ccRCC. Several lines of evidence from *in vivo* and *in vitro* data support the above idea. First, RNF20 expression was decreased in ccRCC tumors compared with normal kidney tissues. Furthermore, low RNF20 expression was associated with poor survival regardless of *VHL* mutation status in ccRCC patients, implying that RNF20 might oppose ccRCC progression in a *VHL*-independent manner. Second, ectopic expression of RNF20 repressed SREBP1c and cell proliferation in both *VHL* wild-type ACHN and *VHL* depleted A498 ccRCC cell lines. Third, the levels of SREBP1c and tumor growth were reduced by RNF20 overexpression *in vivo* ccRCC xenograft tumors.

RNF20 has been reported as a putative tumor suppressor (Shema et al., 2008), possibly functioning through interaction with p53 and its presence at the promoter of p53 target genes (Kim et al., 2005). RNF20-promoted histone H2B monoubiquitination is elevated at the coding regions of p53 target genes upon their activation (Minsky et al., 2008). Suppression of RNF20 results in a decrease in p53 expression, which leads to increase in cell migration and tumorigenesis. Also, downregulation of RNF20 increases tumor growth (Shema et al., 2008).

RNF20 promoter contains prominent CpG islands and is hypermethylated in breast cancer tumors (Shema et al., 2008). Consistent with these reports, I observed that DNA methyltransferase inhibitor RG108 treatment to ACHN ccRCC cell lines substantially increased the level of RNF20 mRNA, but not in HRCE and HEK293 normal kidney cell lines, implying that RNF20 promoter hypermethylation, at least partly, may serve to dampen RNF20 expression in ccRCC. Together, I suggest that RNF20 would act as a potential tumor suppressor

and is downregulated in ccRCC.

3. SREBP1c promotes lipogenesis and cell proliferation in ccRCC

Accumulating evidences have demonstrated that activated SREBP1c enhances lipogenesis in certain cancers (Griffiths et al., 2013; Guo et al., 2014). In addition, SREBP1c promotes lipid metabolism and tumor development, potentiating progression and migration, leading to poor prognosis in certain cancers (Guo et al., 2009; Huang et al., 2012). Previous studies have shown that lipogenic enzymes such as FASN and SCD1 are increased in various cancers (Igal, 2010; Menendez and Lupu, 2007). Moreover, drugs targeting against SREBP1c-driven lipogenesis have been shown as anti-cancer effects in glioblastoma therapy (Guo et al., 2009). However, it remains unclear whether SREBP1 and lipogenic genes might be associated with ectopic lipid storage and cell proliferation in ccRCC.

In this study, I demonstrated that SREBP1c and lipogenic activities are upregulated in ccRCC tumors and promote ccRCC cell proliferation. In TCGA analyses, the mRNA levels of SREBP1 and lipogenic genes were elevated in ccRCC tumors compared with normal kidney tissues, which were correlated with poor prognosis in ccRCC patients. In addition, I verified that ectopic SREBP1c overexpression stimulated ccRCC cell proliferation. These observations warrant a potential consideration of pharmacological inhibitors for lipogenesis as anti-cancer drugs against ccRCC. Accordingly, the SREBP inhibitor betulin repressed ccRCC cell proliferation by inhibiting SREBP1 and lipogenesis. Given the hyperactivation of SREBP1 and lipogenesis along with RNF20 downregulation in ccRCC, unfettered SREBP1 may promote ccRCC tumor development via lipogenic

activation. Therefore, it is plausible that SREBP1 and lipogenic pathways might be potential therapeutic targets against ccRCC.

4. SREBP1c-PTTG1 axis potentiates cell cycle progression and tumorigenesis

Recently, it has been reported that SREBP1c is involved in not only fatty acid synthesis but also cell cycle progression (Bengoechea-Alonso and Ericsson, 2006; Jeon et al., 2013; Williams et al., 2013). For example, CDK1/cyclin B-mediated phosphorylation stabilizes and activates SREBP1c during mitosis (Bengoechea-Alonso and Ericsson, 2006). In addition, miR-33, which is one of the SREBP-responsive miRNAs, inhibits the expression of the CDK6 and cyclin D1, thereby reducing cell proliferation and cell cycle progression in Huh7 and A549 cells (Cirera-Salinas et al., 2012). In glioma and cervical cancers, suppression of SREBP1 represses tumor growth via inducing G_1 cell cycle arrest and apoptosis (Bengoechea-Alonso and Ericsson, 2006; Williams et al., 2013). Furthermore, it has been shown that betulin inhibits lung cancer cell proliferation by downregulating cell-cycle regulators such as cyclin B1, D, and E (Li et al., 2014).

Here, I have identified that PTTG1 is a novel target gene of SREBP1c and involved in cell cycle progression and tumorigenesis in ccRCC. PTTG1 (also known as securin, EAP1, and TUTR1) is an anaphase inhibitor that prevents premature chromosome separation through inhibition of separase activity and also interacts with p53, which leads to inhibit p53-dependent transcription and apoptosis (Draviam et al., 2004; Jallepalli and Lengauer, 2001). Besides, PTTG1 appears to function as a transcription factor, which promotes the transcription of

several genes, such as *c-Myc*, *cyclin D3*, *FGF2*, and *MMP2* (Dominguez et al., 1998; Tong and Eigler, 2009). Thus, it seems that PTTG1 participates in several key cellular events such as gene transcription, cell transformation, angiogenesis, metabolism, apoptosis, DNA repair, genetic instability, and mitotic control (Bradshaw and Kakar, 2007; Vlotides et al., 2007). Recently, PTTG1 has been categorized as an oncogene because PTTG1 is overexpressed in numerous tumors including pituitary, thyroid, glioma, hepatic, colorectal, and renal cancers (Bradshaw and Kakar, 2007; Vlotides et al., 2007). In accordance with the previous reports (Wondergem et al., 2012), high PTTG1 expression was associated with advanced tumor stage and poor survival in ccRCC, whereas PTTG1 expression was negatively correlated with RNF20 expression. Notably, SREBP1c potently stimulated the levels of PTTG1 mRNA, protein, and several cell-cycle regulators, leading to cancer cell proliferation in ccRCC. In contrast, PTTG1 knockdown via siRNA decreased the mRNA levels of cell-cycle regulatory genes without change of lipogenic activity. In addition, pharmacological inhibition of lipogenesis with TOFA or C75 did not change the mRNA level of PTTG1 in ccRCC cell lines. These data indicate that SREBP1c could stimulate PTTG1 level, probably, in a lipogenesis-independent manner. Together, these data suggest that SREBP1c could regulate not only lipid metabolism but also cell cycle progression by regulating different set of genes, which would eventually coalesce to drive tumor development in ccRCC. Nevertheless, further studies are required to clarify whether lipogenic pathway might affect PTTG1 and cell cycle progression in other tissues and/or different types of cancers.

In conclusion, I have elucidated a novel mechanism of lipid metabolism which RNF20 downregulates SREBP1c upon fasting. Furthermore, this work provides a clue to understand how SREBP1c is rapidly regulated by fasting signals to prevent futile lipogenic activation. Because there is a positive correlation between lipogenic activity and metabolic complications such as obesity, NAFLD, and certain cancers, it is likely that RNF20 might be a metabolic tumor suppressor in certain cancers associated with increased lipid metabolism. In addition, I have investigated whether RNF20 might be involved in tumorigenesis in ccRCC, which is characterized by ectopic intracellular lipid storage. This study indicates that downregulation of RNF20 stimulates tumorigenesis following SREBP1c activation in ccRCC, accompanied with poor prognosis. Conversely, RNF20 overexpression repressed lipogenesis and cell proliferation by inhibiting SREBP1c in cultured ccRCC cells and xenograft studies. Notably, PTTG1 was identified as a novel SREBP1c target gene that plays a crucial role in cell cycle control in ccRCC. Taken together, RNF20 suppresses tumorigenesis by inhibiting SREBP1c-mediated lipogenesis and cell cycle regulation in ccRCC. I believe that this work establishes the key role of RNF20-SREBP1c axis for the control of lipogenesis and cell cycle progression, which may shed light on the development of therapeutic strategies in ccRCC.

References

Amemiya-Kudo, M., Shimano, H., Yoshikawa, T., Yahagi, N., Hasty, A.H., Okazaki, H., Tamura, Y., Shionoiri, F., Iizuka, Y., Ohashi, K., *et al.* (2000). Promoter analysis of the mouse sterol regulatory element-binding protein-1c gene. J Biol Chem *275*, 31078-31085.

Arai, E., Ushijima, S., Fujimoto, H., Hosoda, F., Shibata, T., Kondo, T., Yokoi, S., Imoto, I., Inazawa, J., Hirohashi, S., *et al.* (2009). Genome-wide DNA methylation profiles in both precancerous conditions and clear cell renal cell carcinomas are correlated with malignant potential and patient outcome. Carcinogenesis *30*, 214-221.

Bakan, I., and Laplante, M. (2012). Connecting mTORC1 signaling to SREBP-1 activation. Curr Opin Lipidol *23*, 226-234.

Becker, T.C., Noel, R.J., Coats, W.S., Gomez-Foix, A.M., Alam, T., Gerard, R.D., and Newgard, C.B. (1994). Use of recombinant adenovirus for metabolic engineering of mammalian cells. Methods Cell Biol *43 Pt A*, 161-189.

Bengoechea-Alonso, M.T., and Ericsson, J. (2006). Cdk1/cyclin B-mediated phosphorylation stabilizes SREBP1 during mitosis. Cell Cycle *5*, 1708-1718.

Bernal, J.A., Luna, R., Espina, A., Lazaro, I., Ramos-Morales, F., Romero, F., Arias, C., Silva, A., Tortolero, M., and Pintor-Toro, J.A. (2002). Human securin interacts with p53 and modulates p53-mediated transcriptional activity and apoptosis. Nat Genet *32*, 306-311.

Berry, M.N., and Friend, D.S. (1969). High-yield preparation of isolated rat liver parenchymal cells: a biochemical and fine structural study. The Journal of cell biology *43*, 506-520.

Bizeau, M.E., MacLean, P.S., Johnson, G.C., and Wei, Y. (2003). Skeletal muscle sterol regulatory element binding protein-1c decreases with food deprivation and increases with feeding in rats. The Journal of nutrition *133*, 1787-1792.

Bradshaw, C., and Kakar, S.S. (2007). Pituitary tumor transforming gene: an important gene in normal cellular functions and tumorigenesis. Histology and histopathology *22*, 219-226.

Bretscher, M.S., and Raff, M.C. (1975). Mammalian plasma membranes. Nature *258*, 43-49.

Briggs, M.R., Yokoyama, C., Wang, X., Brown, M.S., and Goldstein, J.L. (1993). Nuclear protein that binds sterol regulatory element of low density lipoprotein receptor promoter. I. Identification of the protein and delineation of its target nucleotide sequence. The Journal of biological chemistry *268*, 14490-14496.

Brown, M.S., and Goldstein, J.L. (1997). The SREBP pathway: regulation of cholesterol metabolism by proteolysis of a membrane-bound transcription factor. Cell *89*, 331-340.

Chen, W., Hill, H., Christie, A., Kim, M.S., Holloman, E., Pavia-Jimenez, A., Homayoun, F., Ma, Y., Patel, N., Yell, P., *et al.* (2016). Targeting Renal Cell Carcinoma with a HIF-2 antagonist. Nature.

Chintharlapalli, S., Papineni, S., Ramaiah, S.K., and Safe, S. (2007). Betulinic acid inhibits prostate cancer growth through inhibition of specificity protein transcription factors. Cancer Res *67*, 2816-2823.

Cho, H., Du, X., Rizzi, J.P., Liberzon, E., Chakraborty, A.A., Gao, W., Carvo, I., Signoretti, S., Bruick, R., Josey, J.A., *et al.* (2016). On-Target Efficacy of a HIF2alpha Antagonist in Preclinical Kidney Cancer Models. Nature.

Cirera-Salinas, D., Pauta, M., Allen, R.M., Salerno, A.G., Ramirez, C.M., Chamorro-Jorganes, A., Wanschel, A.C., Lasuncion, M.A., Morales-Ruiz, M., Suarez, Y., *et al.* (2012). Mir-33 regulates cell proliferation and cell cycle progression. Cell Cycle *11*, 922-933.

Cohen, J.C., Horton, J.D., and Hobbs, H.H. (2011). Human fatty liver disease: old questions and new insights. Science *332*, 1519-1523.

Cole, A.J., Clifton-Bligh, R., and Marsh, D.J. (2015). Histone H2B monoubiquitination: roles to play in human malignancy. Endocrine-related cancer *22*, T19-33.

Currie, E., Schulze, A., Zechner, R., Walther, T.C., and Farese, R.V., Jr. (2013). Cellular fatty acid metabolism and cancer. Cell Metab *18*, 153-161.

DeBerardinis, R.J., Lum, J.J., Hatzivassiliou, G., and Thompson, C.B. (2008). The biology of cancer: metabolic reprogramming fuels cell growth and proliferation. Cell Metab *7*, 11-20.

Dentin, R., Liu, Y., Koo, S.H., Hedrick, S., Vargas, T., Heredia, J., Yates, J., 3rd, and Montminy, M. (2007). Insulin modulates gluconeogenesis by inhibition of the coactivator TORC2. Nature *449*, 366-369.

Dif, N., Euthine, V., Gonnet, E., Laville, M., Vidal, H., and Lefai, E. (2006). Insulin activates human sterol-regulatory-element-binding protein-1c (SREBP-1c) promoter through SRE motifs. The Biochemical journal *400*, 179-188.

Divecha, N., and Irvine, R.F. (1995). Phospholipid signaling. Cell *80*, 269-278.

Dominguez, A., Ramos-Morales, F., Romero, F., Rios, R.M., Dreyfus, F., Tortolero, M., and Pintor-Toro, J.A. (1998). hpttg, a human homologue of rat pttg, is overexpressed in hematopoietic neoplasms. Evidence for a transcriptional activation function of hPTTG. Oncogene *17*, 2187-2193.

Drabkin, H.A., and Gemmill, R.M. (2010). Obesity, cholesterol, and clear-cell renal cell carcinoma (RCC). Adv Cancer Res *107*, 39-56.

Draviam, V.M., Xie, S., and Sorger, P.K. (2004). Chromosome segregation and genomic stability. Curr Opin Genet Dev *14*, 120-125.

Du, X., Kristiana, I., Wong, J., and Brown, A.J. (2006). Involvement of Akt in ER-to-Golgi transport of SCAP/SREBP: a link between a key cell proliferative pathway and membrane synthesis. Molecular biology of the cell *17*, 2735-2745.

Eberle, D., Clement, K., Meyre, D., Sahbatou, M., Vaxillaire, M., Le Gall, A., Ferre, P., Basdevant, A., Froguel, P., and Foufelle, F. (2004a). SREBF-1 gene polymorphisms are associated with obesity and type 2 diabetes in French obese and diabetic cohorts. Diabetes *53*, 2153-2157.

Eberle, D., Hegarty, B., Bossard, P., Ferre, P., and Foufelle, F. (2004b). SREBP transcription factors: master regulators of lipid homeostasis. Biochimie *86*, 839-848.

Farmer, S.R. (2006). Transcriptional control of adipocyte formation. Cell Metab *4*, 263-273.

Ferre, P., and Foufelle, F. (2010). Hepatic steatosis: a role for de novo lipogenesis and the transcription factor SREBP-1c. Diabetes Obes Metab *12 Suppl 2*, 83-92.

Flier, J.S., and Hollenberg, A.N. (1999). ADD-1 provides major new insight into the mechanism of insulin action. Proceedings of the National Academy of Sciences of the United States of America *96*, 14191-14192.

Foretz, M., Carling, D., Guichard, C., Ferre, P., and Foufelle, F. (1998). AMP-activated protein kinase inhibits the glucose-activated expression of fatty acid synthase gene in rat hepatocytes. J Biol Chem *273*, 14767-14771.

Foretz, M., Pacot, C., Dugail, I., Lemarchand, P., Guichard, C., Le Liepvre, X., Berthelier-Lubrano, C., Spiegelman, B., Kim, J.B., Ferre, P., *et al.* (1999). ADD1/SREBP-1c is required in the activation of hepatic lipogenic gene expression by glucose. Mol Cell Biol *19*, 3760-3768.

Foufelle, F., Gouhot, B., Perdereau, D., Girard, J., and Ferre, P. (1994). Regulation of lipogenic enzyme and phosphoenolpyruvate carboxykinase gene expression in cultured white adipose tissue. Glucose and insulin effects are antagonized by cAMP. European journal of biochemistry / FEBS *223*, 893-900.

Giandomenico, V., Simonsson, M., Gronroos, E., and Ericsson, J. (2003). Coactivator-dependent acetylation stabilizes members of the SREBP family of transcription factors. Molecular and cellular biology *23*, 2587-2599.

Girard, J., Perdereau, D., Foufelle, F., Prip-Buus, C., and Ferre, P. (1994). Regulation of lipogenic enzyme gene expression by nutrients and hormones. FASEB J *8*, 36-42.

Griffiths, B., Lewis, C.A., Bensaad, K., Ros, S., Zhang, Q., Ferber, E.C., Konisti, S., Peck, B., Miess, H., East, P., *et al.* (2013). Sterol regulatory element binding protein-dependent regulation of lipid synthesis supports cell survival and tumor growth. Cancer Metab *1*, 3.

Guo, D., Bell, E.H., Mischel, P., and Chakravarti, A. (2014). Targeting SREBP-1-driven lipid metabolism to treat cancer. Curr Pharm Des *20*, 2619-2626.

Guo, D., Prins, R.M., Dang, J., Kuga, D., Iwanami, A., Soto, H., Lin, K.Y., Huang, T.T., Akhavan, D., Hock, M.B., *et al.* (2009). EGFR signaling through an Akt-SREBP-1-dependent, rapamycin-resistant pathway sensitizes glioblastomas to antilipogenic therapy. Sci Signal *2*, ra82.

Ham, M., Choe, S.S., Shin, K.C., Choi, G., Kim, J.W., Noh, J.R., Kim, Y.H., Ryu, J.W., Yoon, K.H., Lee, C.H., *et al.* (2016). Glucose-6-phosphate dehydrogenase deficiency improves insulin resistance with reduced adipose tissue inflammation in obesity. Diabetes.

Hanahan, D., and Weinberg, R.A. (2000). The hallmarks of cancer. Cell *100*, 57-70.
Hanahan, D., and Weinberg, R.A. (2011). Hallmarks of cancer: the next generation. Cell *144*, 646-674.

He, T.C., Zhou, S., da Costa, L.T., Yu, J., Kinzler, K.W., and Vogelstein, B. (1998). A simplified system for generating recombinant adenoviruses. Proceedings of the National Academy of Sciences of the United States of America *95*, 2509-2514.

Hebbard, L., and George, J. (2011). Animal models of nonalcoholic fatty liver disease. Nature reviews Gastroenterology & hepatology *8*, 35-44.

Hensley, C.T., Wasti, A.T., and DeBerardinis, R.J. (2013). Glutamine and cancer: cell biology, physiology, and clinical opportunities. J Clin Invest *123*, 3678-3684.

Hirano, Y., Murata, S., Tanaka, K., Shimizu, M., and Sato, R. (2003). Sterol regulatory element-binding proteins are negatively regulated through SUMO-1 modification independent of the ubiquitin/26 S proteasome pathway. The Journal of biological chemistry *278*, 16809-16819.

Hirano, Y., Yoshida, M., Shimizu, M., and Sato, R. (2001). Direct demonstration of rapid degradation of nuclear sterol regulatory element-binding proteins by the ubiquitin-proteasome pathway. J Biol Chem *276*, 36431-36437.

Horiguchi, A., Asano, T., Asano, T., Ito, K., Sumitomo, M., and Hayakawa, M. (2008). Pharmacological inhibitor of fatty acid synthase suppresses growth and invasiveness of renal cancer cells. J Urol *180*, 729-736.

Horton, J.D., Bashmakov, Y., Shimomura, I., and Shimano, H. (1998a). Regulation of sterol regulatory element binding proteins in livers of fasted and refed mice. Proc Natl Acad Sci U S A *95*, 5987-5992.

Horton, J.D., Goldstein, J.L., and Brown, M.S. (2002). SREBPs: activators of the complete program of cholesterol and fatty acid synthesis in the liver. J Clin Invest *109*, 1125-1131.

Horton, J.D., Shimomura, I., Brown, M.S., Hammer, R.E., Goldstein, J.L., and Shimano, H. (1998b). Activation of cholesterol synthesis in preference to fatty acid synthesis in liver and adipose tissue of transgenic mice overproducing sterol regulatory element-binding protein-2. J Clin Invest *101*, 2331-2339.

Hsu, P.P., and Sabatini, D.M. (2008). Cancer cell metabolism: Warburg and beyond. Cell *134*, 703-707.

Huang, W.C., Li, X., Liu, J., Lin, J., and Chung, L.W. (2012). Activation of androgen receptor, lipogenesis, and oxidative stress converged by SREBP-1 is responsible for regulating growth and progression of prostate cancer cells. Mol Cancer Res *10*, 133-142.

Hwang, W.W., Venkatasubrahmanyam, S., Ianculescu, A.G., Tong, A., Boone, C., and Madhani, H.D. (2003). A conserved RING finger protein required for histone H2B monoubiquitination and cell size control. Mol Cell *11*, 261-266.

Igal, R.A. (2010). Stearoyl-CoA desaturase-1: a novel key player in the mechanisms of cell proliferation, programmed cell death and transformation to cancer. Carcinogenesis *31*, 1509-1515.

Ishii, S., Iizuka, K., Miller, B.C., and Uyeda, K. (2004). Carbohydrate response element binding protein directly promotes lipogenic enzyme gene transcription. Proc Natl Acad Sci U S A *101*, 15597-15602.

Jackson, R.L., Morrisett, J.D., and Gotto, A.M., Jr. (1976). Lipoprotein structure and metabolism. Physiol Rev *56*, 259-316.

Jallepalli, P.V., and Lengauer, C. (2001). Chromosome segregation and cancer: cutting through the mystery. Nat Rev Cancer *1*, 109-117.

Jang, H., Lee, G.Y., Selby, C.P., Lee, G., Jeon, Y.G., Lee, J.H., Cheng, K.K., Titchenell, P., Birnbaum, M.J., Xu, A., *et al.* (2016). SREBP1c-CRY1 signalling represses hepatic glucose production by promoting FOXO1 degradation during refeeding. Nat Commun *7*, 12180.

Janowski, B.A., Willy, P.J., Devi, T.R., Falck, J.R., and Mangelsdorf, D.J. (1996). An oxysterol signalling pathway mediated by the nuclear receptor LXR alpha. Nature *383*, 728-731.

Jensen, M.D. (1997). Lipolysis: contribution from regional fat. Annu Rev Nutr *17*, 127-139.

Jeon, T.I., Esquejo, R.M., Roqueta-Rivera, M., Phelan, P.E., Moon, Y.A., Govindarajan, S.S., Esau, C.C., and Osborne, T.F. (2013). An SREBP-responsive microRNA operon contributes to a regulatory loop for intracellular lipid homeostasis. Cell Metab *18*, 51-61.

Jeong, H.W., Lee, J.W., Kim, W.S., Choe, S.S., Shin, H.J., Lee, G.Y., Shin, D., Lee, J.H., Choi, E.B., Lee, H.K., *et al.* (2010). A nonthiazolidinedione peroxisome proliferator-activated receptor alpha/gamma dual agonist CG301360 alleviates insulin resistance and lipid dysregulation in db/db mice. Molecular pharmacology *78*, 877-885.

Jiang, G., and Zhang, B.B. (2003). Glucagon and regulation of glucose metabolism. American journal of physiology Endocrinology and metabolism *284*, E671-678.

Jitrapakdee, S. (2012). Transcription factors and coactivators controlling nutrient and hormonal regulation of hepatic gluconeogenesis. The international journal of biochemistry & cell biology *44*, 33-45.

Jo, H., Choe, S.S., Shin, K.C., Jang, H., Lee, J.H., Seong, J.K., Back, S.H., and Kim, J.B. (2013). Endoplasmic reticulum stress induces hepatic steatosis via increased expression of the hepatic very low-density lipoprotein receptor. Hepatology *57*, 1366-1377.

Kaelin, W.G., Jr. (2008). The von Hippel-Lindau tumour suppressor protein: O2 sensing and cancer. Nat Rev Cancer *8*, 865-873.

Kalaany, N.Y., Gauthier, K.C., Zavacki, A.M., Mammen, P.P., Kitazume, T., Peterson, J.A., Horton, J.D., Garry, D.J., Bianco, A.C., and Mangelsdorf, D.J. (2005). LXRs regulate the balance between fat storage and oxidation. Cell Metab *1*, 231-244.

Karmen, A., Whyte, M., and Goodman, D.S. (1963). Fatty Acid Esterification and Chylomicron Formation during Fat Absorption. 1. Triglycerides and Cholesterol Esters. J Lipid Res *4*, 312-321.

Kersten, S. (2001). Mechanisms of nutritional and hormonal regulation of lipogenesis. EMBO Rep *2*, 282-286.

Kim, J., Hake, S.B., and Roeder, R.G. (2005). The human homolog of yeast BRE1 functions as a transcriptional coactivator through direct activator interactions. Mol Cell *20*, 759-770.

Kim, J.B., Sarraf, P., Wright, M., Yao, K.M., Mueller, E., Solanes, G., Lowell, B.B., and Spiegelman, B.M. (1998). Nutritional and insulin regulation of fatty acid synthetase and leptin gene expression through ADD1/SREBP1. J Clin Invest *101*, 1-9.

Kim, J.B., and Spiegelman, B.M. (1996). ADD1/SREBP1 promotes adipocyte differentiation and gene expression linked to fatty acid metabolism. Genes Dev *10*, 1096-1107.

Kim, J.B., Spotts, G.D., Halvorsen, Y.D., Shih, H.M., Ellenberger, T., Towle, H.C., and Spiegelman, B.M. (1995). Dual DNA binding specificity of ADD1/SREBP1 controlled by a single amino acid in the basic helix-loop-helix domain. Mol Cell Biol *15*, 2582-2588.

Kim, K.H., Lee, G.Y., Kim, J.I., Ham, M., Won Lee, J., and Kim, J.B. (2010). Inhibitory effect of LXR activation on cell proliferation and cell cycle progression through lipogenic activity. J Lipid Res *51*, 3425-3433.

Kim, K.H., Song, M.J., Yoo, E.J., Choe, S.S., Park, S.D., and Kim, J.B. (2004). Regulatory role of glycogen synthase kinase 3 for transcriptional activity of ADD1/SREBP1c. J Biol Chem *279*, 51999-52006.

Kim, K.H., Yoon, J.M., Choi, A.H., Kim, W.S., Lee, G.Y., and Kim, J.B. (2009). Liver X receptor ligands suppress ubiquitination and degradation of LXRalpha by displacing BARD1/BRCA1. Mol Endocrinol *23*, 466-474.

Krebs, H.A. (1948). The tricarboxylic acid cycle. Harvey Lect *Series 44*, 165-199.

Kuhajda, F.P. (2000). Fatty-acid synthase and human cancer: new perspectives on its role in tumor biology. Nutrition *16*, 202-208.

Kumadaki, S., Karasawa, T., Matsuzaka, T., Ema, M., Nakagawa, Y., Nakakuki, M., Saito, R., Yahagi, N., Iwasaki, H., Sone, H., *et al.* (2011). Inhibition of ubiquitin ligase F-box and WD repeat domain-containing 7alpha (Fbw7alpha) causes hepatosteatosis through Kruppel-like factor 5 (KLF5)/peroxisome proliferator-activated receptor gamma2 (PPARgamma2) pathway but not SREBP-1c protein in mice. J Biol Chem *286*, 40835-40846.

Kumadaki, S., Matsuzaka, T., Kato, T., Yahagi, N., Yamamoto, T., Okada, S., Kobayashi, K., Takahashi, A., Yatoh, S., Suzuki, H., *et al.* (2008). Mouse Elovl-6 promoter is an SREBP target. Biochem Biophys Res Commun *368*, 261-266.

Lands, W.E. (1965). Lipid Metabolism. Annu Rev Biochem *34*, 313-346.

Lee, G.Y., Jang, H., Lee, J.H., Huh, J.Y., Choi, S., Chung, J., and Kim, J.B. (2014a). PIASy-mediated sumoylation of SREBP1c regulates hepatic lipid metabolism upon fasting signaling. Mol Cell Biol *34*, 926-938.

Lee, J.H., Lee, G.Y., Jang, H., Choe, S.S., Koo, S.H., and Kim, J.B. (2014b). Ring finger protein20 regulates hepatic lipid metabolism through protein kinase A-dependent sterol regulatory element binding protein1c degradation. Hepatology *60*, 844-857.

Lee, Y.S., Lee, H.H., Park, J., Yoo, E.J., Glackin, C.A., Choi, Y.I., Jeon, S.H., Seong, R.H., Park, S.D., and Kim, J.B. (2003). Twist2, a novel ADD1/SREBP1c interacting protein, represses the transcriptional activity of ADD1/SREBP1c. Nucleic acids research *31*, 7165-7174.

Leung, K., and Munck, A. (1975). Peripheral actions of glucocorticoids. Annual review of physiology *37*, 245-272.

Li, L., and Kaelin, W.G., Jr. (2011). New insights into the biology of renal cell carcinoma. Hematol Oncol Clin North Am *25*, 667-686.

Li, X.D., Zhang, Y.J., and Han, J.C. (2014). Betulin inhibits lung carcinoma proliferation through activation of AMPK signaling. Tumour Biol *35*, 11153-11158.

Li, Y., Xu, S., Mihaylova, M.M., Zheng, B., Hou, X., Jiang, B., Park, O., Luo, Z., Lefai, E., Shyy, J.Y., *et al.* (2011). AMPK phosphorylates and inhibits SREBP activity to attenuate hepatic steatosis and atherosclerosis in diet-induced insulin-resistant mice. Cell metabolism *13*, 376-388.

Li, Z., Bowerman, S., and Heber, D. (2005). Health ramifications of the obesity epidemic. The Surgical clinics of North America *85*, 681-701, v.

Liang, G., Yang, J., Horton, J.D., Hammer, R.E., Goldstein, J.L., and Brown, M.S. (2002). Diminished hepatic response to fasting/refeeding and liver X receptor agonists in mice with selective deficiency of sterol regulatory element-binding protein-1c. J Biol Chem *277*, 9520-9528.

Linehan, W.M., and Ricketts, C.J. (2013). The metabolic basis of kidney cancer. Semin Cancer Biol *23*, 46-55.

Liscovitch, M., and Cantley, L.C. (1994). Lipid second messengers. Cell *77*, 329-334.

Lu, M., and Shyy, J.Y. (2006). Sterol regulatory element-binding protein 1 is negatively modulated by PKA phosphorylation. American journal of physiology Cell physiology *290*, C1477-1486.

Magana, M.M., Koo, S.H., Towle, H.C., and Osborne, T.F. (2000). Different sterol regulatory element-binding protein-1 isoforms utilize distinct co-regulatory factors to activate the promoter for fatty acid synthase. The Journal of biological chemistry *275*, 4726-4733.

Marchesini, G., Brizi, M., Bianchi, G., Tomassetti, S., Bugianesi, E., Lenzi, M., McCullough, A.J., Natale, S., Forlani, G., and Melchionda, N. (2001). Nonalcoholic fatty liver disease: a feature of the metabolic syndrome. Diabetes *50*, 1844-1850.

Medes, G., Thomas, A., and Weinhouse, S. (1953). Metabolism of neoplastic tissue. IV. A study of lipid synthesis in neoplastic tissue slices in vitro. Cancer Res *13*, 27-29.

Menendez, J.A., and Lupu, R. (2007). Fatty acid synthase and the lipogenic phenotype in cancer pathogenesis. Nat Rev Cancer *7*, 763-777.

Minsky, N., Shema, E., Field, Y., Schuster, M., Segal, E., and Oren, M. (2008). Monoubiquitinated H2B is associated with the transcribed region of highly expressed genes in human cells. Nat Cell Biol *10*, 483-488.

Muoio, D.M., and Newgard, C.B. (2006). Obesity-related derangements in metabolic regulation. Annu Rev Biochem *75*, 367-401.

Naar, A.M., Beaurang, P.A., Zhou, S., Abraham, S., Solomon, W., and Tjian, R. (1999). Composite co-activator ARC mediates chromatin-directed transcriptional activation. Nature *398*, 828-832.

Nakamura, K., Kato, A., Kobayashi, J., Yanagihara, H., Sakamoto, S., Oliveira, D.V., Shimada, M., Tauchi, H., Suzuki, H., Tashiro, S., *et al.* (2011). Regulation of homologous recombination by RNF20-dependent H2B ubiquitination. Mol Cell *41*, 515-528.

Nguyen, P., Leray, V., Diez, M., Serisier, S., Le Bloc'h, J., Siliart, B., and Dumon, H. (2008). Liver lipid metabolism. J Anim Physiol Anim Nutr (Berl) *92*, 272-283.

Ookhtens, M., Kannan, R., Lyon, I., and Baker, N. (1984). Liver and adipose tissue contributions to newly formed fatty acids in an ascites tumor. Am J Physiol *247*, R146-153.

Osborne, T.F. (2000). Sterol regulatory element-binding proteins (SREBPs): key regulators of nutritional homeostasis and insulin action. J Biol Chem *275*, 32379-32382.

Owen, J.L., Zhang, Y., Bae, S.H., Farooqi, M.S., Liang, G., Hammer, R.E., Goldstein, J.L., and Brown, M.S. (2012). Insulin stimulation of SREBP-1c processing in transgenic rat hepatocytes requires p70 S6-kinase. Proc Natl Acad Sci U S A *109*, 16184-16189.

Pearce, J. (1983). Fatty acid synthesis in liver and adipose tissue. Proc Nutr Soc *42*, 263-271.

Ponugoti, B., Kim, D.H., Xiao, Z., Smith, Z., Miao, J., Zang, M., Wu, S.Y., Chiang, C.M., Veenstra, T.D., and Kemper, J.K. (2010). SIRT1 deacetylates and inhibits SREBP-1C activity in regulation of hepatic lipid metabolism. J Biol Chem *285*, 33959-33970.

Porstmann, T., Santos, C.R., Griffiths, B., Cully, M., Wu, M., Leevers, S., Griffiths, J.R., Chung, Y.L., and Schulze, A. (2008). SREBP activity is regulated by mTORC1 and contributes to Akt-dependent cell growth. Cell Metab *8*, 224-236.

Postic, C., Dentin, R., Denechaud, P.D., and Girard, J. (2007). ChREBP, a transcriptional regulator of glucose and lipid metabolism. Annu Rev Nutr *27*, 179-192.

Punga, T., Bengoechea-Alonso, M.T., and Ericsson, J. (2006). Phosphorylation and ubiquitination of the transcription factor sterol regulatory element-binding protein-1 in response to DNA binding. J Biol Chem *281*, 25278-25286.

Qiu, B., Ackerman, D., Sanchez, D.J., Li, B., Ochocki, J.D., Grazioli, A., Bobrovnikova-Marjon, E., Diehl, J.A., Keith, B., and Simon, M.C. (2015). HIF2alpha-Dependent Lipid Storage Promotes Endoplasmic Reticulum Homeostasis in Clear-Cell Renal Cell Carcinoma. Cancer discovery *5*, 652-667.

Rankin, E.B., Tomaszewski, J.E., and Haase, V.H. (2006). Renal cyst development in mice with conditional inactivation of the von Hippel-Lindau tumor suppressor. Cancer Res *66*, 2576-2583.

Rezende, R.B., Drachenberg, C.B., Kumar, D., Blanchaert, R., Ord, R.A., Ioffe, O.B., and Papadimitriou, J.C. (1999). Differential diagnosis between monomorphic clear cell adenocarcinoma of salivary glands and renal (clear) cell carcinoma. Am J Surg Pathol *23*, 1532-1538.

Ricketts, C.J., Morris, M.R., Gentle, D., Brown, M., Wake, N., Woodward, E.R., Clarke, N., Latif, F., and Maher, E.R. (2012). Genome-wide CpG island methylation analysis implicates novel genes in the pathogenesis of renal cell carcinoma. Epigenetics *7*, 278-290.

Sakai, J., Rawson, R.B., Espenshade, P.J., Cheng, D., Seegmiller, A.C., Goldstein, J.L., and Brown, M.S. (1998). Molecular identification of the sterol-regulated luminal protease that cleaves SREBPs and controls lipid composition of animal cells. Mol Cell *2*, 505-514.

Saltiel, A.R., and Kahn, C.R. (2001). Insulin signalling and the regulation of glucose and lipid metabolism. Nature *414*, 799-806.

Santos, C.R., and Schulze, A. (2012). Lipid metabolism in cancer. The FEBS journal *279*, 2610-2623.

Schaefer, E.J., Eisenberg, S., and Levy, R.I. (1978). Lipoprotein apoprotein metabolism. J Lipid Res *19*, 667-687.

Schroepfer, G.J., Jr. (1981). Sterol biosynthesis. Annu Rev Biochem *50*, 585-621.

Schulze, A., and Harris, A.L. (2012). How cancer metabolism is tuned for proliferation and vulnerable to disruption. Nature *491*, 364-373.

Seo, J.B., Moon, H.M., Kim, W.S., Lee, Y.S., Jeong, H.W., Yoo, E.J., Ham, J., Kang, H., Park, M.G., Steffensen, K.R., *et al.* (2004a). Activated liver X receptors

stimulate adipocyte differentiation through induction of peroxisome proliferator-activated receptor gamma expression. Molecular and cellular biology *24*, 3430-3444.

Seo, J.B., Moon, H.M., Noh, M.J., Lee, Y.S., Jeong, H.W., Yoo, E.J., Kim, W.S., Park, J., Youn, B.S., Kim, J.W., *et al.* (2004b). Adipocyte determination- and differentiation-dependent factor 1/sterol regulatory element-binding protein 1c regulates mouse adiponectin expression. The Journal of biological chemistry *279*, 22108-22117.

Shabb, J.B. (2001). Physiological substrates of cAMP-dependent protein kinase. Chemical reviews *101*, 2381-2411.

Shao, W., and Espenshade, P.J. (2012). Expanding roles for SREBP in metabolism. Cell Metab *16*, 414-419.

Sharman, D.F. (1973). The catabolism of catecholamines. Recent studies. British medical bulletin *29*, 110-115.

Shema, E., Kim, J., Roeder, R.G., and Oren, M. (2011). RNF20 inhibits TFIIS-facilitated transcriptional elongation to suppress pro-oncogenic gene expression. Mol Cell *42*, 477-488.

Shema, E., Tirosh, I., Aylon, Y., Huang, J., Ye, C., Moskovits, N., Raver-Shapira, N., Minsky, N., Pirngruber, J., Tarcic, G., *et al.* (2008). The histone H2B-specific ubiquitin ligase RNF20/hBRE1 acts as a putative tumor suppressor through selective regulation of gene expression. Genes Dev *22*, 2664-2676.

Shen, C., and Kaelin, W.G., Jr. (2013). The VHL/HIF axis in clear cell renal carcinoma. Semin Cancer Biol *23*, 18-25.

Shimano, H. (2001). Sterol regulatory element-binding proteins (SREBPs): transcriptional regulators of lipid synthetic genes. Prog Lipid Res *40*, 439-452.

Shimano, H., Horton, J.D., Shimomura, I., Hammer, R.E., Brown, M.S., and Goldstein, J.L. (1997). Isoform 1c of sterol regulatory element binding protein is less active than isoform 1a in livers of transgenic mice and in cultured cells. J Clin Invest *99*, 846-854.

Shimomura, I., Shimano, H., Horton, J.D., Goldstein, J.L., and Brown, M.S. (1997). Differential expression of exons 1a and 1c in mRNAs for sterol regulatory element binding protein-1 in human and mouse organs and cultured cells. J Clin Invest *99*, 838-845.

Soyal, S.M., Nofziger, C., Dossena, S., Paulmichl, M., and Patsch, W. (2015). Targeting SREBPs for treatment of the metabolic syndrome. Trends Pharmacol Sci *36*, 406-416.

Spiegel, S., Foster, D., and Kolesnick, R. (1996). Signal transduction through lipid second messengers. Current opinion in cell biology *8*, 159-167.

Sundqvist, A., Bengoechea-Alonso, M.T., Ye, X., Lukiyanchuk, V., Jin, J., Harper, J.W., and Ericsson, J. (2005). Control of lipid metabolism by phosphorylation-dependent degradation of the SREBP family of transcription factors by SCF(Fbw7). Cell Metab *1*, 379-391.

Tang, J.J., Li, J.G., Qi, W., Qiu, W.W., Li, P.S., Li, B.L., and Song, B.L. (2011). Inhibition of SREBP by a small molecule, betulin, improves hyperlipidemia and insulin resistance and reduces atherosclerotic plaques. Cell Metab *13*, 44-56.

Taniguchi, C.M., Emanuelli, B., and Kahn, C.R. (2006). Critical nodes in signalling pathways: insights into insulin action. Nat Rev Mol Cell Biol *7*, 85-96.

Tarcic, O., Pateras, I.S., Cooks, T., Shema, E., Kanterman, J., Ashkenazi, H., Boocholez, H., Hubert, A., Rotkopf, R., Baniyash, M., *et al.* (2016). RNF20 Links Histone H2B Ubiquitylation with Inflammation and Inflammation-Associated Cancer. Cell Rep *14*, 1462-1476.

Tong, Y., and Eigler, T. (2009). Transcriptional targets for pituitary tumor-transforming gene-1. J Mol Endocrinol *43*, 179-185.

Tong, Y., Tan, Y., Zhou, C., and Melmed, S. (2007). Pituitary tumor transforming gene interacts with Sp1 to modulate G1/S cell phase transition. Oncogene *26*, 5596-5605.

Tontonoz, P., Kim, J.B., Graves, R.A., and Spiegelman, B.M. (1993). ADD1: a novel helix-loop-helix transcription factor associated with adipocyte determination and differentiation. Mol Cell Biol *13*, 4753-4759.

Valera, V.A., and Merino, M.J. (2011). Misdiagnosis of clear cell renal cell carcinoma. Nat Rev Urol *8*, 321-333.

Vander Heiden, M.G., Cantley, L.C., and Thompson, C.B. (2009). Understanding the Warburg effect: the metabolic requirements of cell proliferation. Science *324*, 1029-1033.

Vlotides, G., Eigler, T., and Melmed, S. (2007). Pituitary tumor-transforming gene: physiology and implications for tumorigenesis. Endocr Rev *28*, 165-186.

von Roemeling, C.A., Marlow, L.A., Wei, J.J., Cooper, S.J., Caulfield, T.R., Wu, K., Tan, W.W., Tun, H.W., and Copland, J.A. (2013). Stearoyl-CoA desaturase 1 is a novel molecular therapeutic target for clear cell renal cell carcinoma. Clin Cancer Res *19*, 2368-2380.

Walker, A.K., Jacobs, R.L., Watts, J.L., Rottiers, V., Jiang, K., Finnegan, D.M., Shioda, T., Hansen, M., Yang, F., Niebergall, L.J., *et al.* (2011). A conserved SREBP-1/phosphatidylcholine feedback circuit regulates lipogenesis in metazoans. Cell *147*, 840-852.

Walker, A.K., Yang, F., Jiang, K., Ji, J.Y., Watts, J.L., Purushotham, A., Boss, O., Hirsch, M.L., Ribich, S., Smith, J.J., *et al.* (2010). Conserved role of SIRT1 orthologs in fasting-dependent inhibition of the lipid/cholesterol regulator SREBP. Genes Dev *24*, 1403-1417.

Wang, C., Xu, C., Sun, M., Luo, D., Liao, D.F., and Cao, D. (2009). Acetyl-CoA carboxylase-alpha inhibitor TOFA induces human cancer cell apoptosis. Biochem Biophys Res Commun *385*, 302-306.

Wang, X., Briggs, M.R., Hua, X., Yokoyama, C., Goldstein, J.L., and Brown, M.S. (1993). Nuclear protein that binds sterol regulatory element of low density lipoprotein receptor promoter. II. Purification and characterization. J Biol Chem *268*, 14497-14504.

Wang, X., Sato, R., Brown, M.S., Hua, X., and Goldstein, J.L. (1994). SREBP-1, a membrane-bound transcription factor released by sterol-regulated proteolysis. Cell *77*, 53-62.

Wang, Y., Viscarra, J., Kim, S.J., and Sul, H.S. (2015). Transcriptional regulation of hepatic lipogenesis. Nat Rev Mol Cell Biol *16*, 678-689.

Williams, K.J., Argus, J.P., Zhu, Y., Wilks, M.Q., Marbois, B.N., York, A.G., Kidani, Y., Pourzia, A.L., Akhavan, D., Lisiero, D.N., *et al.* (2013). An essential requirement for the SCAP/SREBP signaling axis to protect cancer cells from lipotoxicity. Cancer Res *73*, 2850-2862.

Wondergem, B., Zhang, Z., Huang, D., Ong, C.K., Koeman, J., Hof, D.V., Petillo, D., Ooi, A., Anema, J., Lane, B., *et al.* (2012). Expression of the PTTG1 oncogene is associated with aggressive clear cell renal cell carcinoma. Cancer Res *72*, 4361-4371.

Wood, A., Krogan, N.J., Dover, J., Schneider, J., Heidt, J., Boateng, M.A., Dean, K., Golshani, A., Zhang, Y., Greenblatt, J.F., *et al.* (2003). Bre1, an E3 ubiquitin ligase

required for recruitment and substrate selection of Rad6 at a promoter. Mol Cell *11*, 267-274.

Yamamoto, T., Shimano, H., Inoue, N., Nakagawa, Y., Matsuzaka, T., Takahashi, A., Yahagi, N., Sone, H., Suzuki, H., Toyoshima, H., *et al.* (2007). Protein kinase A suppresses sterol regulatory element-binding protein-1C expression via phosphorylation of liver X receptor in the liver. The Journal of biological chemistry *282*, 11687-11695.

Yang, T., Espenshade, P.J., Wright, M.E., Yabe, D., Gong, Y., Aebersold, R., Goldstein, J.L., and Brown, M.S. (2002). Crucial step in cholesterol homeostasis: sterols promote binding of SCAP to INSIG-1, a membrane protein that facilitates retention of SREBPs in ER. Cell *110*, 489-500.

Yellaturu, C.R., Deng, X., Cagen, L.M., Wilcox, H.G., Mansbach, C.M., 2nd, Siddiqi, S.A., Park, E.A., Raghow, R., and Elam, M.B. (2009). Insulin enhances post-translational processing of nascent SREBP-1c by promoting its phosphorylation and association with COPII vesicles. J Biol Chem *284*, 7518-7532.

Yellaturu, C.R., Deng, X., Cagen, L.M., Wilcox, H.G., Park, E.A., Raghow, R., and Elam, M.B. (2005). Posttranslational processing of SREBP-1 in rat hepatocytes is regulated by insulin and cAMP. Biochemical and biophysical research communications *332*, 174-180.

Yu, R., Heaney, A.P., Lu, W., Chen, J., and Melmed, S. (2000). Pituitary tumor transforming gene causes aneuploidy and p53-dependent and p53-independent apoptosis. J Biol Chem *275*, 36502-36505.

Zechner, R., Strauss, J.G., Haemmerle, G., Lass, A., and Zimmermann, R. (2005). Lipolysis: pathway under construction. Curr Opin Lipidol *16*, 333-340.

Zhang, Y., Yin, L., and Hillgartner, F.B. (2003). SREBP-1 integrates the actions of thyroid hormone, insulin, cAMP, and medium-chain fatty acids on ACCalpha transcription in hepatocytes. Journal of lipid research *44*, 356-368.

Zhao, X., Feng, D., Wang, Q., Abdulla, A., Xie, X.J., Zhou, J., Sun, Y., Yang, E.S., Liu, L.P., Vaitheesvaran, B., *et al.* (2012). Regulation of lipogenesis by cyclin-dependent kinase 8-mediated control of SREBP-1. The Journal of clinical investigation *122*, 2417-2427.

Zhou, G., Myers, R., Li, Y., Chen, Y., Shen, X., Fenyk-Melody, J., Wu, M., Ventre, J., Doebber, T., Fujii, N., *et al.* (2001). Role of AMP-activated protein kinase in mechanism of metformin action. J Clin Invest *108*, 1167-1174.

국문 초록

지방대사는 에너지 항상성, 신호전달 경로, 세포막 구조를 조절함으로써 세포의 성장과 생존에 중요한 역할을 수행한다. 그러므로 지방대사의 이상 조절은 대사성 질환 및 종양 형성과 밀접하게 연관되어 있다. 간에서 다량으로 발현하는 전사인자인 sterol regulatory element-binding protein 1c (SREPB1c)는 인슐린에 의해 활성화되어 지방대사물 생합성을 촉진하는 역할을 관장한다. 반면 공복시 SREBP1c는 억제됨으로써 불필요한 지방대사물의 생합성을 제어하는데 그에 대한 기전 연구가 불분명한 상황이다. 이와 함께 암세포에서 SREBP1c의 활성화는 종양의 발생, 진행 및 전이를 촉진함으로써 궁극적으로 환자의 낮은 생존 예후와 연관되어 있다. 그러나 암세포에서 SREBP1c가 어떻게 지방대사물의 축적과 종양 발생을 촉진하는지에 대해서는 분자수준의 연구가 부족한 상황이다.

본 연구를 통해 SREBP1c 전사인자의 유비퀴틴화를 통한 분해를 매개하는 E3 ubiquitin ligase로 ring finger protein 20 (RNF20)을 동정하였다. 간세포에서 RNF20는 단식 조건에서 활성화되는 protein kinase A (PKA) 신호전달을 거쳐 그 발현이 증가하며, 이로 인해 SREBP1c 활성 및 지방대사물 생합성 프로그램이 통제되는 새로운 기전을 규명하였다. 나아가 SREBP1c와 지방대사물 생합성이 증가되어 있는 *db*/*db* 생쥐 모델의 간 조직 특이적 RNF20 과발현은 SREBP1c와 지방대사물 생합성

관련인자들의 발현 감소를 통하여 궁극적으로 지방간을 개선시켰다. 이상의 결과들을 통하여 공복 시 RNF20가 SREBP1c를 제거함으로써 불필요한 지방대사물 생합성이 억제되는 지방대사 항상성 조절 기전을 새롭게 제시하였다.

과도한 지방대사물 축적이 동반되는 신장암에서 RNF20는 억제되며 동시에 SREBP1c는 활성화됨을 관찰하였다. 신장암 종양 조직에서 RNF20 발현이 감소되어 있지만 지방대사물 생합성 관련 유전자의 발현은 증가되어 있으며, RNF20 발현이 낮게 관찰되는 신장암 환자의 낮은 생존 예후를 발견하였다. 신장암 세포주와 이종 이식 실험 결과, RNF20 과발현에 의해 SREBP1c가 억제됨으로써 지방대사물 생합성과 세포증식이 감소함을 관찰하였다. 본 연구를 통해 pituitary tumor-transforming gene 1 (PTTG1)을 SREBP1c의 새로운 표적 유전자로 동정하였으며, 신장암 세포에서 SREBP1c에 의한 PTTG1 유도가 세포주기 조절에 있어 중요한 역할을 수행함을 밝혔다. 또한, 신장암 세포에서 유전자 넉다운과 SREBP1c 억제 약물인 베틀린은 SREBP1c의 저해뿐 아니라 PTTG1과 세포주기 조절 유전자들의 발현을 감소시킴으로써 세포증식을 억제함을 관찰하였다.

본 연구를 통하여 RNF20-SREBP1c 신호전달 경로는 지방대사물 생합성 및 세포주기를 조절함으로써 지방대사 항상성 유지와 신장암 종양 형성 과정에도 깊이 연관되어 있음을 규명하였다. 그러므로 RNF20는 SREBP1c 제어를 통하여 지방대사 및 세포주기 조절에 중요한

기능을 담당함으로써 대사성 질환 및 특정 종양 치료제 발굴을 위한 표적으로 제안할 수 있다.

주요어: RNF20, SREBP1c, PTTG1, PKA, 유비퀴틴화, 지방생합성, 종양 형성, 신장암

학번: 2011-30914